

# Ligand and Substrate Migration in Human Indoleamine 2,3-Dioxygenase



Zur Erlangung des akademischen Grades eines  
DOKTORS DER NATURWISSENSCHAFTEN  
(Dr. rer. nat.)

Fakultät für Chemie und Biowissenschaften  
Karlsruher Institut für Technologie (KIT) - Universitätsbereich

genehmigte  
DISSERTATION  
von  
Dipl.-Biol. Elena Nickel  
aus  
Ahlen

Dekan:	Prof. Dr. Martin Bastmeyer
Referent:	Prof. Dr. Gerd Ulrich Nienhaus
Korreferent:	Prof. Dr. Anne Ulrich

Tag der mündlichen Prüfung: 16. Dezember 2011



# Contents

<b>List of Figures</b>	<b>V</b>
<b>List of Abbreviations</b>	<b>VII</b>
<b>1 Introduction</b>	<b>1</b>
1.1 Indoleamine 2,3-Dioxygenase . . . . .	1
1.1.1 The Various Functions of Heme Proteins . . . . .	1
1.1.2 Function of IDO and TDO . . . . .	2
1.1.3 hIDO - In the Focus of Research . . . . .	3
1.1.4 Structure and Dynamics of hIDO . . . . .	5
1.2 Protein-Ligand Interactions . . . . .	7
1.2.1 Dissociation Reaction . . . . .	7
1.2.2 Ligand Binding in Mb . . . . .	7
1.3 Spectroscopy . . . . .	11
1.3.1 Principle of UV/Vis Spectroscopy . . . . .	13
1.3.2 UV/Vis Spectroscopy of Proteins . . . . .	14
1.3.3 IR Spectroscopy . . . . .	15
1.3.4 IR Spectroscopy of Proteins . . . . .	16
1.3.5 Using CO as a Probe . . . . .	17
1.4 Outline of the Work . . . . .	18
<b>2 Materials and Methods</b>	<b>21</b>
2.1 The Vector Coding for hIDO . . . . .	21
2.2 Mutagenesis . . . . .	22
2.3 Expression and Purification . . . . .	23
2.4 Absorbance Spectroscopy . . . . .	24
2.4.1 UV/Vis Spectroscopy . . . . .	24
2.4.1.1 Sample Preparation . . . . .	24
2.4.1.2 Time-Resolved Spectroscopy . . . . .	25
2.5 Fourier Transform Infrared Spectroscopy . . . . .	26
2.5.1 Sample Preparation . . . . .	26

## CONTENTS

---

2.5.2	Setup for Infrared Cryospectroscopy Measurements . . . . .	27
2.5.3	The FTIR Spectrometer . . . . .	27
2.5.4	FTIR Absorbance Difference Spectra . . . . .	29
2.5.5	Isothermal Kinetic Measurements . . . . .	30
2.5.6	Temperature Derivative Spectroscopy (TDS) . . . . .	30
2.5.6.1	Theoretical Background . . . . .	30
2.5.6.2	TDS in Application . . . . .	33
2.5.6.3	Contour Plots - Presentation of the TDS Data . . . . .	33
2.5.6.4	Temperature Dependence of Transmission Spectra and TDS . . . . .	34
2.5.7	Illumination Protocols (IPs) . . . . .	36
<b>3</b>	<b>Probing the Active Site</b>	<b>37</b>
3.1	UV/Vis and FTIR Absorbance Spectra at Ambient Temperature . . . . .	38
3.2	Temperature Effect on Active Site Conformations . . . . .	39
3.3	4-K FTIR Absorbance Spectra . . . . .	42
3.4	Point Mutations at the Active Site . . . . .	45
3.5	Binding of L-Trp Analogues . . . . .	51
3.6	Binding of D-Trp in hIDO Variants . . . . .	53
3.7	Conclusions . . . . .	54
<b>4</b>	<b>Probing the Protein Matrix</b>	<b>57</b>
4.1	Existence of Ligand Docking Sites in hIDO-CO and hIDO-CO/L-Trp . . . . .	58
4.2	Ligand Dynamics in the Docking Sites . . . . .	59
4.3	hIDO-CO: Docking Sites and Ligand Migration . . . . .	63
4.4	hIDO-CO/L-Trp: Docking Sites and Ligand Migration . . . . .	69
4.5	L-Trp Analogues . . . . .	74
4.6	Conclusions . . . . .	77
<b>5</b>	<b>L-Trp Migration</b>	<b>79</b>
5.1	Photolysis at $T \geq 200$ K . . . . .	79
5.2	Photolysis at $T < 200$ K . . . . .	82
5.3	Tracking L-Trp in the Enzyme . . . . .	83
5.4	Monitoring the Heme . . . . .	83
5.5	Conclusions . . . . .	88
<b>6</b>	<b>Ligand Binding at Ambient Temperature</b>	<b>91</b>
6.1	Spectroscopic and Kinetic Changes upon L-Trp Addition . . . . .	91
6.2	Spectroscopic and Kinetic Properties of MLT-, D-Trp- and S-Trp- bound hIDO . . . . .	100
6.3	Conclusions . . . . .	105

---

<b>7</b>	<b>Conclusions and Discussion</b>	<b>107</b>
7.1	Two Modes of L-Trp Binding . . . . .	107
7.2	Evidence of a Second Inhibitory Binding Site . . . . .	109
7.3	Substrate Binding and Catalytic Activity . . . . .	110
7.4	Inhibition of hIDO by 1-MT . . . . .	111
7.5	hIDO, hIDO2 and TDO: Three Proteins Converting L-Trp . . . . .	112
7.6	Outlook . . . . .	112
<b>8</b>	<b>Summary</b>	<b>115</b>
	Summary . . . . .	115
	<b>Zusammenfassung</b>	<b>118</b>
<b>A</b>	<b>List of Primers</b>	<b>i</b>
<b>B</b>	<b>Chemical Structures of L-Trp, D-Trp, S-Trp and MLT</b>	<b>iii</b>
<b>C</b>	<b>List of Equations</b>	<b>v</b>
	<b>Bibliography</b>	<b>xix</b>
	Danksagung . . . . .	xxi
	List of Publications . . . . .	xxiii
	List of Poster . . . . .	xxv
	Lebenslauf . . . . .	xxvii



# List of Figures

1.1	Conversion of L-Trp . . . . .	2
1.2	Michaelis-Menten Plot of hIDO Activity . . . . .	4
1.3	Active Site Structure and Entrance to the Distal Pocket of hIDO . . .	6
1.4	Reaction Energy Surface of a Three-State Model . . . . .	8
1.5	Electromagnetic Spectrum . . . . .	12
1.6	Electronic Transitions Observed by UV/Vis Spectroscopy . . . . .	13
1.7	UV/Vis Spectra of hIDO . . . . .	15
1.8	Molecular Potential Energy Curves for a Diatomic Molecule . . . . .	16
1.9	Back-Bonding . . . . .	18
2.1	Expression Region of the Vector pET-15b-hIDO . . . . .	21
2.2	Scheme of the Flash Photolysis System . . . . .	26
2.3	FTIR Spectroscopy Setup, Interferogram and Transmission Spectrum	28
2.4	Schematic Representation of TDS . . . . .	31
2.5	Illumination Protocols . . . . .	36
3.1	Vis and FTIR Absorbance Spectra of hIDO-CO and hIDO-CO/L-Trp at RT . . . . .	38
3.2	Temperature Dependence of hIDO-CO FTIR Absorbance Spectra . .	40
3.3	Fit of 4-K FTIR Absorbance Spectra of hIDO-CO and hIDO-CO/L-Trp	42
3.4	Amino Acid Sequence of hIDO . . . . .	45
3.5	Active Site Structures of wt hIDO and hIDO Variants . . . . .	46
3.6	Alignment of Amino Acid Sequences of xcTDO and hIDO . . . . .	47
3.7	Comparison of Vis Spectra of wt hIDO-CO and hIDO-CO Variants without and with L-Trp . . . . .	48
3.8	Comparison of 4-K FTIR Absorbance Spectra of wt hIDO-CO and hIDO-CO Variants without and with L-Trp . . . . .	50
3.9	Spectra of hIDO-CO with Different L-Trp Analogues . . . . .	52
3.10	4-K FTIR Spectra of wt hIDO-CO and Variants with D-Trp . . . . .	53
3.11	Scheme of Interactions between hIDO and L-Trp/D-Trp . . . . .	55

LIST OF FIGURES

---

4.1	Photolysis Difference Spectra of hIDO-CO and hIDO-CO/L-Trp . . .	59
4.2	TDS maps of hIDO-CO . . . . .	60
4.3	Effect of Ligand Dynamic in Docking Sites on the Photoproduct Bands	61
4.4	Development of Photoproduct Bands of hIDO-CO with Temperature	62
4.5	Geminate Recombination of CO in hIDO-CO . . . . .	64
4.6	Assignment of Photoproduct Bands in hIDO-CO . . . . .	65
4.7	Variant G261A hIDO-CO: Assignment of Photoproduct Bands D <sub>1</sub> and D <sub>2</sub> . . . . .	67
4.8	Comparison of Photolysis Yield in hIDO-CO and hIDO-CO/L-Trp . .	70
4.9	Geminate Rebinding of CO in hIDO-CO/L-Trp . . . . .	71
4.10	Recombination of CO in hIDO-CO/L-Trp at T > 160 K . . . . .	72
4.11	Comparison of FTIR Difference Spectra and CO Recombination in hIDO-CO with Different L-Trp Analogous . . . . .	75
5.1	CO Recombination Kinetics in hIDO-CO/L-Trp . . . . .	81
5.2	Formation of hIDO-CO/—L-Trp after Photolysis at T < 200 K . . .	82
5.3	Tracking L-Trp in the Protein Matrix . . . . .	84
5.4	CO Recombination in hIDO-CO/L-Trp at Different Temperatures Observed by Vis Spectroscopy . . . . .	85
5.5	CO Recombination at Different L-Trp Concentrations . . . . .	86
5.6	Analysis of CO and L-Trp Binding to hIDO-CO/L-Trp at Different L-Trp Concentrations . . . . .	87
5.7	Scheme of L-Trp Migration in hIDO . . . . .	89
6.1	Visible Spectra of Deoxy and CO-Bound hIDO and hIDO/L-Trp . . .	92
6.2	Development of Visible Spectra and Time Traces of hIDO-CO upon Increasing L-Trp Concentrations . . . . .	94
6.3	Analysis of the Bimolecular Recombination Process of CO in hIDO- CO with Increasing L-Trp Concentration . . . . .	95
6.4	Development of the Fractions of hIDO-CO, hIDO-CO/L-Trp' and hIDO-CO/L-Trp" with Increasing L-Trp Concentration . . . . .	97
6.5	hIDO-CO/L-Trp and hIDO-CO/L-Trp' Contribute to the Soret Band Shift . . . . .	100
6.6	Development of Visible Spectra and Kinetic Traces upon Addition of of Various Substrates to hIDO-CO . . . . .	101
6.7	Analysis of Bimolecular CO Recombination in Samples with Different L-Trp Analogues . . . . .	103
B.1	Chemical Structures of L-Trp, D-Trp, S-Trp and MLT . . . . .	iii

## List of Abbreviations

1-MT	1-Methyl-DL-tryptophan
CHES	2-(N-cyclohexylamino)ethane sulfonic acid
CN	Cyanide
CO	Carbon monoxide
CS	Conformational substate
DNA	Deoxyribonucleic acid
D-Trp	D-tryptophan
<i>E. coli</i>	<i>Escherichia coli</i>
FTIR	Fourier transform infrared
FWHM	Full width at half maximum
hIDO	Human indoleamine 2,3-dioxygenase
hTDO	Human tryptophan 2,3-dioxygenase
IDO	Indoleamine 2,3-dioxygenase
IP	Illumination protocol
IR	Infrared
KPB	Potassium phosphate buffer
L-Trp	L-tryptophan
Mb	Myoglobin
MbCO	Carbonmonoxide-ligated myoglobin
MbO <sub>2</sub>	Oxygen-ligated myoglobin
MDT	1-Methyl-D-tryptophan
MLT	1-Methyl-L-tryptophan
NaCl	Sodium chloride
NFK	N-formylkynurenine
NO	Nitric oxide
NOS	Nitric oxide synthase
O <sub>2</sub>	Oxygen
PI	4-Phenylimidazole
PrnB	Second enzyme in the pyrrolnitril biosynthesis pathway
RT	Room temperature
S-Trp	3-(Thianaphthen-3-yl)-L-alanine
TDO	Tryptophan 2,3-dioxygenase
TDS	Temperature derivative spectroscopy
Trp	Tryptophan
UV	Ultraviolet
Vis	Visible
wt	Wildtype
xcTDO	Tryptophan 2,3-dioxygenase of <i>Xanthomonas campestris</i>

Table 1: 1-Letter Code of Standard Amino Acids

A	alanine	G	glycine	M	methionine	S	serine
C	cysteine	H	histidine	N	asparagine	T	threonine
D	aspartate	I	isoleucine	P	proline	V	valine
E	glutamate	K	lysine	Q	glutamine	W	tryptophan
F	phenylalanine	L	leucine	R	arginine	Y	tyrosine





# Chapter 1

## Introduction

### 1.1 Indoleamine 2,3-Dioxygenase

#### 1.1.1 The Various Functions of Heme Proteins

The functions of proteins are diverse. They act as enzymes, transporters or are part of the cellular structure. Just as diverse as their functions are their sizes and structures. They include small single-domain proteins, but also protein complexes formed by two and more protein subunits. Many proteins contain prosthetic groups, tightly bound cofactors such as metal ions, phosphates or lipids.

Heme proteins contain a prosthetic heme group consisting of an iron atom in the center of a porphyrin molecule. This heme group is crucial for the functionality of the proteins. Its environment is responsible for the diversity of the functions heme proteins perform<sup>[1]</sup>. For decades, heme proteins have been known to serve as transporter and storage proteins for small diatomic ligands such as oxygen (O<sub>2</sub>), carbon monoxide (CO) or nitric oxide (NO)<sup>[2]</sup>. In the blood, hemoglobin assures the transport of O<sub>2</sub> from the respiratory organs to the different tissues of the body<sup>[3]</sup>. Myoglobin (Mb), a small globular heme protein, is responsible for O<sub>2</sub> transport within muscle tissue<sup>[4-6]</sup>. In addition, heme proteins are involved in diatomic gas sensing<sup>[7,8]</sup> and electron transport<sup>[9-11]</sup>. Several heme proteins in the human body were found to be involved in catalysis, among them cytochrome P450<sup>[12]</sup>, nitric oxide synthase (NOS)<sup>[13]</sup> and tryptophan 2,3-dioxygenase (TDO)<sup>[14]</sup>. The enzymes of the cytochrome P450 superfamily are monooxygenases inserting one atom of the oxygen molecule into an organic substrate. NOS metabolizes arginine by a two-step reaction to NO, an important cell signaling molecule. The dioxygenase TDO carries out the first and rate-limiting step of the kynurenine pathway, which is the major route of the tryptophan (W) metabolism in humans. The same reaction is catalyzed by another heme-containing enzyme, indoleamine 2,3-dioxygenase (IDO).

### 1.1.2 Function of IDO and TDO

L-tryptophan (L-Trp) is an essential amino acid in humans. More than 95% of the dietary L-Trp is metabolized via the kynurenine pathway <sup>[15]</sup> leading to formation of nicotinamide adenine dinucleotide. Only a small amount is converted to the neurotransmitter serotonin <sup>[16]</sup>.

IDO and TDO catalyze the degradation of L-Trp to N-formylkynurenine (NFK) in the initial step of the kynurenine pathway (Figure 1.1). The catalytic reaction of the enzymes is initiated by the reduction of the heme iron. Recent studies propose cytochrome *b*<sub>5</sub> as the electron transfer partner of IDO *in vivo* <sup>[17,18]</sup>. Subsequently, the ligand O<sub>2</sub> binds to the heme iron and, in close vicinity to the ligand, the substrate L-Trp binds inside the distal pocket. In the reaction, both atoms of an oxygen molecule are inserted across the C<sub>2</sub> = C<sub>3</sub> double bond of the L-Trp indole moiety.

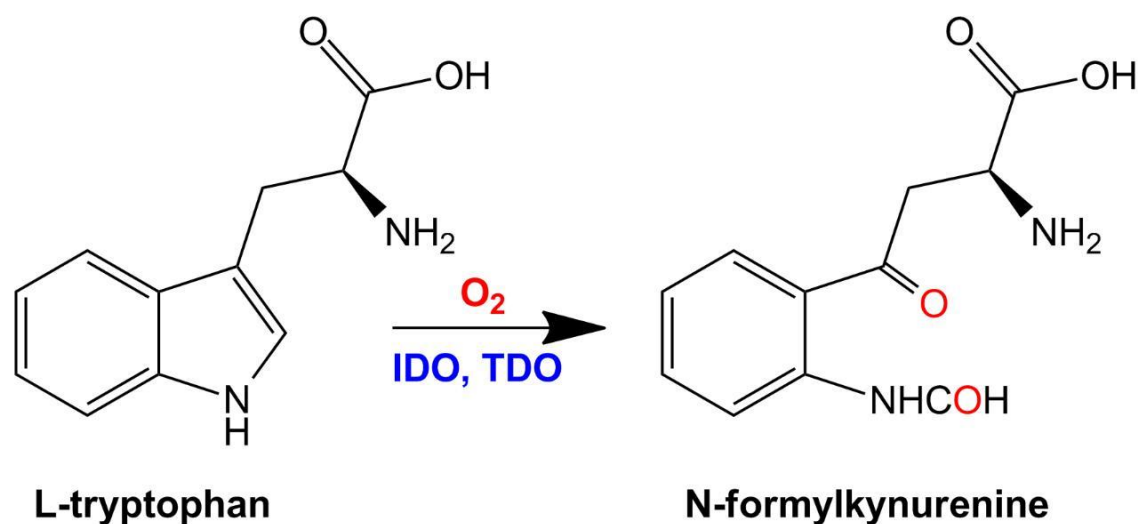


Figure 1.1: Conversion of L-Trp. IDO and TDO catalyze the reaction of L-Trp and O<sub>2</sub> to N-formylkynurenine.

Despite catalyzing the same reaction, there are major differences between TDO and IDO. TDO is widely distributed across the different biological domains including eukaryotes and bacteria whereas IDO is only found in mammals <sup>[19]</sup>. Just recently, some IDO-like proteins were identified in yeast and bacteria <sup>[20,21]</sup>. Furthermore, TDO and IDO exhibit differences in their structures. TDO is a homotetrameric protein <sup>[22]</sup> whereas IDO acts as a monomeric molecule <sup>[23]</sup>. Although some key amino

acids at the active site are similar, the sequence identity between IDO and TDO is only about 10%<sup>[24]</sup>. Whereas human TDO (hTDO) is predominantly found in the liver, human IDO (hIDO) is widely distributed across non-hepatic tissue. One of the major differences between TDO and IDO is their substrate specificity. TDO converts only L-Trp and some of its derivatives substituted at the 5- and 6-position of the indole moiety<sup>[25]</sup>. IDO exhibits much less substrate specificity, converting various indole derivatives such as D-tryptophan (D-Trp), serotonin or tryptamine<sup>[23]</sup>.

### 1.1.3 hIDO - In the Focus of Research

IDO was discovered by Hayaishi and coworkers in 1967<sup>[26]</sup>. The protein, purified from rabbit intestine, was initially shown to convert D-Trp. Until the early 1990s, extensive studies on the functional and structural properties of rabbit IDO were performed<sup>[27-33]</sup>. In 1990, Tone and coworkers published the primary structure of hIDO<sup>[34]</sup>. However, only since hIDO was found to be connected to various (patho)-physiological conditions including depression, the escape of tumors from the cell immune surveillance, or Alzheimer's disease, the enzyme moved back into the focus of research<sup>[16,35-39]</sup>.

The expression of hIDO is induced by proinflammatory cytokines such as interferon  $\gamma$ , lipopolysaccharides, and tumor necrosis factor, which are linked to a variety of immune-related (patho)-physiological conditions<sup>[40]</sup>. Local overexpression of hIDO results in the depletion of L-Trp and, simultaneously, in the accumulation of tryptophan metabolites. Increased levels of quinolic acid, a neurotoxic intermediate of the kynurenine pathway, may lead to neuro-degeneration in Alzheimer's disease<sup>[39]</sup>. The intermediate 3-hydroxykynurenine was shown to be linked to the formation of cataractous lenses<sup>[41,42]</sup>. Local depletion of L-Trp suppresses bacterial growth<sup>[43,44]</sup>. However, the depletion also results in the suppression of T-cell proliferation promoting immunetolerance<sup>[45]</sup>. This phenomenon prevents the T-cell mediated rejection of the allogenic fetus<sup>[46]</sup>. At the same time, it is responsible for the immune escape of tumor cells.

In humans, two IDOs have been identified, IDO1 and IDO2. Human IDO2 was only recently described and shares 43% sequence identity with human IDO1<sup>[47,48]</sup>. These proteins are found in different tissues and exhibit different kinetic properties<sup>[49]</sup>. This work will focus on the enzyme human IDO1, in the following denoted as hIDO.

Since hIDO was identified as a therapeutic target, its inhibition has been the issue of many studies. One difficulty in finding suitable inhibitors is based on the necessity to be specific to hIDO; simultaneous inhibition of IDO2 and TDO must be excluded. The list of tested inhibitors is long<sup>[49-51]</sup>. Early studies focused on consecutive inhibitors that either replace the ligand O<sub>2</sub> or the substrate L-Trp. Sono and coworkers studied inhibitors, such as 4-phenylimidazole (PI) or norharman that

bind directly to the heme iron and, thereby, hinder the association of the ligand<sup>[52]</sup>. They also investigated the binding of different structural analogues of L-Trp, among them 1-methyl-DL-tryptophan (1-MT) and  $\beta$ -3-benzofuran-DL-alanine<sup>[53]</sup>.

Yeh and coworkers tested the activity of hIDO towards L-Trp and D-Trp (Figure 1.2)<sup>[54]</sup>. For D-Trp and for low concentrations of L-Trp, the activity of hIDO exhibits typical Michaelis-Menten behavior. However, at high L-Trp concentrations, significant substrate inhibition is observed (Figure 1.2 a). Similar results were obtained with rabbit IDO<sup>[26]</sup>. These results suggest the existence of a second, inhibitory L-Trp binding site in hIDO, a possible target for therapeutics.

To date, the most potent inhibitor is the L-Trp analogue 1-methyl-L-tryptophan (MLT), which is derived from L-Trp by adding a methyl group to the indole nitrogen. Still, the molecule is only a weak competitive inhibitor<sup>[48]</sup>. The search for more suitable inhibitors is ongoing.

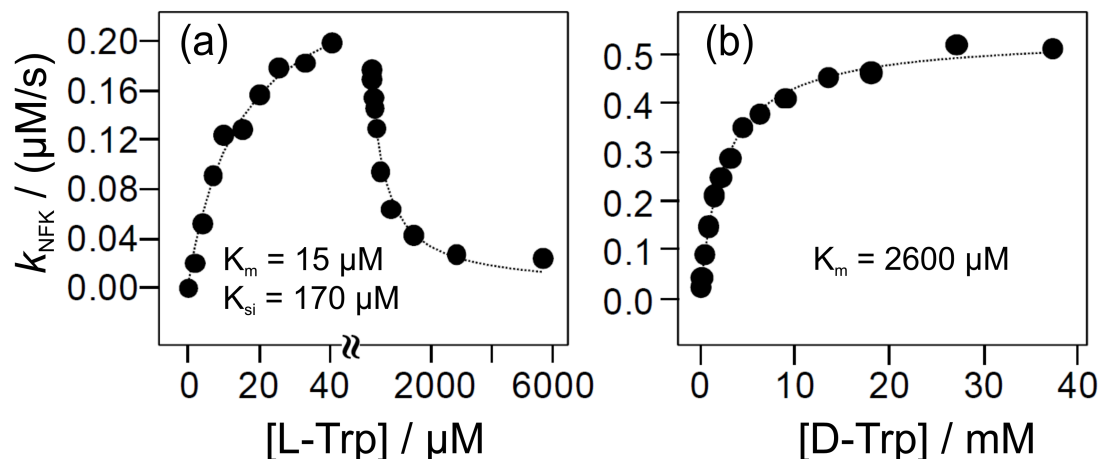


Figure 1.2: Michaelis-Menten plot of the hIDO reaction forming NFK from (a) L-Trp and (b) D-Trp. The experiment was performed under air-saturated conditions with 91 nM hIDO at pH 7.4.<sup>[54]</sup>

### 1.1.4 Structure and Dynamics of hIDO

Monomeric hIDO has a molecular weight of  $\approx 45$  kDa. In 2006, the crystal structure of recombinant hIDO was solved by Sugimoto et al.<sup>[55]</sup>. The structures of the PI-bound (resolution 2.3 Å) and the cyanide (CN)-bound (resolution 3.4 Å) forms were solved, both representing inactive states of the protein (PDB entry codes: 2D0T and 2D0U). Figure 1.3 depicts the active site of CN-bound hIDO (panel a) and the suspected entrance to the distal heme pocket (panel b). In the following, all amino acids are abbreviated by the 1-letter code (List of Abbreviations, Table 1).

The mainly  $\alpha$ -helical polypeptide chain of the protein is folded into two domains that sandwich the heme moiety in between. The heme pocket is covered by the smaller domain, whereas the larger  $\alpha$ -helical domain anchors the prosthetic heme group. The heme molecule is covalently bonded to the proximal H346. A loop (residues 250 - 267) connects the two domains. A highly conserved section of this loop (residues 260 - 265; Figure 1.3 a, green), expected to provide the flexibility for large-scale motions of the protein, is part of the distal pocket.

A flexible loop outside the heme pocket consisting of residues 360 to 380 could not be solved in the crystal structure. The framing residues that were solved are marked in cyan, S359, Q360, G380 and G381 (Figure 1.3 a). Upon substrate binding, the loop is expected to become ordered and close off the heme pocket, analogously to findings in TDO<sup>[24,40]</sup> and PrnB<sup>[21]</sup>, the second enzyme in the pyrrolnitril biosynthesis pathway.

With S167 (Figure 1.3 a, magenta) as the only exception, the distal pocket is devoid of polar residues. However, mutagenesis studies revealed that S167 is neither involved in the catalytic activity nor in substrate recognition<sup>[55,56]</sup>. Moreover, mutagenesis studies showed the importance of the amino acids R231 (orange) and F226 and F227 (blue) for the catalytic activity of hIDO towards L-Trp<sup>[55]</sup>. The PI-bound form of ferric ( $\text{Fe}^{3+}$ ) hIDO revealed that the phenyl group of the inhibitor PI interacts with F163 (blue) via  $\pi - \pi$  stacking.

The crystal structures of hIDO showed a rather spacious heme pocket (Figure 1.3 b)<sup>[55]</sup>. In addition to PI (green) bound at the heme iron, two buffer molecules (2-(N-cyclohexylamino)ethane sulfonic acid (CHES)) (yellow) were found in the distal pocket. The crystal structure revealed interactions of the CHES molecules with the protein matrix and the heme moiety. It is considerable that the binding positions of these molecules at least partly overlap with the binding site of the substrate.

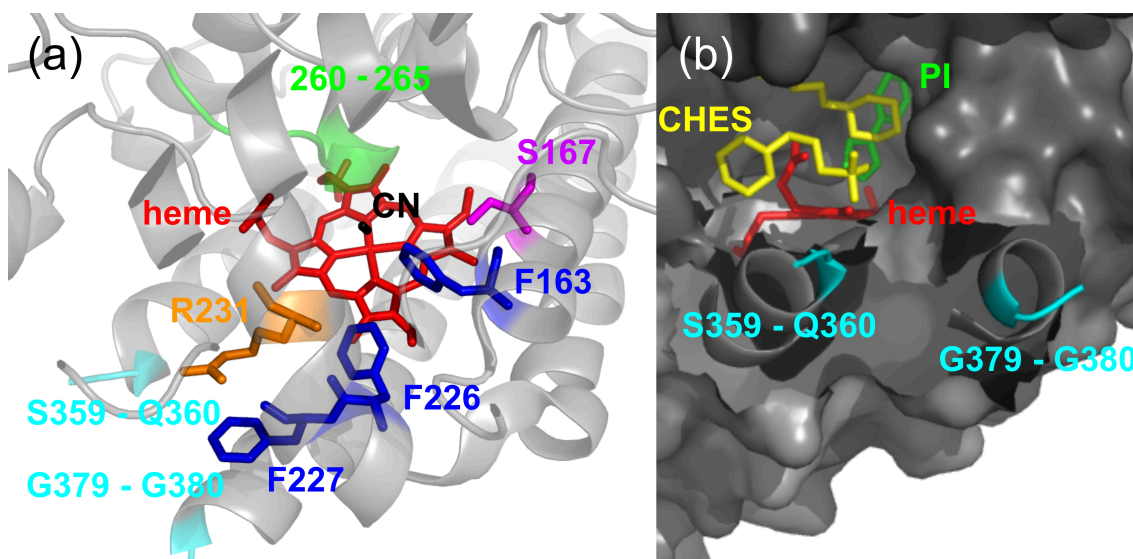
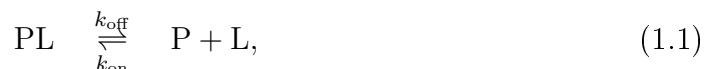


Figure 1.3: (a) Structure of the distal side of CN-bound hIDO and (b) the putative entrance to the distal pocket of PI-bound hIDO. (a) The distal heme pocket includes the heme moiety (red), the ligand CN (black) and several amino acids such as F163, F226 and F227 (blue), R231 (orange), S167 (magenta) and the conserved amino acid residues 260 to 265 (green). Amino acids S359, Q360, G380 and G381 (cyan) frame the flexible loop that was not solved in the crystal structure. (b) The distal pocket accommodating two CHES buffer molecules (yellow) and the inhibitor PI (green). Indicated in cyan are the framing amino acids (S359, Q360, G380 and G381) of the outside loop. Images were created with PyMol<sup>[57]</sup>. (PDB entry codes: 2D0T and 2D0U<sup>[55]</sup>)

## 1.2 Protein-Ligand Interactions

### 1.2.1 Dissociation Reaction

The dissociation of a protein-ligand complex, PL, into a ligand, L, and a protein, P, can be described by the reaction



where  $k_{\text{off}}$  and  $k_{\text{on}}$  are the dissociation and the association rate coefficients, respectively. The equilibrium at which the associated and the dissociated forms of the protein-ligand complex exist in equal concentrations is given by the dissociation coefficient,  $K_{\text{d}}$ , defined as

$$K_{\text{d}} = \frac{k_{\text{off}}}{k_{\text{on}}} = \frac{[\text{L}][\text{P}]}{[\text{PL}]}. \quad (1.2)$$

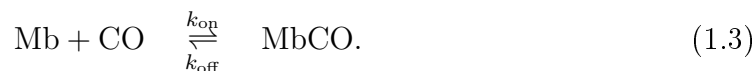
$[\text{L}]$ ,  $[\text{P}]$  and  $[\text{PL}]$  are the concentrations of ligand, protein and the protein-ligand complex.

Equilibrium studies provide information about the  $K_{\text{d}}$  between the protein and the ligand. The rate coefficients,  $k_{\text{on}}$  and  $k_{\text{off}}$ , yielding information about the time it takes for a reaction to occur, can only be obtained by time-resolved experiments.

### 1.2.2 Ligand Binding in Mb

The kinetics of ligand binding have been especially well studied in Mb, which is often used as a model system for heme proteins. In 1957, Gibson found that the bond between a ligand, such as  $\text{O}_2$  or  $\text{CO}$ , and the heme iron in Mb can be disrupted by visible light<sup>[58]</sup>. This property of the iron-ligand bond is utilized in flash photolysis experiments to observe the recombination process of the ligand to the heme iron after the ligand was photolyzed by a short laser pulse. The photoproduct yield on the nanosecond time scale for oxyMb ( $\text{MbO}_2$ ) is between 30 - 70%<sup>[59,60]</sup>. For CO-ligated Mb ( $\text{MbCO}$ ) it is 100%, making the  $\text{MbCO}$  complex a perfect example to study ligand binding in heme proteins<sup>[61]</sup>.

Until the early seventies, the process of  $\text{CO}$  binding to Mb was considered a simple one-step reaction<sup>[62]</sup> described by



However, flash photolysis experiments on MbCO over a wide temperature range revealed multiple intermediate steps in the ligand recombination process<sup>[61]</sup>. The kinetic intermediates were shown to result from protein relaxation and movements of the ligand within the protein<sup>[63,64]</sup>.

After photolysis at cryogenic temperatures ( $< 180$  K), CO is trapped at defined sites in the protein matrix<sup>[63,65,66]</sup>. Immediately after the photolysis flash, the CO ligand resides at a primary docking site, site B, located in close vicinity to the heme iron<sup>[67-69]</sup>. From this position, the ligand can either rebind to the heme iron or migrate to further, secondary docking sites in the protein matrix. In Mb, two additional secondary docking sites could be identified, named C and D sites<sup>[63,64,70-73]</sup>. A time resolved x-ray crystallography study of Anfinrud and coworkers on the crystal structure of the Mb mutant L29F MbCO impressively demonstrated the migration of the ligand within the protein<sup>[66]</sup>.

Up to now, well-defined transient ligand docking sites in the protein matrix have been identified in several heme proteins, among them human neuroglobin<sup>[74]</sup>, human hemoglobin<sup>[75]</sup> or dehaloperoxidase from the worm *Amphitrite ornata*<sup>[76]</sup>.

After flash photolysis of MbCO at ambient temperature, the CO ligand is either trapped inside the protein or escapes into the solvent. The recombination process at room temperature was first described by Austin et al.<sup>[61]</sup>. They observed a biphasic recombination process in Mb including a fast and a slow rebinding step. Eaton and coworkers published a simplified model to describe the rebinding kinetics in MbCO<sup>[77]</sup>. They introduced a three-state model including three protein states: the protein in the ligand-bound state, A, the protein with the photodissociated ligand in the protein matrix, B, and the dissociated state, S, with the ligand in the solvent (Figure 1.4).

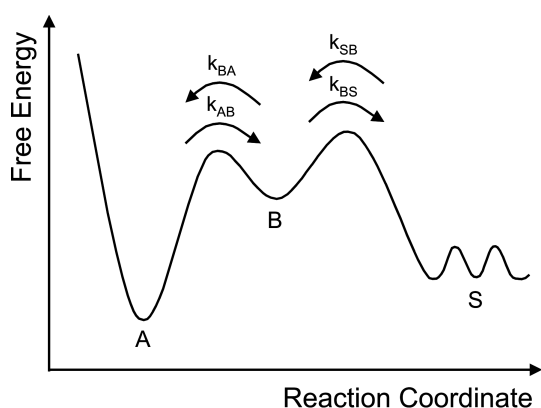


Figure 1.4: The reaction energy surface of a three-state model. The scheme includes the protein in the ligand-bound state, A, state B, where the ligand resides within the protein matrix, and state S, where the ligand escaped into the solvent. The transitions between the states are described by the rate coefficients  $k_{AB}$ ,  $k_{BA}$ ,  $k_{BS}$  and  $k_{SB}$ .

The scheme in Figure 1.4 depicts the three protein states, A, B and S. The rate coefficients  $k_{AB}$ ,  $k_{BA}$ ,  $k_{BS}$  and  $k_{SB}$  connect the three states. The rate coefficient  $k_{AB}$  is much smaller than the other rate coefficients. Hence, for simplicity, we set  $k_{AB} \approx 0$ . Additionally, we assume that internal and bimolecular recombination are sufficiently separated in time, which implies that  $k_{SB} \ll k_{BA}, k_{BS}$ .

The temporal development of the fraction of photodissociated proteins  $N(t)$  is given by:

$$N(t) = 1 - N_A(t) = N_B(t) + N_S(t), \quad (1.4)$$

where  $N_A(t)$  is the fraction of ligand-bound protein,  $N_B(t)$  is the fraction of proteins that rebind the ligand geminately and  $N_S(t)$  is the fraction of proteins that rebind the ligand from the solvent. Due to the initial conditions in a flash photolysis experiment, the reaction starts with  $N_A = N_S = 0$ , while  $N_B = 1$ , indicating that immediately after photolysis, all ligands are photodissociated and reside inside the protein. From the protein matrix, they can either rebind directly to the heme iron or escape into the solvent. The recombination process can be described by two exponential decays:

$$N(t) = N_B \cdot e^{-\lambda_B t} + N_S \cdot e^{-\lambda_S t}, \quad (1.5)$$

where  $N_B$  represents the fraction of proteins that rebind geminately and  $N_S$  denotes the fractions of proteins that rebinds the ligands from the solvent. The amplitudes are given by

$$N_B = \frac{k_{BA}}{k_{BA} + k_{BS}} \quad (1.6)$$

and

$$N_S = \frac{k_{BS}}{k_{BA} + k_{BS}}. \quad (1.7)$$

The apparent rate coefficients are given by

$$\lambda_B = k_{BA} + k_{BS} = \frac{k_{BA}}{N_B} \quad (1.8)$$

and

$$\lambda_S = k_{SB} \cdot N_B = k_{SB} \frac{k_{BA}}{k_{BA} + k_{BS}} = k_{BA} \frac{k_{SB}}{k_{BS}} \frac{k_{BS}}{k_{BA} + k_{BS}}. \quad (1.9)$$

$\lambda_B$  represents the depletion of the intermediate state B. This apparent rate coefficient is independent of the ligand concentration because the identical ligand that was initially photolyzed rebinds to the heme iron of the protein. In contrast, the apparent rate coefficient,  $\lambda_S$ , describing the bimolecular rebinding from the solvent, is dependent on both, the ligand concentration in the solvent and the protein concentration.

If the concentration of one reactant will not change appreciably as the reaction proceeds, the reaction can be considered being a pseudo-first order reaction. Experimentally, this condition is provided by using one reactant in excess so that its concentration will remain essentially constant in comparison to the concentration of the second reactant. In our flash photolysis experiments, the concentration of the ligand ( $[CO] = 1 \text{ mM}$ ) in the solvent is much larger than the protein concentration ( $[hIDO] \approx 10 \text{ }\mu\text{M}$ ). Introducing a first order rate coefficient,  $k_{SB} = k'_{SB}[CO]$ , that depends linearly on the ligand concentration, yields the proportionality of the apparent rate coefficient and the CO concentration:

$$\lambda_S \propto [CO]. \quad (1.10)$$

More detailed information about ligand and protein interactions can be found in literature<sup>[2,78–80]</sup>.

## 1.3 Spectroscopy

Spectroscopy is the study of the interaction between electromagnetic radiation and matter. Electromagnetic radiation is described by the concept of wave-particle duality implying the description of radiation as both, a continuous electromagnetic wave and as particles. The energy of a photon, the quantum of electromagnetic interaction, is given by

$$E = h\nu \quad \text{and} \quad \nu = c \cdot \tilde{\nu} = \frac{c}{\lambda}, \quad (1.11)$$

where  $E$  is the energy of the photon,  $h$  is the Planck's constant and  $\nu$  is the frequency.  $\nu$  is given by the speed of light,  $c$ , and the wavenumber,  $\tilde{\nu}$ . Alternatively to the wavenumber,  $\tilde{\nu}$ , radiation is often described by the wavelength,  $\lambda$ , which is connected to the wavenumber by  $\tilde{\nu} = \frac{1}{\lambda}$ . As seen from Equation 1.11, the energy of radiation is proportional to its frequency and the wavenumber and inverse proportional to the wavelength.

The spectrum of electromagnetic radiation extends from waves with wavelengths of  $> 1$  km up to  $\gamma$ -rays with wavelengths smaller than  $10^{-11}$  m (Figure 1.5). In between, we find radio waves (1 m - 10 km), infrared (IR) radiation (780 nm - 1 mm), visible (Vis) and ultraviolet (UV)-light (380 - 780 nm and 1 - 380 nm) and x-rays (10 pm - 1 nm). Various experimental methods utilize radiation of different wavelength to study biological molecules. X-ray diffraction studies obtain structural information on the atomic level of molecules requiring crystallization of the molecule. UV/Vis, IR and nuclear magnetic resonance spectroscopy provide information of the structure and dynamics of proteins.

In this work, UV/Vis and IR spectroscopy are used to study the interaction between protein, ligand and substrate. The observation of changes in the absorbance of the prosthetic heme group of the protein via UV/Vis spectroscopy and changes of the stretching vibration of the ligand CO via IR spectroscopy are used complementarily.

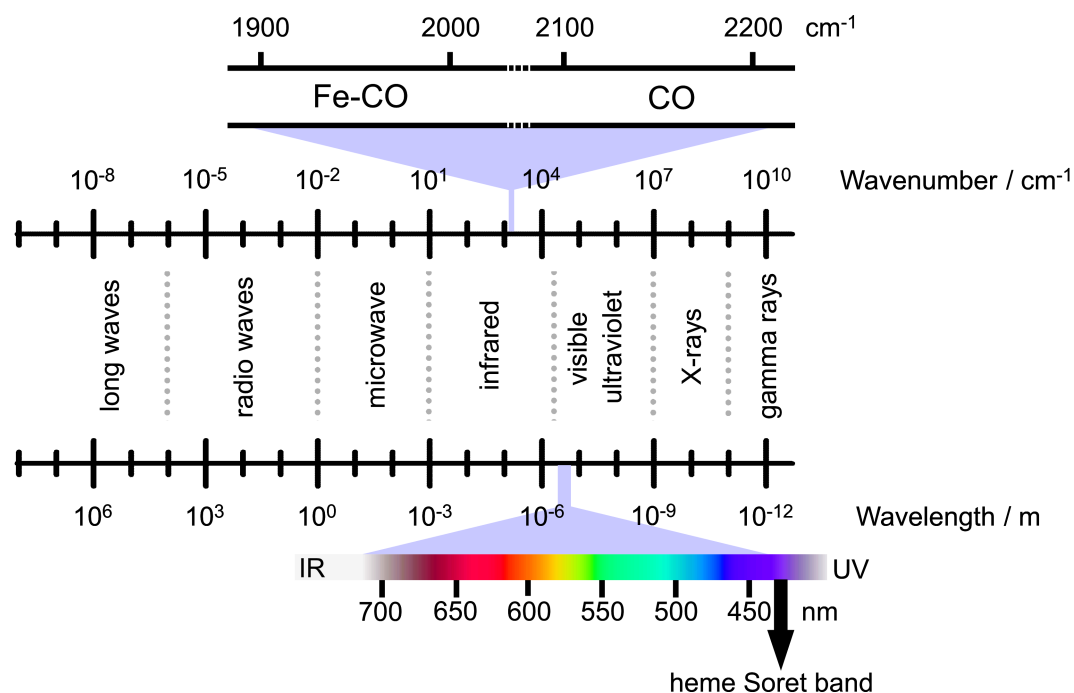


Figure 1.5: Electromagnetic spectrum. The spectral absorbance range of heme-bound and gaseous CO (Fe-CO and CO) as well as the absorbance region of the heme Soret band are highlighted.

The absorption of radiation is measured as a function of its frequency or wavelength. The wavelength-dependent absorbance,  $A(\lambda)$ , is given by Lambert-Beer's law,

$$A(\lambda) = \log\left(\frac{I_0}{I}\right) = \varepsilon(\lambda)cl, \quad (1.12)$$

which describes the logarithmic dependency between the transmission  $T$  and the absorbance  $A$  that holds true for homogenous samples. In Equation 1.12,  $I_0$  is the incident light intensity striking the sample, whereas  $I$  describes the light intensity after passing a sample with a concentration  $c$  and a path length  $l$ .  $\varepsilon(\lambda)$  is the wavelength-dependent extinction coefficient with the unit [M<sup>-1</sup>cm<sup>-1</sup>]. With the concentration in [M] and the path length  $l$  in [cm] the absorbance  $A$  is unitless. Sometimes, a pseudo unit 'optical density' [OD] is used.

### 1.3.1 Principle of UV/Vis Spectroscopy

Light in the UV/Vis spectral range interacts with the electrons of a chromophore. The valence electrons of an atom determine the formation of a chemical bond. The interaction between the atomic orbitals give rise to formation of molecular orbitals, representing regions in a molecule where an electron is likely to be found. Molecular orbitals are separated into binding ( $n$ ,  $\sigma$  and  $\pi$ ) and non-binding orbitals ( $\sigma^*$ ,  $\pi^*$ ). In the non-excited state of a molecule, the ground state, the electrons populate the lower lying orbitals, typically the binding orbitals. By the interaction of a photon with an electron, the photon can be absorbed and transfers the electron into a higher lying, often a non-binding orbital (Figure 1.6 a). The molecule is in its excited state. One requirement for photon absorption is that the photon energy equals the energetic difference between the ground state and the excited state of a molecule and, thereby, fulfils the resonance condition between these two states of the chromophore.

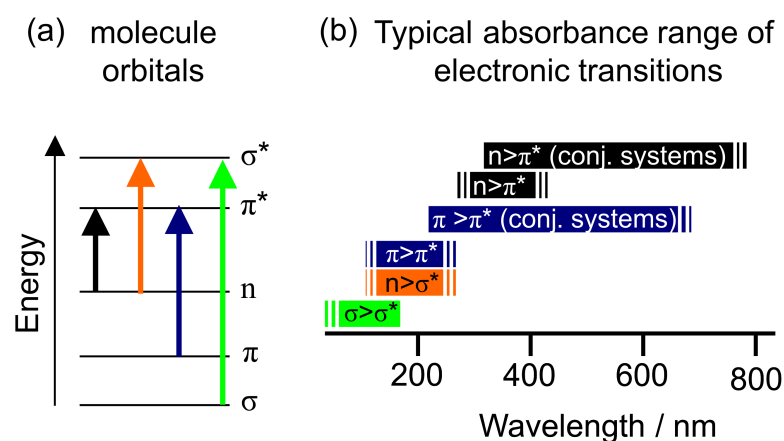


Figure 1.6: Electronic transitions observed by UV/Vis spectroscopy. (a) Electronic transition between the different molecule orbitals. (b) Absorbance ranges of the different electronic transitions<sup>[81]</sup>.

The energy difference between the two molecular orbitals determines the absorbed energy and, therefore, the absorbance spectrum.  $\sigma \rightarrow \sigma^*$  and  $n \rightarrow \sigma^*$  transitions absorb light in the low UV range<sup>[82]</sup>.  $\pi \rightarrow \pi^*$  transition can be observed in the high UV range. The more pronounced the delocalization of a  $\pi$  system, the more the absorbed energy shifts to the visible range (Figure 1.6 b). In addition, low d-d transition bands, based on the excitation of an electron in a d-orbital of a metal to another d-orbital of higher energy, and charge transfer bands, caused by the transition of an electron from a metal orbital into an empty ligand orbital, are observed in the visible range.

The molecular structure of a chromophore and its local environment determine the energies of particular molecular orbitals and thus the absorption properties. Changes in the structure and/or the environment of the chromophore will affect the energy levels and thus the absorption properties of the system.

### 1.3.2 UV/Vis Spectroscopy of Proteins

Proteins exhibit absorbance bands in the UV/Vis spectral range, which arise from light absorption by the peptide bonds, the amino acid side chains and the prosthetic groups.

For the peptide bond, the energetically lowest transition ( $n \rightarrow \pi^*$ ) is observed at 210 to 220 nm, whereas the  $\pi \rightarrow \pi^*$  transition shows an absorbance band at 190 nm. The conjugated  $\pi$  systems of the aromatic amino acids W, Y and F absorb between 230 and 300 nm, with W exhibiting the highest extinction coefficient. The absorbance bands of the aromatic amino acids are often utilized to determine the protein concentration.

Biochromophores with a conjugated  $\pi$  electron system, in which the electrons are delocalized over the whole system, typically absorb in the visible region. The higher the degree of delocalization, the more the absorbance shifts to longer wavelengths. In the green fluorescent protein, GFP, the chromophore is autocatalytically formed from a part of the polypeptide chain (residues S-Y-G)<sup>[83]</sup>. More often, the absorption in the visible region is related to prosthetic groups such as porphyrines, carotenoids or flavins.

Heme proteins exhibit a typical absorbance spectrum based on  $\pi \rightarrow \pi^*$  transitions of the heme prosthetic group. The most prominent absorbance band is the Soret band at  $\approx 400$  nm. Further bands are the Q bands, also denoted as  $\alpha$  and  $\beta$  bands, which are found at  $\approx 550$  nm. The absorbance bands are sensitive to the oxidation and the ligation states of the heme iron. Additionally, changes in the environment of the heme group, for example, induced by the formation of hydrogen bonds to the propionate groups of the heme, can cause changes in the absorbance bands. Figure 1.7 shows UV/Vis spectra of hIDO in different oxidation and ligation states. Met hIDO denotes the protein with the heme iron in the oxidized state ( $\text{Fe}^{3+}$ ) and with a water molecule bound to the heme iron (black line). The absorbance spectrum of met hIDO exhibits a Soret band at 404 nm, Q bands at 499 and 533 nm and a heme charge-transfer band at 633 nm. The absorbance band observed in the UV range of the spectrum is due to the aromatic amino acid side chains. Deoxy hIDO (blue line) with the heme iron in the reduced state ( $\text{Fe}^{2+}$ ) exhibits a Soret band at 429 nm. The absorbance spectrum of CO-ligated hIDO, hIDO-CO, shows a Soret band at 420 nm and Q bands at 538 nm ( $\beta$  band) and 570 nm ( $\alpha$  band).

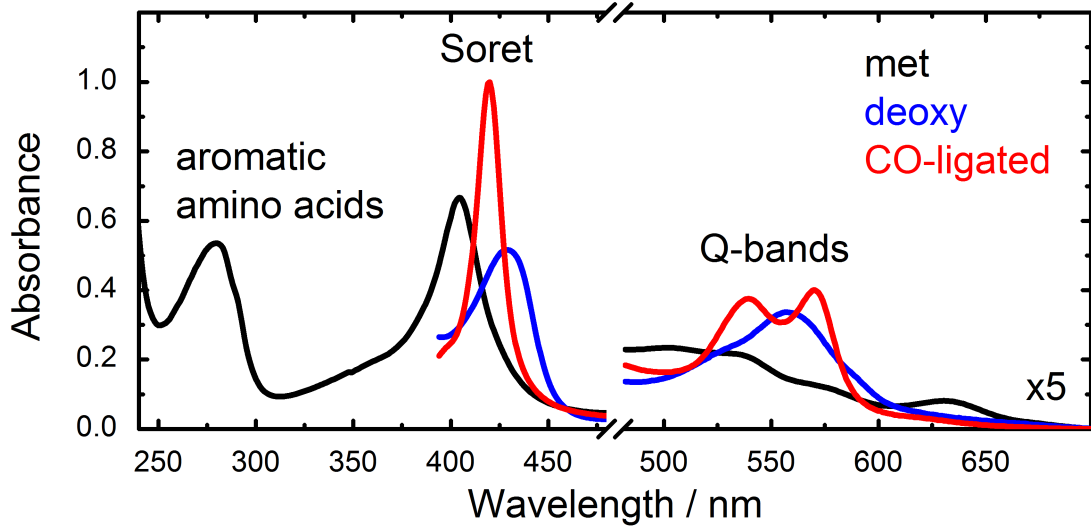


Figure 1.7: UV/Vis spectra of hIDO in different oxidation and ligation states, met hIDO (black), deoxy hIDO (blue) and CO-ligated hIDO (red).

### 1.3.3 IR Spectroscopy

Light in the IR region of the electromagnetic spectrum excites vibrations in a molecule. In a first approximation, the vibration of a bond in a diatomic molecule can be described by the model of a harmonic oscillator with a frequency  $\nu$ ,

$$\nu = \frac{1}{2\pi} \sqrt{\frac{k}{\mu}}. \quad (1.13)$$

Here,  $k$  is the force constant of the bond and  $\mu$  is the reduced mass of the molecule, given by

$$\mu = \frac{m_1 m_2}{m_1 + m_2} \quad (1.14)$$

with  $m_1$  and  $m_2$  representing the masses of the two atoms.

The potential energy,  $V$ , as a function of the interatomic distance  $R$  depends on the equilibrium bond length,  $R_e$ , and the force constant of the bond,  $k$ :

$$V(R) = \frac{1}{2} k (R - R_e)^2. \quad (1.15)$$

As apparent from Equation 1.15, the potential energy is described by a parabola (dotted line in Figure 1.8). However, the actual potential energy of a diatomic molecule deviates from the function of a parabola. Its potential energy is better

described by the Morse potential (solid line in Figure 1.8), which implies that the repulsion of two atoms at internuclear distances below  $R_e$  increases stronger than in an harmonic oscillator. Additionally, it includes that, with increasing distance between the two atoms, the potential energy approaches a level where the two atoms dissociate.

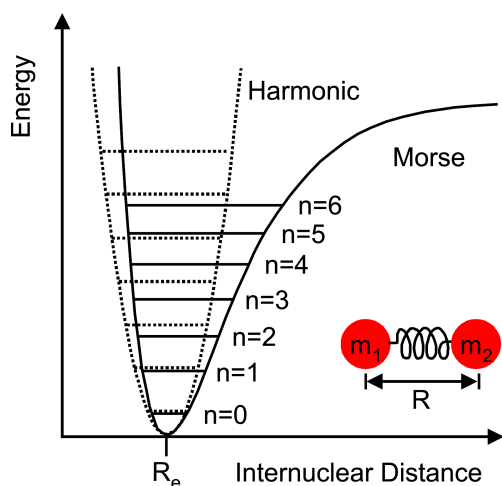


Figure 1.8: Molecular potential energy curves for a diatomic molecule.

According to the rules of quantum mechanics, a transition from the ground to an excited vibrational state occurs upon absorption of a photon, if its energy coincides with the energy difference between the ground and the excited vibrational state. For a harmonic oscillator, the energy levels  $E_n$  are given by

$$E_n = \left(n + \frac{1}{2}\right)h\nu, \quad (1.16)$$

where  $\nu$  is the frequency of the vibration,  $h$  is Plank's constant and  $n = 0, 1, 2, \dots$  is the quantum number representing the energy levels. The selection rule demands  $n$  to be  $\Delta n = \pm 1$ . For the transition to be IR active the molecular dipole moment has to change.

For a simple harmonic oscillator, the spacing between the vibrational levels is constant. In the Morse curve, the spacing between the vibrational levels becomes smaller with higher energies. The dominant transitions from the vibrational ground state to the first excited state, are called first harmonics.

### 1.3.4 IR Spectroscopy of Proteins

Vibrational spectroscopy of proteins, including IR and Raman spectroscopy, can provide information on the secondary structure of proteins, the structure and environment of amino acid side chains or the binding of ligands to a protein. However,

the vibrational spectrum of proteins exhibits a superposition of multiple absorbance bands. Therefore, the assignment of these bands is not unambiguous. Methods such as isotope labeling and site-directed mutagenesis are applied to assign the different bands.

Characteristic bands of polypeptides are the amide bands, which are sensitive to the secondary structure of the protein. The amide I band ( $\approx 1650\text{ cm}^{-1}$ ) is used to elucidate the secondary structure of proteins. It arises primarily from the stretch vibration of the backbone carbonyl of the polypeptide<sup>[84]</sup>. In Mb that has 70 - 80%  $\alpha$ -helix and 20 - 30% unordered structures, Dong et al.<sup>[85]</sup> found a strong amide I band at  $1654\text{ cm}^{-1}$ . Proteins with mostly  $\beta$ -sheets such as immunoglobulin G, show amide I bands at  $\approx 1633$  and  $\approx 1684\text{ cm}^{-1}$ <sup>[86]</sup>. The amide II band ( $\approx 1550\text{ cm}^{-1}$ ) reflects the NH in-plane bending in combination with the C-N stretching vibration of the protein backbone<sup>[84]</sup> and can also be used for secondary structure predictions<sup>[87]</sup>.

### 1.3.5 Using CO as a Probe

The observation of distinct vibrational bands of ligands can provide information about structural changes in a protein. The stretching vibration of CO is a sensitive gauge to probe the active site and the protein matrix of heme proteins. Gaseous CO absorbs at  $2143\text{ cm}^{-1}$ , a region where triple bonds absorb that are rare in proteins. The protein environment modulates the electron density of the CO bond and, therefore, changes the stretching vibration of the ligand. The absorbance bands of CO residing in the protein matrix, the photoproduct bands, are found between  $2090$  and  $2160\text{ cm}^{-1}$ . Heme-bound CO absorbs between  $1870$  and  $2000\text{ cm}^{-1}$  (Figure 1.5). It was shown that the IR spectrum of heme-bound CO can be sensitive towards changes of pH, temperature and the structure in close vicinity of the ligand<sup>[88-90]</sup>.

CO binds covalently to the ferrous heme iron. The formation of a covalent bond of a  $\pi$ -conjugated ligand to a transition metal includes two synergetic processes, electron donation and the back-bonding process<sup>[91]</sup>. In the case of the Fe-CO complex, (1) the electron donation from the  $5\sigma$  orbital of CO into the empty  $d_z$  orbital of the iron and (2) the  $\pi$  back-bonding, where the  $3d\pi$  orbital of the iron overlaps with the anti-bonding  $\pi^*$  orbital of the ligand, result in the decrease of the bond order of the ligand and, consequently, in a decrease of the CO stretching frequency.

Polar residues in close vicinity to the Fe-CO complex change the electron density in the environment of the bound CO, influencing electron donation or electron withdrawal and lead to changes in the back-bonding effect (Figure 1.9)<sup>[92,93]</sup>. A positive charge in the vicinity of the oxygen atom of the heme-bound CO molecule attracts electron density towards the ligand, causing a decrease in the  $\sigma$ -donation and an increase in back-bonding. The bond order of CO is decreased and the frequency  $\nu_{\text{C-O}}$  shifts towards lower values. Simultaneously, the frequency of the Fe-C bond vibration ( $\nu_{\text{Fe-C}}$ ) increases. Vice versa, a negative charge in close vicinity of the oxygen atom results in an increase in bond order of the ligand and, consequently, a frequency shift towards higher values is observed. The frequency of the Fe-C bond,  $\nu_{\text{Fe-C}}$ , decreases. This inverse correlation between the stretching frequency  $\nu_{\text{C-O}}$  and  $\nu_{\text{Fe-C}}$  of the Fe-CO complex that is owed to the back donation of the heme iron<sup>[94,95]</sup> was observed in many heme proteins<sup>[96-99]</sup>. The sensitivity of the stretching vibration of heme-bound CO to its environment makes CO a perfect probe to observe changes at the active sites of heme proteins.

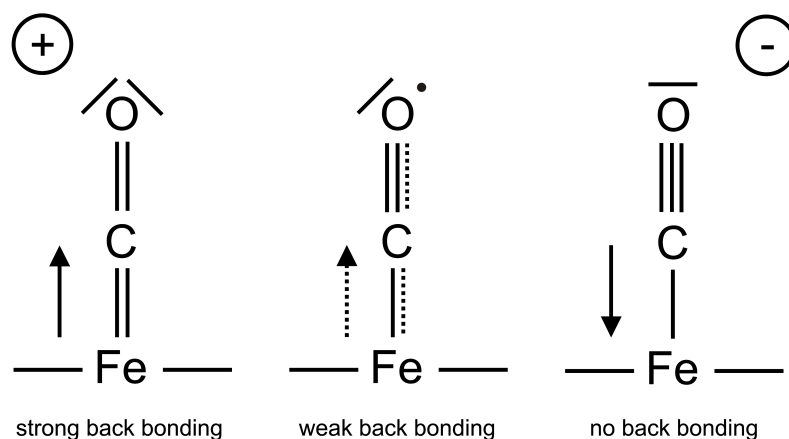


Figure 1.9: Back-bonding

## 1.4 Outline of the Work

In this chapter, the heme protein hIDO was introduced, and its function, the reasons for its relevance in medicine and its structure were briefly discussed. Using Mb as an example, the basics of ligand binding in heme proteins were explained, followed by the theoretical background of UV/Vis and IR spectroscopy and its application in protein research. We have presented the C-O stretching band as a sensitive marker in the IR region of the electromagnetic spectrum.

The second chapter describes the procedures of site-directed mutagenesis, protein expression and purification as well as the sample preparation. The methods of UV/Vis spectroscopy, flash photolysis, Fourier Transform InfraRed (FTIR) spectroscopy and Temperature-Derivative Spectroscopy (TDS) will be introduced.

In the Chapters 3 to 6 we describe and briefly discuss the experimental results. In Chapter 3, experiments are shown, in which we used heme-bound CO to probe the active site structures of CO-ligated hIDO (hIDO-CO). UV/Vis and IR spectra of hIDO-CO and L-Trp-bound hIDO-CO (hIDO-CO/L-Trp) were compared to elucidate changes in the active site structure of hIDO generated by the binding of L-Trp. To identify the amino acids involved in substrate binding, the UV/Vis and IR spectra of selected hIDO variants with and without L-Trp were compared with spectra of wildtype (wt) hIDO. These studies were complemented by binding studies with different L-Trp analogues to wt hIDO and some variants. Subsequently, we utilized the CO ligand to probe transient ligand docking sites in the protein matrix of hIDO (Chapter 4). Using FTIR spectroscopy and TDS, the effect of the substrate binding to hIDO on the accessibility of these sites was analyzed. In Chapter 5, results obtained by isothermal kinetic measurements at different temperatures are shown. FTIR and UV/Vis spectroscopy measurements were used to follow ligand and substrate migration as a function of time and concentration. Chapter 6 focuses on spectroscopic and kinetic measurements at room temperature. The influence of L-Trp and some L-Trp analogues on ligand recombination from the solvent were analyzed in detail.

The last chapter summarizes the results. They are discussed with respect to the latest results in research.

The thesis ends with the appendix, including a list of primers, the structures of L-Trp and L-Trp analogues used in the work, the applied fitting functions and the bibliography.



# Chapter 2

## Materials and Methods

### 2.1 The Vector Coding for hIDO

The chromosomal DeoxyriboNucleic Acid (DNA) of hIDO was inserted into the vector pET-15b (Novagen, Darmstadt, Germany) carrying an N-terminal hexahistidinetag (His-tag) sequence and an ampicillin resistance. This construct was kindly provided by Dr. Hiroshi Sugimoto (Biometal Science Laboratory, Harima Institute, Hyogo, Japan). A map of the expression region of the pET-15b-hIDO construct is shown in Figure 2.1.

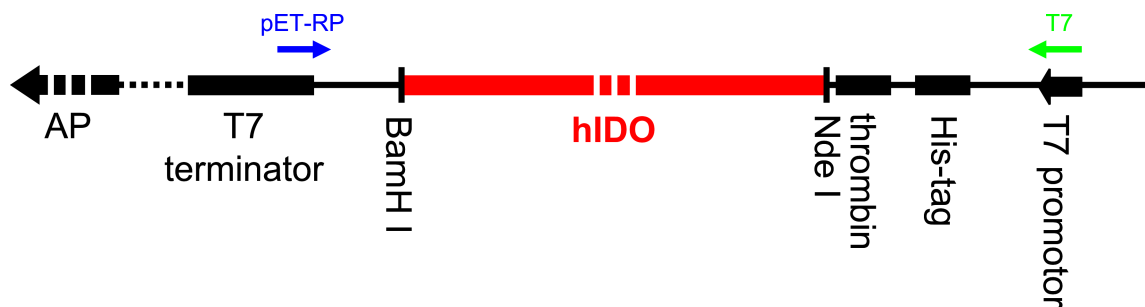


Figure 2.1: Expression region of the pET-15b-hIDO vector construct containing restriction sites BamHI and Nde I, an ampicillin resistance (AP), a T7 promoter and terminator region and coding regions for thrombin and His-tag. The two primer regions used for sequencing are marked by pET-RP and T7.

## 2.2 Mutagenesis

Mutants of hIDO were produced by site-directed mutagenesis. The polymerase chain reaction was carried out on the pET-15b-hIDO vector using custom designed primers. Oligonucleotides were ordered from biomers.net (Ulm, Germany). The sequences of the primers are listed in Table A.1 (Appendix A). The table contains only the forward primers; the reverse primers are complementary. Bases that code for the mutated amino acids are marked in red.

To introduce a point mutation into the gene of interest, the double stranded template DNA (approx. 40 ng) and two complementary primers (each approx. 125 ng) that carry the mutation were mixed with 5  $\mu$ l of *Pfu* DNA polymerase 10x reaction buffer (Promega Corporation, Madison, USA) and an excess of a nucleoside triphosphate mix (200  $\mu$ M) (Promega Corporation, Madison, USA). Amplification was achieved by a temperature cycle protocol. In a first step, the plasmid template was denatured to single stranded DNA by a temperature increase to 95°C. During the first cycle, 1  $\mu$ l of 2-3 u/ $\mu$ l *Pfu* DNA polymerase (Promega Corporation, Madison, USA) was added to the preheated reaction assay. Subsequently, a temperature decrease to 55°C for 1 min allowed the primers to anneal to their complementary DNA sequences of the single stranded template DNA. Primers were elongated at 75°C for 7.5 min. This cycle of denaturation, annealing and elongation was repeated 15 – 20  $\times$  using a thermocycler Mastercycler personal (Eppendorf, Hamburg, Germany). For each particular primer pair, temperatures and times were adjusted. To obtain only the plasmids that host the introduced mutation, the original vector DNA was digested by the DpnI restriction enzyme (Promega Corporation, Madison, USA)(10 u/ $\mu$ l). This enzyme recognizes methylated double stranded DNA sequences and cleaves the plasmid at these sites.

For multiplication of the recombinant DNA, the plasmid carrying the gene coding for hIDO was transformed into competent *E. coli* XL1 blue cells (Stratagene, Santa Clara, USA). A mixture of 1 ng of the pET-15b-hIDO construct and 200  $\mu$ l of competent cells were incubated on ice for 20 – 30 min. A heat shock at 42°C for 45 s caused uptake of the DNA. Cells were put back on ice for 5 min. 900  $\mu$ l of 2YT-medium (10 g/l yeast extract, 16 g/l tryptone, 10 g/l sodium chloride (NaCl)) was added and the cell suspension was shaken for 1 h at 37°C. Subsequently, 50  $\mu$ l of the cell solution were streaked on 2YT agar plates containing 75  $\mu$ g/ $\mu$ l ampicillin and incubated overnight at 37°C. One colony was selected from the plate and transferred to a sufficient volume of 2YT medium containing 75  $\mu$ g/ $\mu$ l ampicillin. The cells were shaken overnight at 220 rpm and 37°C.

The plasmid DNA was isolated using the Wizard Plus SV Minipreps DNA Purification System from Promega Corporation (Madison, USA). The DNA concentration was determined by the absorbance at 260 nm. To verify the insertion of the

mutation, the isolated plasmid was sent to GATC Biotech (Konstanz, Germany) for sequencing. Either the T7 or the pET-RP primer were chosen as sequencing primers. The positions of the primers are marked by green and blue arrows in Figure 2.1.

## 2.3 Expression and Purification

The described expression protocols were slightly modified<sup>[100–102]</sup>. The expression strain used for hIDO and its mutants was *E. coli* BL21 (Stratagene, Santa Clara, USA). Transformation was performed as described for the *E. coli* XL1 blue cells (Chapter 2.1). The cells containing the pET-15b vector hosting the wildtype (wt) or the mutant protein sequence were precultured in 100 ml 2YT-medium containing 50 mg/l ampicillin. Cultures were incubated overnight at 37°C and 220 rpm. The cells were added to a fresh medium (usually 9 l; 6 × 1,5 l) containing 50 mg/l ampicillin and 50 mg/l L-tryptophan and were grown at 37°C and 160 rpm to an optical density of 0.9 at 600 nm. The cell cultures were then cooled to 30°C and 2 ml/l of both 0.5 M ethylenediaminetetraacetic acid solution and 3.5 mM hemin dissolved in 10 mM NaOH were added. Subsequently, the bacterial cultures were shaken at 27°C and 160 rpm for ≈ 15 min before induction by 1 mM isopropyl beta-D-1-thiogalactopyranoside. The cells were grown to an absorbance of ≈ 3 OD at 600 nm. Cells were collected by centrifugation for 20 min at 5,100 rpm and 4°C (Sigma 4-16K, Rotor 11150). The cell pellet was stored at −20°C.

At 4°C, cells were lysed and protein was purified. The cell pellet was resuspended in binding buffer I (50 mM potassium phosphate buffer (KPB), pH 7, 300 mM NaCl, 20 mM imidazole and 20 mM mercaptoethanol) at a ratio 1:1 (vol/vol). After adding protease inhibitor following the manufacturer's instruction (Roche, Grenzach-Wyhlen, Germany) and 1 mg/ml lysozyme (Roche, Grenzach-Wyhlen, Germany), the cells were ruptured by sonication with a Brandelin electronic sonifier (Berlin, Germany). To prevent overheating, the cell suspension was put on ice for 4 min after each 2-min sonication step (total sonification time: 1 min/ml cell suspension). Subsequently, the lysis solution was centrifuged for 20 min at 20,000 rpm and 4°C (Sigma 3-30K, Rotor 19776-H). The supernatant was thoroughly mixed for 30 min with Nickel (Ni)-Sepharose<sup>TM</sup> 6 Fast Flow (GE Healthcare, Little Chalfont, UK) that had been equilibrated with binding buffer I. A column was loaded with the hIDO-bound Ni-Sepharose and washed with binding buffer II containing 50 mM KPB, pH 7, 300 mM NaCl, 50 mM imidazole and 20 mM mercaptoethanol until the absorbance at 280 nm and 260 nm had decayed to zero. The protein was eluted with elution buffer (50 mM KPB, pH 7, 300 mM NaCl, 500 mM imidazole, 20 mM mercaptoethanol). Appropriate fractions of purified protein were pooled and concentrated in a Vivaspin 20 ultrafiltration spin column (Satorius Stedim biotech, Aubagne, France) at 7,600 rpm at 4°C (Sigma 3-30K,

Rotor 19776-H). After concentration, the buffer was exchanged to 100 mM KPB, pH 7, using a NAP<sup>TM</sup> 10 Column (Sephadex<sup>TM</sup>, Little Chalfont, UK). Imidazole-free protein fractions were collected and concentrated again as described above. Smaller volumes of protein were concentrated with Nanosep 10K/30K Omega centrifugal devices (Pall Life Science, Port Washington, USA). The purity of the protein was controlled by the ratio of the absorbance at the Soret peak at 404 nm (ferric hIDO) and the absorbance at 280 nm.

The protein was stored at  $-80^{\circ}\text{C}$  either in 100 mM KPB, pH 7, after freezing the sample rapidly in liquid nitrogen or in 55%/45% (vol/vol) glycerol/100 mM KPB, pH 7.

## 2.4 Absorbance Spectroscopy

### 2.4.1 UV/Vis Spectroscopy

UV/Vis spectroscopy is a convenient method to determine the concentration of organic compounds and biological macromolecules. The concentrations of the substrate stock solutions of L- and D-Trp ( $\epsilon_{280} = 5,502 \text{ M}^{-1}\text{cm}^{-1}$ ), 3-(Thianaphthen-3-yl)-L-alanine (S-Trp) ( $\epsilon_{289} \approx 2,694 \text{ M}^{-1}\text{cm}^{-1}$ ) and MLT ( $\epsilon_{286} \approx 5,470 \text{ M}^{-1}\text{cm}^{-1}$ ) were inferred from the absorption at the 280, 289 and 286 nm, respectively. The absorption was measured with a commercial dual-beam spectrometer Varian Cary 100 Scan (Agilent Technologies, Santa Clara, USA). The spectrometer was also used for determining the concentration and purity of hIDO ( $\epsilon_{404} = 172 \text{ mM}^{-1}\text{cm}^{-1}$ ) and its mutants<sup>[102]</sup>.

By default, spectra of the samples used for flash photolysis and FTIR spectroscopy were measured before data collection to verify the concentration and the coordination state of the heme.

Spectra at cryogenic temperatures were measured with a modernized Cary 14 from On-Line Instrument Systems (Borgart, USA) with a resolution of 1 nm. Samples were photolyzed with a Xenon Lamp (75 W).

Unless stated differently, samples for UV/Vis spectroscopy and flash photolysis measurements were prepared as described in Chapter 2.4.1.1.

#### 2.4.1.1 Sample Preparation

100 mM KPB, pH 7, was sealed in a glass cuvette ( $1 \times 1 \times 3 \text{ cm}^3$ ) and equilibrated with CO gas (purity at least 99.97 %). A sodium dithionite solution was prepared under 1 atm CO and diluted in the prepared buffer solution to a final concentration of up to 10 mM. Concentrated protein from a stock solution was added to a final concentration of 10 to 100  $\mu\text{M}$ . For the titration experiments, a substrate solution was prepared in 100  $\mu\text{M}$  KPB, pH 7, and equilibrated with CO gas. The substrate

concentration of the solution was determined based on the UV/Vis absorption spectrum. An increasing volume of this solution was added in steps to the protein sample.

For experiments at cryogenic temperatures, the protein was dissolved in a cryo-solvent (75%/25% (vol/vol) glycerol/400 mM KPB, pH 8) instead of aqueous solvent. After sample preparation, the anaerobic protein solution was sealed in a home-build plastic cuvette ( $10 \times 10 \times 2.5$  mm<sup>3</sup>). The cuvette was fitted into an oxygen-free copper block that was mounted on a cold finger of a closed cycle helium refrigerator cryostat (model 22, CTI Cryogenics, Mansfield, USA). A diver's helmet with quartz windows served as a vacuum shroud. Evacuation of the sample in the shroud permits experiments in the temperature range from 10 to 320 K. The sample temperature was detected by a silicon temperature sensor diode. Sample temperature was regulated with a digital temperature controller (model 330 (flash photolysis setup) or DRC-93CA (Olis 14 setup for UV/Vis spectroscopy), LakeShore Cryotronics, Westerville, USA).

### 2.4.1.2 Time-Resolved Spectroscopy

#### Flash Photolysis System

The protein samples were photodissociated by a 6 ns pulse (full width at half maximum (FWHM)) of a frequency doubled Nd:YAG (neodymium-doped yttrium aluminium garnet) laser (Surelite II, Continuum, Santa Clara, USA). After photolysis, relaxation to the equilibrium state was monitored with light from a tungsten source. The light intensity,  $I(t)$ , at a particular wavelength,  $\lambda$ , was detected as a function of time by a photomultiplier tube (model R 5600U, Hamamatsu Photonics Deutschland GmbH, Herrsching am Ammersee, Germany). The signals from 10 ns to 50  $\mu$ s and from 2  $\mu$ s to 1,000 s were recorded with a digital storage oscilloscope (model TDS520, Tektronix, Beaverton, USA) and with a home-built logarithmic time-base digitizer (Wondertoy II), respectively. The experimental setup was controlled by different LabView programs (LabView release 4, National Instruments, Austin, USA). A scheme of the home-built flash photolysis system is shown in Figure 2.2.

#### Analysis of Flash Photolysis Data

The absorbance change,  $\Delta A(t)$ , as a function of time is calculated as

$$\Delta A(t) = -\log\left(\frac{I(t)}{I(t_{<0})}\right), \quad (2.1)$$

with light intensity,  $I(t)$ , as a function of time and  $I(t_{<0})$  describing the light intensity before the laser flash. 5 to 100 transients were averaged to achieve one kinetic

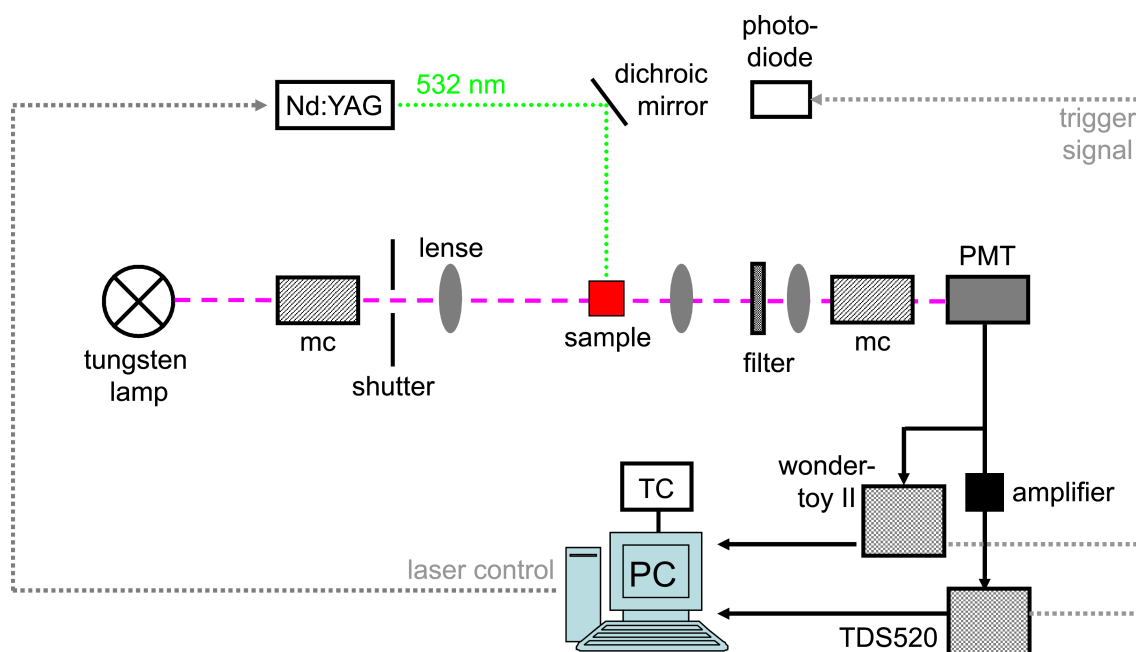


Figure 2.2: Scheme of the flash photolysis system. mc, monochromator; PMT, photomultiplier tube; Nd:YAG, neodymium-doped yttrium aluminium garnet laser; TC, temperature controller. Graphic modified from Nienhaus et al.<sup>[78]</sup>.

trace for each experimental condition. The kinetic traces were fitted with exponential decays (Appendix C). From the time courses at ambient temperature, two parameters could be extracted, describing bimolecular rebinding of the ligand. The fraction of CO that escapes into the solvent is represented by the amplitude  $N_S$ .  $k_{SB}$  describes the rate coefficient for recombination from the solvent.

## 2.5 Fourier Transform Infrared Spectroscopy

### 2.5.1 Sample Preparation

If not stated otherwise, samples for Fourier Transform InfraRed (FTIR) experiments were prepared as follows. The protein dissolved in 53%/47% (vol/vol) glycerol/100 mM KPb, pH 7, was stirred under 1 atm CO for 45 min. Anaerobically prepared sodium dithionite was added in a 10-fold molar excess. Subsequently, the sample was stirred for another 15 min to ensure reduction of the heme iron and CO ligation. The final protein concentration varied between 0.8 and 2 mM. For substrate-saturated conditions, the substrate was added as a solid. To obtain definite substrate concentrations, a substrate stock solution in 100 mM KPb, pH 7,

was equilibrated with CO in the presence of sodium dithionite. An appropriate volume of the stock solution was added to the protein sample and stirred for an additional 15 min. To separate undissolved substrate and aggregated protein, the sample solution was centrifuged for 15 min at 5,000 rpm (Hettich Zentrifugen EBA 12, Tuttlingen, Germany). 1 to 2  $\mu\text{l}$  of the protein solution were loaded into the sample holder.

The sample holder composed of an oxygen-free high conductivity copper block enclosed two calcium fluoride windows, which are separated by a 75  $\mu\text{m}$  thick Mylar spacer; the sample is sandwiched in between the two windows.

### 2.5.2 Setup for Infrared Cryospectroscopy Measurements

The sample holder was mounted on the cold finger of a closed-cycle helium refrigerator (model SRDK-205AW, Sumitomo, Tokyo, Japan). The sample temperature can be regulated between 3 and 320 K by a silicon temperature sensor diode and a digital temperature controller (model 330, Lake Shore Cryotronics, Westerville, USA). The sample was photolyzed by a Green Line Laser MGL-532 (Changchun New Industries opto-electronics Teeh. CO, LTD., Changchun, China) delivering  $\approx 150$  mW output at 532 nm. By a setup of mirrors and a beam splitter, the laser beam was focused onto the sample from both sides (Figure 2.3).

### 2.5.3 The FTIR Spectrometer

The FTIR transmission spectra were measured with an IFS 66v/S FTIR spectrometer from Bruker (Karlsruhe, Germany) at a resolution of 2  $\text{cm}^{-1}$ . Spectra in the mid-infrared range were recorded with an indium antimonide (InSb) detector (detection range:  $\approx 1800 - 4000$   $\text{cm}^{-1}$ ). A scheme of the experimental setup is shown in Figure 2.3 a. The heart of the spectrometer is a Michelson interferometer that generates an interferogram (Figure 2.3 b), describing the intensity  $I(x)$  of the IR beam as a function of the position  $x$  of the moving mirror (M2). The measured interferogram can be converted into a transmission spectrum by applying a Fourier transformation.

Polychromatic radiation is emitted by a mid-IR light source and divided by a beamsplitter (BS). One part is directed onto a fixed mirror (M1) while the second part is reflected by M2. The reflected beams interfere before crossing the sample and, subsequently, hitting the detector. In case of a polychromatic light source, the interferogram is characterized by a position of highest intensity, the center burst, and decreasing intensities at either side. The center burst identifies the position of maximal constructive interference where the optical path difference  $\delta$  is zero or, equivalently, the position of M2 is  $x = 0$ . At any other mirror position, only

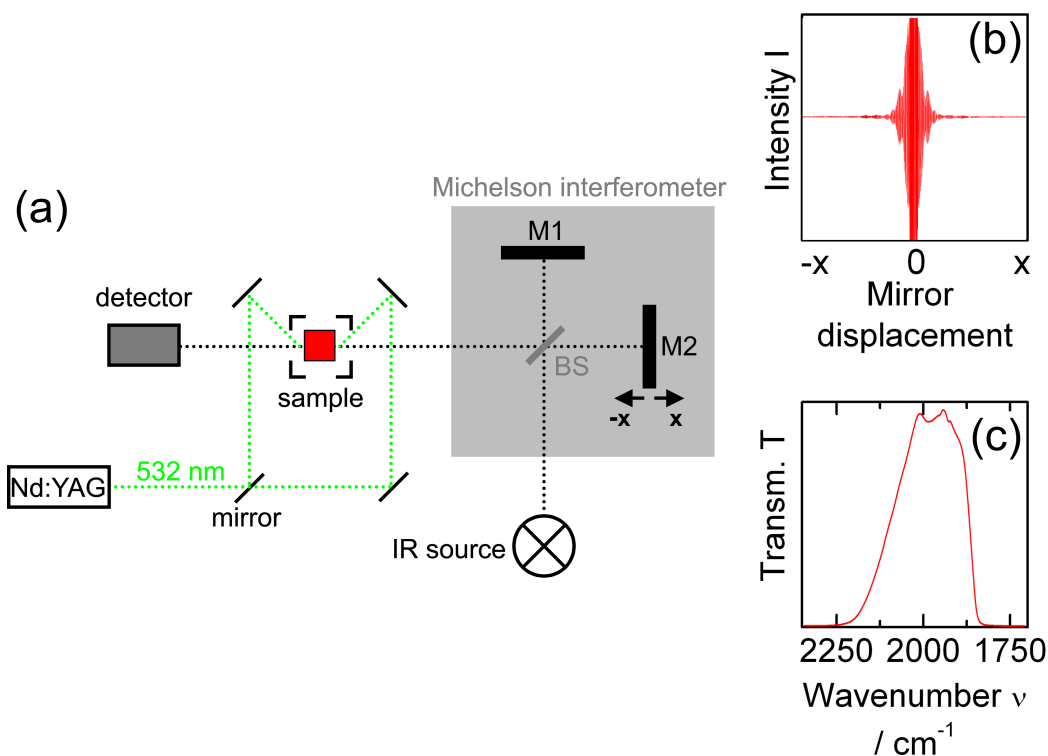


Figure 2.3: (a) FTIR spectroscopy setup. Nd:YAG, neodymium-doped yttrium aluminium garnet laser; M1, fixed mirror, M2, moving mirror; BS, beamsplitter. (b) Interferogram of a polychromatic light source. (c) Calculated transmission spectrum.

a certain wavelength  $\lambda$  equals a multiple of the optical path difference  $\delta$  ( $\lambda = \frac{x}{2}$ ) and, therefore, features constructive interference. If  $\delta$  corresponds to odd integer multiples of  $\frac{1}{2}\lambda$  ( $\lambda = \frac{x}{4}$ ) the beams interfere destructively.

For monochromatic light modulated by the Michelson interferometer, the intensity  $I'(x)$  is described by a periodic cosine shaped function:

$$I'(x) = I^*(\nu)\cos(2\pi\nu x). \quad (2.2)$$

Here,  $x$  is the position of M2.  $\nu$  represents the wavenumber and  $I^*(\nu)$  the intensity of the radiation at wavenumber  $\nu$ .

This characteristic of monochromatic light is used to determine the position  $x$  of mirror M2. A beam of a He/Ne-laser follows the same optical path as the IR beam. A cosine shaped interferogram is detected that serves for internal distance calibration.

Taking into account that a certain fraction of the interfering beam of polychromatic IR light is absorbed by the sample, the overall intensity  $I(x)$  is described as:

$$I(x) = \int_0^{\infty} I(x, \nu) S(\nu) d\nu. \quad (2.3)$$

The term  $S(\nu)$  gives the transmission spectrum after passing the sample. Assuming the interferogram is perfectly symmetric, the transmission spectrum of the sample is obtained by the following inverse Fourier transform:

$$S(\nu) = \text{const.} \int_0^{\infty} [I'(x) - I(0)] \cos(2\pi\nu x) dx. \quad (2.4)$$

A characteristic transmission spectrum of hIDO-CO is shown in Figure 2.3 c. The spectrum was recorded with an InSb detector using a filter absorbing light  $\approx 2100 \text{ cm}^{-1}$  for optimal detection of the signal in the range of the photoproduct bands.

### 2.5.4 FTIR Absorbance Difference Spectra

Absorbance spectra  $\Delta A$  are calculated as the negative logarithm of the ratio of two transmission spectra.  $S_{dark}$  and  $S_{met}$  represent the transmission spectra of ligand-bound and ligand-free protein, respectively. The subtraction of the dark and the met transmission spectra yields the absorbance signal generated by the heme-bound ligand,

$$\Delta A = -\log \left( \frac{S_{dark}}{S_{met}} \right) = \log S_{met} - \log S_{dark}. \quad (2.5)$$

Spectra calculated by this equation will be termed as **FTIR absorbance difference spectra** in this work.

The **FTIR photolysis difference spectrum** is calculated as

$$\Delta A = -\log \left( \frac{S_{light}}{S_{dark}} \right) = \log S_{dark} - \log S_{light}, \quad (2.6)$$

with  $S_{light}$  being the transmission spectrum recorded after photolysis. The difference spectrum displays the absorption changes generated by photolysis.

In a CO-ligated heme protein, the bond between the CO and the heme iron can be broken by light. After photolysis at cryogenic temperatures, the CO is trapped in the protein matrix. Whereas the heme-bound CO gives rise to absorption bands (A bands) in the spectral region between 1870 and 2000  $\text{cm}^{-1}$ , the bands of photodissociated CO (photoproduct bands) are found between 2090 and 2160  $\text{cm}^{-1}$ . The FTIR photolysis difference spectrum displays both, the bands of heme-bound CO and the photoproduct bands. They are presented with negative and positive amplitudes, respectively, indicating the missing CO at the heme iron and the new CO population in the protein matrix.

Typically, the photoproduct bands are much smaller than the bands of heme-bound CO due to their lower extinction coefficient. For better presentation, the absorbance of these bands are multiplied by a factor of 10 if not stated differently.

## 2.5.5 Isothermal Kinetic Measurements

Isothermal perturbation and relaxation experiments monitor absorbance changes in the sample during and subsequent to illumination. During the experiment, the temperature is kept constant. At first, the sample is exposed to illumination by laser light for an extended period of time. A steady state may be achieved. If the photolysis light is switched off, relaxation back to equilibrium might be observed. During illumination and in the dark, FTIR transmission spectra are recorded on a logarithmic timescale. Absorbance difference spectra were calculated as described in Equation 2.6. The reference 'dark' transmission spectrum is recorded immediately before illumination.

## 2.5.6 Temperature Derivative Spectroscopy (TDS)

### 2.5.6.1 Theoretical Background

A non-isothermal approach to study rate processes with distributed enthalpy barriers is Temperature Derivative Spectroscopy (TDS)<sup>[103,104]</sup>. TDS is a temperature ramp protocol that measures relaxation to equilibrium after perturbation as a function of temperature. At first, a non-equilibrium intermediate is introduced by photolysis at low temperatures where relaxation is essentially completely suppressed. Subsequently, the temperature  $T$  is increased linearly with time  $t$  with a rate  $\beta$  (5 or 10  $\frac{\text{mK}}{\text{s}}$ ), starting at an initial temperature  $T_i$  (see Figure 2.4 a),

$$T = T_i + \beta t. \quad (2.7)$$

The photolyzed fraction at time  $t$  is described by  $N(t)$  (Figure 2.4 c). At temperatures below the glass transition temperature, geminate rebinding of ligands is described by a first-order rate process,

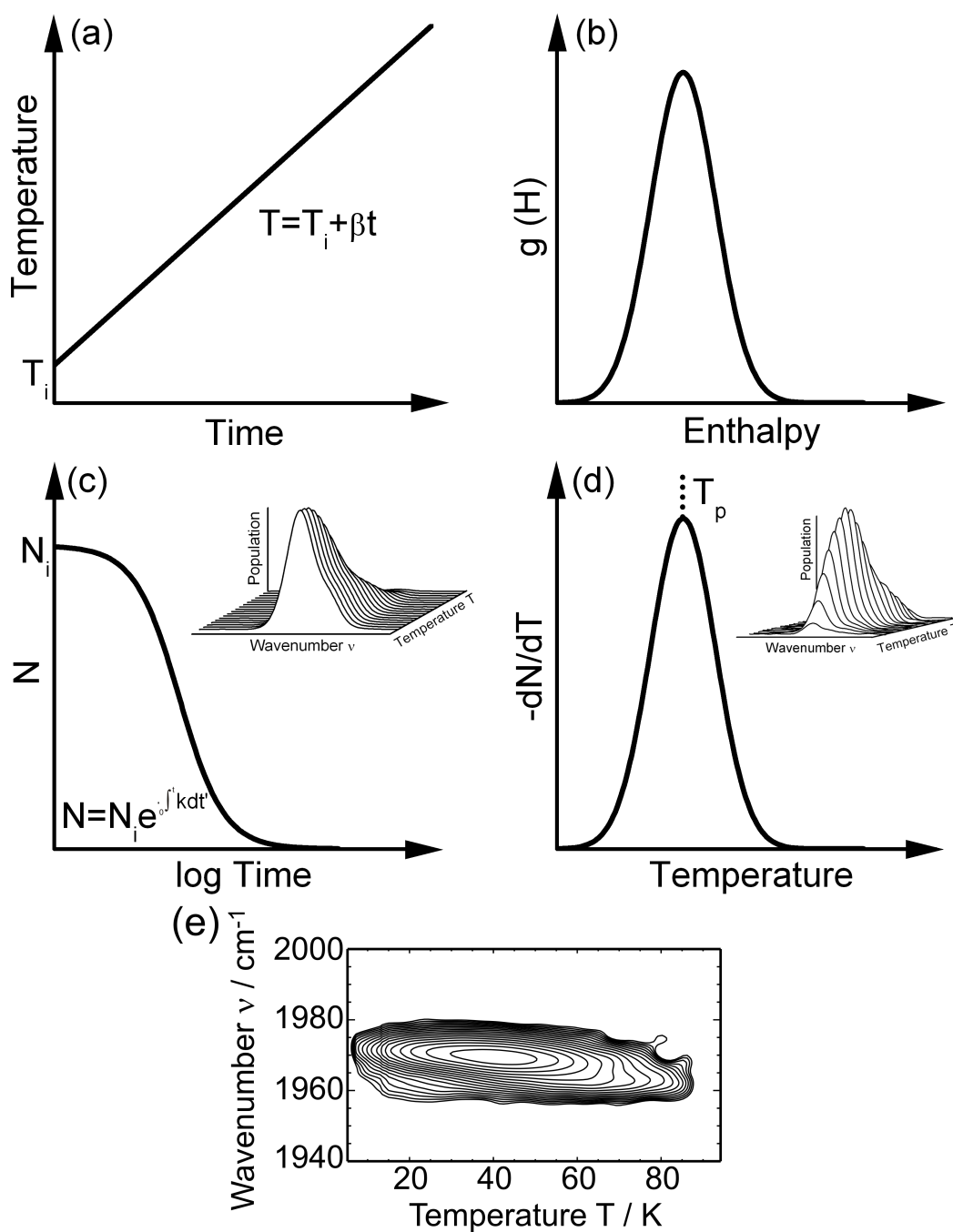


Figure 2.4: Schematic representation of TDS. (a) Linear temperature ramp. (b) Distribution of recombination barriers  $g(H)$ . (c) Time dependence of fraction  $N$  of photolyzed protein. (d) Consecutive differences of  $N(t)$ . (e) TDS data are represented in a contour plot.

$$\frac{dN}{dt} = -kN, \quad (2.8)$$

where  $k$  is the rate coefficient. Solving the differential Equation 2.8 gives the photolyzed population  $N$  describes an exponential decay. The experimental conditions allow the substitution of time  $t$  by the temperature  $T$  according to Equation 2.7:

$$\frac{dN}{dT} = \frac{-N_i}{\beta} \cdot k \cdot e^{-\int_{T_i}^T \frac{k}{\beta} dT'} = \frac{-N_i}{\beta} \cdot k \cdot e^{-\Theta}, \quad (2.9)$$

where  $k \cdot e^{-\Theta}$  is the resolution function. To quantify the integral over temperature,  $\Theta$ , the rate coefficient  $k$  given by the Arrhenius relation can be used:

$$k = A \left( \frac{T}{T_r} \right) e^{\left( \frac{H}{RT} \right)}. \quad (2.10)$$

Here,  $A \left( \frac{T}{T_r} \right)$  is the Arrhenius pre-exponential factor. The term  $\left( \frac{T}{T_r} \right)$  describes a linear temperature dependence with  $T_r$  being the reference temperature set to 100 K.  $R$  denotes the gas constant and  $H$  the activation enthalpy barrier.

Therefore,  $\Theta$  yields

$$\Theta = \frac{AT_r}{\beta} \left[ \left( \frac{T}{T_r} \right)^2 \cdot E_3 \left( \frac{H}{RT} \right) - \left( \frac{T_i}{T_r} \right)^2 \cdot E_3 \left( \frac{H}{RT_i} \right) \right], \quad (2.11)$$

with

$$E_3(x) = \int_1^\infty \frac{e^{(-xt)}}{t^3} dt. \quad (2.12)$$

Equation 2.11 demonstrates the dependence of the resolution of the experiment on the enthalpy  $H$ , the pre-exponential factor  $A$  and the heating rate  $\beta$ . Consequently, the resolution function broadens continuously with temperature. Finally, the distribution of the activation enthalpy barriers,  $g(H)$ , of a protein ensemble has to be considered (Figure 2.4 b),

$$\frac{dN}{dT} = -\frac{N_i}{\beta} \int_0^\infty k e^{(-\Theta)} g(H) dH. \quad (2.13)$$

The term  $dN/dT$  is proportional to the barrier distribution,  $g(H)$ , broadened by the resolution function. Berendzen and Braunstein (1990) showed that the relation between barrier height  $H$  and peak temperature  $T_p$ , the temperature at which  $-dN/dT$  is maximal, is approximately linear for a given Arrhenius factor  $A$  (Equation 2.14)<sup>[104]</sup>. Thus, the temperature axis can be cast into an enthalpy axis.

$$T_p = \frac{H}{R \ln(A\tau_c)}, \quad (2.14)$$

with  $\tau_c$  as the characteristic time for a TDS measurement, which is  $\approx 100$  s for typical parameters of our experiments.

$$\tau_c = \frac{RT_p^2}{\beta(H + RT_p)} \left( \frac{T_p}{T_r} \right). \quad (2.15)$$

### 2.5.6.2 TDS in Application

During a TDS experiment, one transmission spectrum  $S(\nu, T)$  is acquired every Kelvin. In the quantitative TDS analysis,  $dN/dT$  is determined numerically by taking differences between transmission spectra at successive temperatures. The absorbance spectrum,  $A(\nu, T_i)$ , at an initial temperature  $T_i$ , calculated from transmission spectra taken before and after illumination, represents the total photolyzed population,  $N_i$ . With increasing temperature,  $T$ , more and more of the photolyzed species  $N$  recovers to the equilibrium bound state. We assume that the change in the photolyzed population,  $\Delta N$ , is proportional to the change in the integrated absorbance  $\int \Delta A d\nu$ . Absorbance difference spectra are calculated by:

$$\Delta A(\nu, T) = A(\nu, T - \frac{1}{2}K) - A(\nu, T + \frac{1}{2}K). \quad (2.16)$$

The assumption that the change in absorbance,  $\Delta A$ , is proportional to the re-binding population,  $N$ , is not necessarily valid. Both, the bands of heme-bound CO and photodissociated CO may show intrinsic temperature dependences<sup>[105,106]</sup>. The behavior tends to be misinterpreted as recombination. Absorbance differences may also be related to temperature dependent intensity changes or peak shifts.

### 2.5.6.3 Contour Plots - Presentation of the TDS Data

TDS data are presented as two-dimensional contour plots. The absorbance changes,  $\Delta A$ , are plotted on a surface spanned by the temperature ( $T$ ) and wavenumber ( $\nu$ ) axes as shown in Figure 2.4e. Contours are usually spaced logarithmically to enhance small-amplitude features. Solid and dotted lines indicate an absorbance increase and decrease, respectively.

#### 2.5.6.4 Temperature Dependence of Transmission Spectra and TDS

FTIR transmission spectra of hIDO show intrinsic changes in shape and intensity due to variations in temperature. To avoid TDS signals from these intrinsic band changes, absorbance spectra are calculated as shown in Equation 2.6 for each kelvin. Hence, before starting a TDS measurement, reference 'dark' transmission spectra,  $S_{dark}(\nu, T)$ , of the ligated sample were recorded at every kelvin over the whole TDS temperature range. These spectra are used as reference spectra for the TDS transmission spectra,  $S_{light}(\nu, T)$ , collected after illumination. Both the spectra taken before and after illumination exhibit an intrinsic temperature dependence. Therefore, absorbance difference spectra calculated by Equation 2.6 only display the changes due to CO recombination.

An advanced method to compensate for intrinsic temperature-induced band changes at any given temperature is described below. Reference transmission spectra,  $S_{refc}(\nu, T)$ , were calculated by Equation 2.17, where  $S_{light}(\nu, T_i)$  is the transmission spectrum taken at the TDS starting temperature,  $T_i$ , after photolysis.  $S_{dark}(\nu, T)$  gives the temperature-dependent reference transmission spectra recorded at each kelvin before illumination. The fraction of molecules in the photolyzed state at temperature  $T$  are represented by  $x(T)$ .

$$S_{refc}(\nu, T) = x \cdot S_{light}(\nu, T_i) + (1 - x) \cdot S_{dark}(\nu, T). \quad (2.17)$$

According to Equation 2.16 the corrected FTIR absorbance difference spectra  $\Delta A(\nu, T)$  are obtained by:

$$\begin{aligned} \Delta A(\nu, T) &= A(\nu, T - \frac{1}{2}K) - A(\nu, T + \frac{1}{2}K) \\ &= -\log \left[ \frac{S_{light}(\nu, T - \frac{1}{2}K)}{S_{refc}(\nu, T - \frac{1}{2}K)} \right] + \log \left[ \frac{S_{light}(\nu, T + \frac{1}{2}K)}{S_{refc}(\nu, T + \frac{1}{2}K)} \right] \\ &= -\log \left[ \frac{S_{light}(\nu, T - \frac{1}{2}K)}{x \cdot S_{light}(\nu, T_i) + (1 - x) \cdot S_{dark}(\nu, T - \frac{1}{2}K)} \right] + \\ &\quad + \log \left[ \frac{S_{light}(\nu, T + \frac{1}{2}K)}{x \cdot S_{light}(\nu, T_i) + (1 - x) \cdot S_{dark}(\nu, T + \frac{1}{2}K)} \right]. \end{aligned} \quad (2.18)$$

## 2.5. FOURIER TRANSFORM INFRARED SPECTROSCOPY

---

Transmission spectra taken close to the initial temperature  $S_i$  of the TDS measurement are given mainly by the ratio of consecutive transmission spectra.  $x(T)$  is approximately zero. Vice versa, if  $x(T)$  approaches 1 and ligand recombination is almost completed, essentially the 'dark' transmission spectra serve as reference spectra. Between these two extreme cases, the TDS spectra are compensated for temperature dependencies by a linear combination of both terms (Equation 2.18).

### 2.5.7 Illumination Protocols (IPs)

Various illumination procedures at particular temperatures were applied to specifically populate transient ligand docking sites of interest. Figure 2.5 visualizes the IPs including the illumination temperatures and times. Table 2.1 describes the illumination procedures and their purposes.

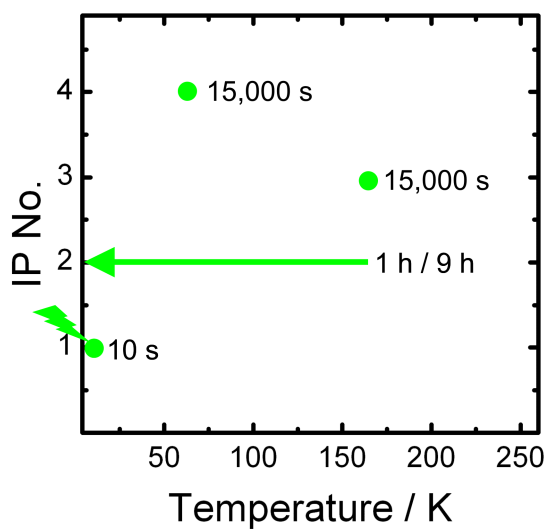


Figure 2.5: Visualization of the applied illumination procedures.

Table 2.1: Applied IPs.

IP No.	description	purpose
1	10 s illumination at 4 K	population of docking sites in close vicinity to the binding site
2	continuous illumination during cooling from 160 - 4 K (cooling time 1 or 9 h)	screening for possible primary and secondary docking sites
3	15,000 s illumination at 160 K	screening for remote docking sites
4	15,000 s illumination at 60 K	selective population of docking site C

## Chapter 3

# Probing the Active Site

hIDO degrades L-Trp to NFK by inserting both atoms of the oxygen molecule into the indole moiety of L-Trp. Therefore, the binding of L-Trp close to the heme-bound O<sub>2</sub> and thus inside the distal heme pocket is necessary. The available crystal structures of hIDO<sup>[55]</sup> reveal an extraordinary large and hydrophobic distal pocket that facilitates L-Trp binding.

For a better understanding of the reaction mechanism of L-Trp conversion and to obtain insight into the substrate specificity of hIDO, a detailed picture of the ternary (protein-ligand-substrate) complex is important. The proper positioning of L-Trp in the distal pocket seems to play a crucial role for efficient conversion of the substrate. Unfortunately, up to date, there is no crystal structure of L-Trp-bound hIDO available and only little information exists about the structure and dynamics of the protein upon binding of ligand and substrate.

To investigate the interactions of the substrate with a ligand-bound protein, the physiological ligand O<sub>2</sub> was replaced by CO in our studies. In the presence of O<sub>2</sub>, L-Trp is subject to permanent conversion, so that at ambient temperature, the observation of the ternary, active complex, in which the enzyme binds ligand and substrate simultaneously, is not possible with steady-state UV/Vis and FTIR spectroscopy.

In this chapter, we utilized CO as an internal gauge to probe the active site structure of hIDO at ambient and cryogenic temperatures. The effect of substrate binding in the distal pocket on the CO stretching bands was observed. Furthermore, we identified amino acids essential for the binding of the substrate using site-directed mutagenesis. The studies were complemented by binding studies with different L-Trp analogues. On the basis of our results we developed a model of the key amino acids in the distal pocket involved in L-Trp binding.

### 3.1 UV/Vis and FTIR Absorbance Spectra at Ambient Temperature

Figure 3.1 a compares the absorbance spectra of CO-ligated hIDO without L-Trp (hIDO-CO) and with L-Trp (hIDO-CO/L-Trp) in the visible region of the spectrum at room temperature (RT). hIDO has a Soret band at 420 nm and Q bands at 538 and 570 nm. Substrate addition causes a significant blue shift of the Soret band from 420 to 416 nm. Less pronounced changes are also observable in the Q bands. The position of the  $\alpha$  band is shifted from 570 to 567 nm. Both the  $\alpha$  and the  $\beta$  bands are affected in shape.

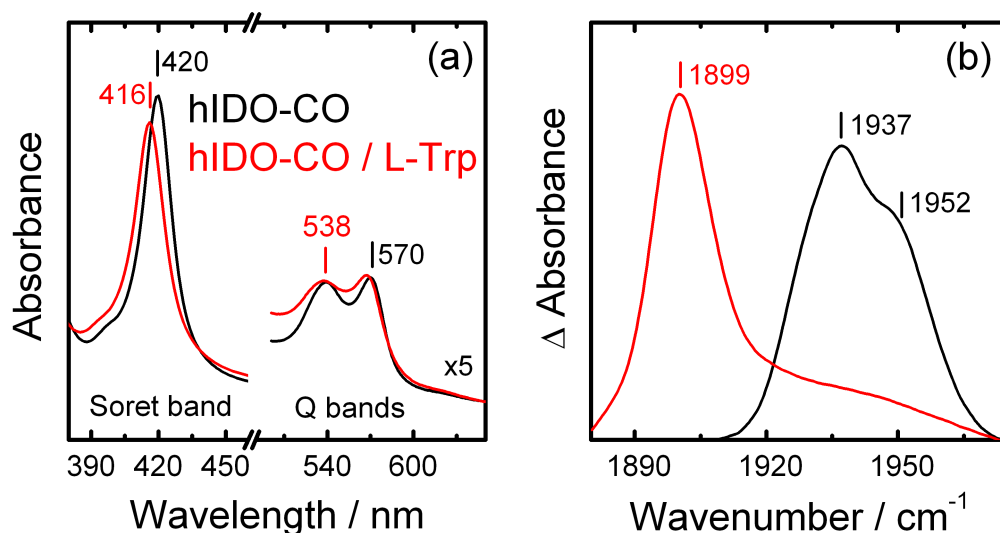


Figure 3.1: (a) Visible and (b) FTIR absorbance difference spectra of hIDO-CO (black lines) and hIDO-CO/L-Trp (red lines) at RT. For better comparison, all spectra were area normalized.

Binding of L-Trp clearly changes the Soret band and the Q bands of hIDO-CO, indicating a direct interaction between the heme group and the L-Trp. Resonance Raman studies showed that L-Trp binding induces conformational changes of the vinyl and propionate groups of the heme, either by direct interaction of the L-Trp with the heme group or by a conformational change in the protein structure<sup>[107]</sup>. Moreover, the crystal structure of hIDO-PI revealed interactions between the amino groups of both CHES buffer molecules with the 7-propionate<sup>[55]</sup>. Predictions of Macchiarulo et al.<sup>[108]</sup> disclose an interaction of the alpha amino group of L-Trp with the heme 7-propionate in an IDO-Fe(III)/superoxide complex. These results support the hypothesis of a direct interaction between L-Trp and the heme group.

Figure 3.1 b shows the FTIR absorbance difference spectra of hIDO-CO and hIDO-CO/L-Trp. In the spectrum of hIDO-CO recorded at ambient temperature, we observe at least two broad bands of heme-bound CO at 1937 and 1952  $\text{cm}^{-1}$ . The CO band at 1937  $\text{cm}^{-1}$  displays a shoulder at  $\approx 1926 \text{ cm}^{-1}$ . Each band of heme-bound CO represents a distinct active site conformation named A state. The addition of L-Trp shifts the bands to a single well defined band at a remarkably low CO stretching frequency of 1899  $\text{cm}^{-1}$ , suggesting an increased structural homogeneity of the active site of hIDO-CO/L-Trp. The broad shoulder at higher wavenumbers indicates a protein fraction that either has not bound L-Trp or, despite binding of L-Trp, has a similar active site conformation as hIDO-CO.

The IR spectra reveal different active site conformations in hIDO-CO. Upon binding of L-Trp, the stretching vibration of heme-bound CO shifts to significantly lower frequencies, indicating an interaction of a positive partial charge with the heme-bound CO oxygen. The results suggest the formation of a hydrogen bond either between the NH-group in the indole moiety of the L-Trp or the  $\text{NH}_3^+$  of the L-Trp backbone with the CO ligand.

## 3.2 Temperature Effect on Active Site Conformations

Proteins in their natural environment are not rigid structures, as often erroneously assumed from the crystal structures. In fact, proteins *in vivo* are wiggling and jiggling. The dynamic behavior of proteins is necessary to enable the variety of biological functions, e.g., the catalytic activity of enzymes.

It was shown that MbCO exhibits different active site conformation, so called taxonomical or conformational substates (CS)<sup>[61,109–111]</sup>. Each of these CS is characterized by a different infrared absorbance band of heme-bound CO, denoted as A band. The equilibrium populations of the CS depend on external conditions such as pH, solvent composition and temperature<sup>[112]</sup>. Below the glass transition temperature, each protein is frozen into a particular substate<sup>[113]</sup>. The examination of each distinct substate is possible. Above the dynamic glass transition temperature of the cryosolvent ( $\approx 180 \text{ K}$ ), conformational transitions between the distinct CS can occur. In this section, we analyze the influence of the temperature on the population of the different CSs in hIDO-CO.

The FTIR absorbance difference spectra of hIDO-CO reveal a variety of CSs. Figure 3.2a shows the development of the spectra as the temperature decreases from 293 to 120 K. The temperature influences the band widths as well as the band positions and their amplitudes<sup>[114]</sup>.

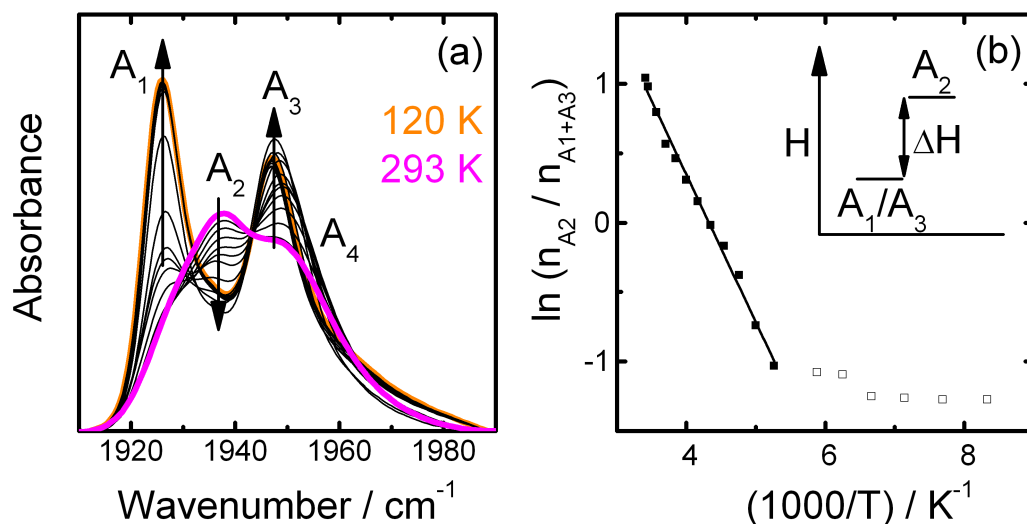


Figure 3.2: Temperature dependence of the absorbance spectra of hIDO-CO between 293 and 120 K. The protein was dissolved in 53%/47% (vol/vol) glycerol/100 mM KPb, pH 7. The sample was cooled at a rate of 0.6 K/min. (a) FTIR absorbance difference spectra. The A band positions are labeled. (b) Van't Hoff plot of hIDO-CO substate area ratios. Each FTIR absorbance spectrum plotted in (a) was fitted with four Gaussian curves representing the four conformational substates,  $A_1$  to  $A_4$ , of hIDO-CO. Using the total curve areas, the ratio of  $A_2$  to  $A_1 + A_3$  (black squares) was calculated. The results were fitted with a straight line. Data below 180 K were not considered for the fit (open squares). Inset: Scheme of relative standard enthalpies of the taxonomic substates.

The line shape of a CO stretching vibration can be approximated by a Gaussian peak function. The ensemble of stretching bands of heme-bound CO were fitted individually with multiple Gaussian functions (Appendix C). For hIDO-CO, the most reliable results were achieved with a fit using four Gaussian lines. Each curve corresponds to one conformational substate of the protein. We name the four substates and their corresponding bands  $A_1$  to  $A_4$ . The development of the relative substate populations with decreasing temperature was analyzed via changes in their

### 3.2. TEMPERATURE EFFECT ON ACTIVE SITE CONFORMATIONS

---

band areas. While the populations of  $A_1$ ,  $A_2$  and  $A_3$  show strong changes above 190 K, the population of  $A_4$  remains almost constant over the entire temperature range. Consequently, we have assumed that there is no exchange between  $A_4$  and the other CSs.

At ambient temperature,  $A_2$  is the preferred CS. A temperature decrease results in the increase of the two bands  $A_1$  and  $A_3$  at the expense of band  $A_2$ . The absorbance difference spectra do not exhibit two well defined isosbestic points which would clearly indicate two-state transition between  $A_2$  and  $A_{1/3}$ . As this may be due to a baseline problem we have assumed that  $A_1$  and  $A_3$  can be considered as one state that exchanges population with  $A_2$ . Therefore,  $A_1$  and  $A_3$  feature the same differences in standard enthalpy  $\Delta H$ , with respect to substate  $A_2$ .

To study the temperature-dependent interconversion between different protein conformations, the area ratio of substate  $A_2$  to the sum of the substates  $A_1$  and  $A_3$  was plotted in a van't Hoff plot (Figure 3.2 b). Van't Hoff described the temperature dependence of an equilibrium constant at constant pressure. The van't Hoff equation yields

$$\ln K = \ln\left(\frac{n_{A_2}}{n_{A_1+A_3}}\right) = -\frac{\Delta H}{R} \cdot \frac{1}{T} + \frac{\Delta S}{R}, \quad (3.1)$$

with the equilibrium constant  $K$ , the temperature  $T$ , the standard enthalpy change of the process  $\Delta H$ , the gas constant  $R$  and the entropy change  $\Delta S$ . To adjust Equation 3.1 to our purposes, we replace the equilibrium constant  $K$  by the terms of  $n_{A_2}/n_{A_1+A_3}$ .  $n$  represents the band areas of the substates of hIDO-CO.

To determine  $\Delta H$  between  $A_2$  and  $A_{1/3}$ , the relative areas and thus the relative populations of the A substates were calculated (Figure 3.2 b). Subsequently, the data above the glass transition temperature were fitted with a straight line. The changes in  $\Delta H$  were calculated from the slope of the line. For the shown example, the change in standard enthalpy is  $\Delta H_{A_2 \rightleftharpoons A_{1/3}} = 8.8$  kJ/mol. The temperature at which the ratio of the substates areas equal one is  $T_{A_2=A_1+A_3} = 231$  K. Above this temperature, conformation  $A_2$  is the favored conformation. Below this temperature, the majority of proteins exist in conformations  $A_1$  plus  $A_3$ . The inset in Figure 3.2 b demonstrates a scheme of the relation of the energy levels and  $\Delta H$  between the conformational states.

The presented results demonstrate the temperature dependence of the relative populations of the distinct hIDO-CO conformations. Under physiological conditions, more than 55% of the protein exists in conformation  $A_2$ . At low temperatures, the substates  $A_1$  and  $A_3$  gain at the expense of  $A_2$ . However, large scale motions of the protein are only activated above the dynamic transition temperature. Below

this temperature, the protein turns into a glass-like structure and investigations of the distinct substates are possible. In the following, we take a closer look at the characteristics of the different substates.

The relative populations of the A substates are not only dependent on the temperature but also, e.g., on the solvent composition, including the water activity, and the rate of cooling<sup>[115]</sup>. This results in a strong variation of population ratios in our experiments. Only slight differences in glycerol concentrations in the samples had a significant effect on the A state population ratio.

### 3.3 4-K FTIR Absorbance Spectra

To determine positions and widths of the A state bands of hIDO-CO and hIDO-CO/L-Trp at 4 K, the 4-K FTIR absorbance difference spectra were also fitted with the Gaussian peak functions (Appendix C). Figure 3.3 shows typical spectra of hIDO-CO and hIDO-CO/L-Trp and the applied fits.

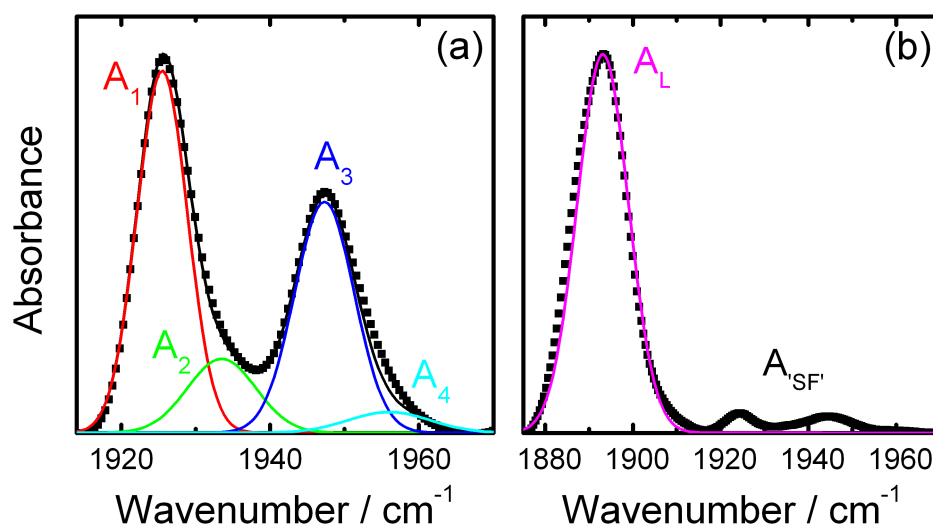


Figure 3.3: 4-K FTIR absorbance difference spectra of (a) hIDO-CO and (b) hIDO-CO/L-Trp fitted with multiple Gaussian peak functions (Appendix C).

Four different CSs were identified in substrate-free hIDO, namely the taxonomic substates  $A_1$ ,  $A_2$ ,  $A_3$  and  $A_4$ . They are represented by IR stretching bands at 1926, 1936, 1948 and 1956  $\text{cm}^{-1}$ , respectively. In the following, we will refer to each of the substates and its assigned band as the A state or the A band. The ensemble of the four A states in substrate-free hIDO-CO will be named  $A_{\text{SF}}$ .

In comparison to the bands  $A_1 - A_3$ , band  $A_4$  is broad (full width at half maximum (FWHM)  $A_4 \approx 15 \text{ cm}^{-1}$ ,  $A_{1-3} \approx 8 - 11 \text{ cm}^{-1}$ ); it is likely that the band represents denatured protein. Experiments with Mb showed that denaturation of the protein causes a blue shift and an intensive broadening of the bands of heme-bound CO<sup>[116,117]</sup> similar to our observation for band  $A_4$  in hIDO-CO. Therefore, we assume that the  $A_4$  state reflects a partly denatured protein conformation. In the following we focus on the three bands of  $A_1$ ,  $A_2$  and  $A_3$ .

A structural interpretation of the A bands of the variant active site conformations is not yet possible. However, a comparison with Mb is helpful to interpret the results. In the small heme protein Mb, three stretching bands of heme-bound CO,  $A_0$  ( $1965 \text{ cm}^{-1}$ ),  $A_1$  ( $1945 \text{ cm}^{-1}$ ) and  $A_3$  ( $1927 \text{ cm}^{-1}$ ) have been resolved by FTIR spectroscopy<sup>[118]</sup>. In the  $A_0$  conformation, the ligand interacts only weakly with its environment as the distal histidine (H64) is swung out of the pocket towards the solvent<sup>[119]</sup>. In comparison to the other conformations, the CO stretching frequency is high. In the substates  $A_1$  and  $A_3$ , the CO interacts with H64<sup>[120]</sup>. The positive partial charge of the  $N_\epsilon$ -H group of the H64 interacts with the oxygen atom of the CO ligand and decreases the CO stretching frequency. In comparison to the  $A_1$  state, H64 in the  $A_3$  conformation is positioned slightly closer to the CO. Based on this information, the IR data of hIDO can be interpreted. In the active site conformation  $A_1$ , the formation of a hydrogen bond between the CO and a close-by amino acid appears as possible. In contrast, interactions of the CO with the protein matrix must be significantly weaker in the  $A_3$  state. Substate  $A_2$  is arranged in between.

The band of heme-bound CO in hIDO-CO/L-Trp was fitted with a single Gaussian peak function (Appendix C). We cannot exclude that the absorbance band consists of multiple bands. Different hIDO-CO/L-Trp substates with only slightly different conformations might exist. For simplification, we will refer to this band/state as the  $A_L$  band/state.  $A_L$  peaks at  $1891 \text{ cm}^{-1}$ . The low frequency underlines the strong interaction between the ligand and a positive partial charge of L-Trp, either the NH in the indole group or the amino group of the backbone of L-Trp. The spectrum of hIDO-CO/L-Trp displays bands similar to the  $A_{SF}$  bands in hIDO-CO. We will refer to these bands as  $A'_{SF'}$  bands. All band positions are listed in Table 3.1.

CHAPTER 3. PROBING THE ACTIVE SITE

---

Table 3.1: Band positions of the stretching vibrations of heme-bound CO in samples of hIDO and hIDO variants with different substrates. All band positions were determined at 4 K.

sample	substrate	stretching frequency of heme-bound CO ( $\text{cm}^{-1}$ )				
		$\pm 1 \text{ cm}^{-1}$				
wt	-		1926 ( $A_1$ )	1936 ( $A_2$ )	1948 ( $A_3$ )	1956 ( $A_4$ )
	L-Trp	$\approx 1893$ ( $A_L$ )				
	D-Trp	(1900)	1922	1930	1945	
	S-Trp		1924	1936	1951	
	MLT	1894				
T367A	-		1926	1936	1948	1956
	L-Trp	1891				
T379A	-		1926	1936	1948	1956
	L-Trp		1926	1936	1948	1956
	D-Trp		1922	1930	1947	1956
R231A	-		1924	1931	1945	1956
	L-Trp		1926	1939	1946	1956
	D-Trp	1903	(1928)	(1950)		
R231E	-		1930	1944	1952	1956
	L-Trp		1927	1944	1952	1956
G261A	-				1947	1959
	L-Trp		1928	1934	1948	1959

### 3.4 Point Mutations at the Active Site

For further investigation of the structural conformations of the hIDO-CO and hIDO-CO/L-Trp active sites, we used site directed mutagenesis. The crystal structure and the mutagenesis studies by Sugimoto et al.<sup>[55]</sup> indicated amino acids presumably relevant for L-Trp binding and catalytic activity in hIDO. On the basis of these results we created the mutants R231A, R231E, G261A and T367A and T379A. The mutated amino acids are highlighted in the primary structure of hIDO shown in Figure 3.4.

```

1 MAHAMENSWT ISKEYHIDEE VGFALPNPQE NLPDFYNDWM FIAKHLPLDI ESGQL RERVE
61 KLNMLSIDHL TDHKSQRLAR LVLGCITMAY VWGKGHGQDVR KVLPRNIAVP YCQLS KKLEL
121 PPILVYADCV LANWKKKDPN KPLTYENMDV LFSFRDGDSC KGFFLVSLLV EIAAA SAIKV
181 IPTVFKAMQM QERDTLLKAL LEIASCLEKA LQVFHQIHDH VNPKAFFSVL RIYLSGWKGN
241 PQLSDGLVYE GFWEDPKEFA GSAGQSSVF QCFDVLLGIQ QTAGGGHAAQ FLQDMRRYMP
301 PAHRNFLCSL ESNPSVREFV LSKGDAGLRE AYDACVKALV SLRSYHLQIV TKYIL IPASQ
361 QPKENKTSED PSKLEAKGTG GTDLMNFLKT VRSTTEKSLL KEG

```

Figure 3.4: Amino acid sequence of hIDO<sup>[55]</sup>. Mutated amino acids are underlined and marked in different colors. The frame indicates the selected amino acids shown in Figure 3.6.

#### Mutation of R231

The crystal structure revealed that amino acid R231 is close to the ligand binding site<sup>[55]</sup>. Its most likely positively charged side chain is directed away from the ligand. Mutagenesis studies showed that the catalytic activity as well as the substrate affinity are drastically reduced in the variant hIDO R231A<sup>[55]</sup>. We replaced R231 both by a nonpolar alanine (A) and a glutamate (E) carrying a negative charge. A scheme of the active site structure (Figure 3.5, top panel) depicts the variants of hIDO R231. R231 is plotted in black, whereas the A and the E residues are overlaid in red and orange, respectively. From the various glutamate positions the one with the highest propability according to PyMol<sup>[57]</sup> (13%) was depicted.

### Mutation of G261

A highly conserved flexible loop (residues 260 to 265) connects the two protein domains of hIDO<sup>[55]</sup>. Comparison of the crystal structures of ferric CN-bound and PI-bound hIDO (hIDO-CN and hIDO-PI) reveals a shift of the loop by 6.5 Å (displacement of G262) upon binding of PI to the heme iron<sup>[121]</sup>. Variant G261A was created to observe if changes in this flexible loop influence the active site structure. The structures of the heme pocket of the wt (black) and the mutant G261A (green) are plotted in Figure 3.5 (bottom panel).

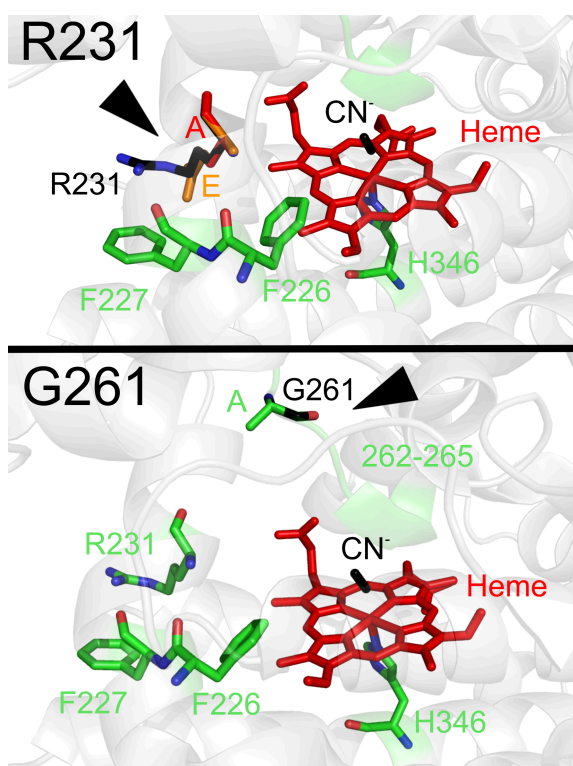


Figure 3.5: Top: Structure of the active sites in wt hIDO, hIDO R231A and hIDO R231E. The wt R231, the mutated A and the mutated E are presented as black, red and orange sticks, respectively. Bottom: Structure of the distal pocket in wt hIDO and hIDO G261A. The wt G261 (black) and the changed A (green) are presented. The arrows point at the mutated amino acids. The structures are based on the crystal structure of hIDO-CN (pdb code: 2D0U)<sup>[55]</sup>. Images were created with PyMol<sup>[57]</sup>.

### Mutations in the Outside Loop

The crystal structure of the binary complex of TDO from *Xanthomonas campestris* (xcTDO) and L-Trp was resolved by Tong and coworkers<sup>[24]</sup>. A comparison of the crystal structures of xcTDO and hIDO demonstrates that both proteins share significant similarities of their amino acids located at the active site. The crystal structure of xcTDO reveals the formation of a hydrogen bond between T254, positioned in a flexible loop, and the carboxylate moiety of L-Trp<sup>[24]</sup>. A complementary



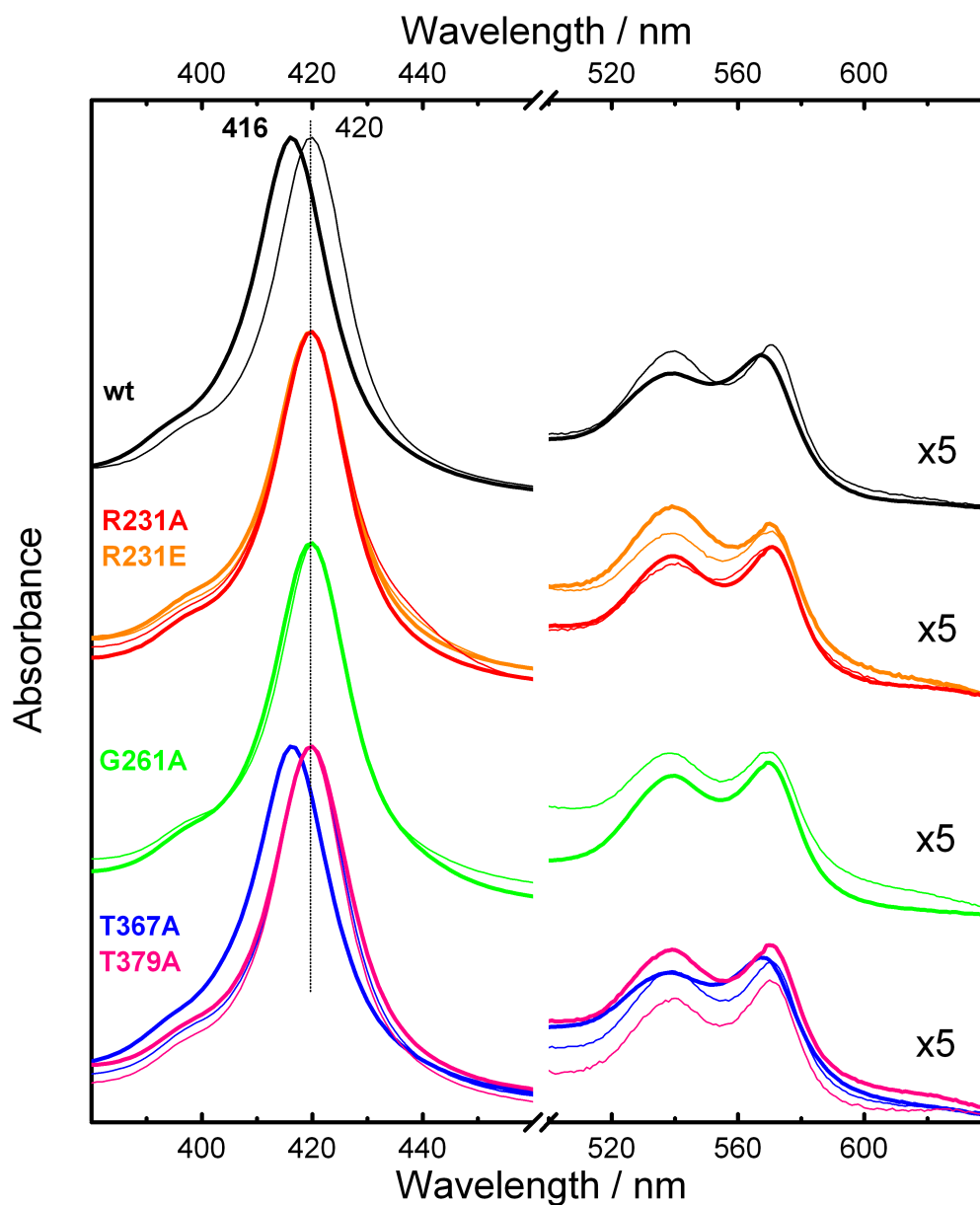


Figure 3.7: Vis spectra of wt hIDO-CO and variants hIDO T367A (blue lines), T379A (pink lines), R231A (red lines), R231E (orange lines) and G261A (green lines) without (thin lines) and with L-Trp (thick lines) at ambient temperature. For better comparison, all spectra were normalized to amplitude 1 at the Soret band maximum. Samples were dissolved in 53%/47% (vol/vol) glycerin/100 mM KPB, pH 7.

The corresponding 4-K FTIR absorbance difference spectra are shown in Figure 3.8. In the left panels, the absorbance spectra of hIDO and variants without substrate are plotted. The right panels display the FTIR absorbance spectra of the identical samples after addition of excess L-Trp.

Figure 3.8 a and b compare the spectra of wt hIDO-CO (black line) and hIDO-CO/L-Trp (back line) with those of the hIDO variants R231A (red line) and R231E (orange line). The FTIR absorbance difference spectra of the L-Trp-free proteins show already significant changes. The spectrum of mutant R231A has at least four overlapping bands similar to the  $A_{SF}$  bands in the wt protein. Interestingly, the spectrum of variant R231E displays one dominant band at  $1944\text{ cm}^{-1}$  with a shoulder at  $1952\text{ cm}^{-1}$  only. A small fraction of the  $A_1$  state exists in this mutant. Upon L-Trp addition, the spectra of the two mutants reveal no significant changes, indicating that the mutants do not bind L-Trp at their active sites.

G261 cannot interact with the bound CO ( $\approx 9\text{ \AA}$ ; G-H to CN ligand)<sup>[121]</sup>. The G261W and G261V mutants were remarkably unstable at room temperature. Eventually, this amino acid is important for proper folding of the protein. Variant G261A was sufficiently stable. Spectra of the variant before and after addition of L-Trp are shown in Figure 3.8 c and d. The absorbance spectrum of mutant G261A displays only the  $A_3$  band with a broad shoulder at  $\approx 1959\text{ cm}^{-1}$  (green line). Analogously to the  $A_4$  band at  $\approx 1956\text{ cm}^{-1}$  in wt hIDO, the shoulder is most likely due to denatured protein (compare Chapter 3.3). Conformations  $A_1$  and  $A_2$  are absent. Apparently, the mutation distorts the flexible loop (residues 260 to 265) and prevents formation of the active site conformations  $A_2$  and  $A_1$ . Upon L-Trp addition, no significant changes in the spectrum are observed, suggesting that the structural distortion of the loop affects the L-Trp binding affinity.

Figure 3.8 e displays the spectra of wt hIDO-CO (black line) and mutants T379A (pink line) and T367A (blue line). The spectra of both variants do not exhibit significant differences with respect to wt hIDO-CO. The spectrum of T367A changes in a similar way to that of wt hIDO-CO after L-Trp addition, indicating that this mutation does not influence L-Trp binding in the heme pocket (Figure 3.8 f). In contrast, in the variant T379A, no  $A_L$  band arises after L-Trp addition, the bands of heme-bound CO remain essentially identical to the bands  $A_{SF}$  in wt hIDO-CO.

In summary: With the exception of the hIDO-CO T367A variant, all mutants show impressive changes in the L-Trp affinity. We could clearly demonstrate the relevance of the amino acids R231 and T379 in the L-Trp binding process. Although the amino acid G261 cannot interact directly with the L-Trp at the active site, it seems to affect the binding affinity by changing the active site structure.

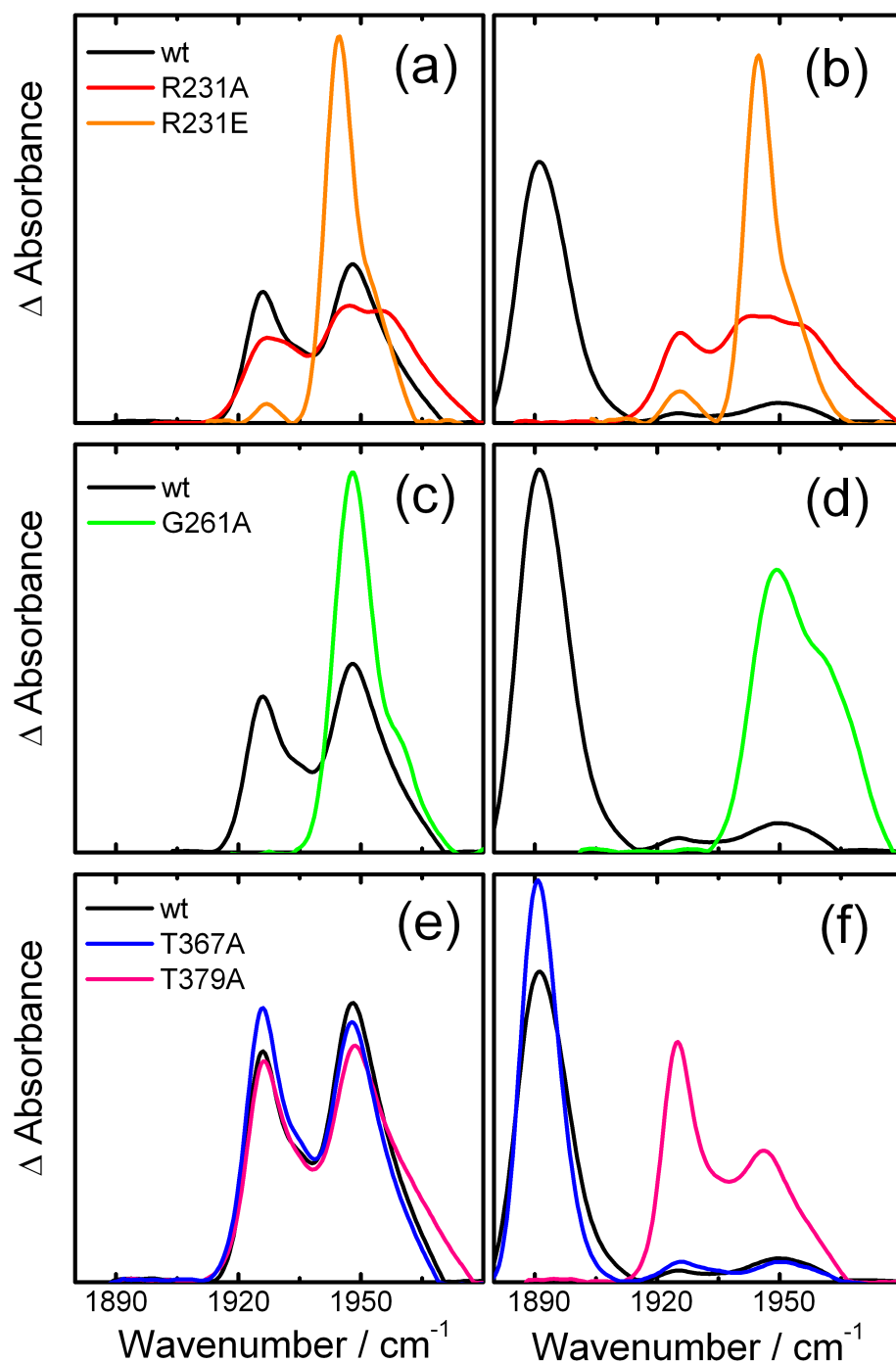


Figure 3.8: 4-K FTIR absorbance difference spectra of wt hIDO-CO and hIDO-CO variants without (left column) and with L-Trp (right column). (a, b) wt hIDO (black), R231A hIDO (red) and R231E (orange). (c,d) wt hIDO (black) and G261A hIDO (green). (e, f) wt hIDO (black) and T367A hIDO (blue) and T379A hIDO (pink). All spectra were area normalized. All band positions are listed in Table 3.1.

### 3.5 Binding of L-Trp Analogues

To elucidate the moieties essential for efficient substrate binding at the active site of hIDO-CO, we picked three different L-Trp analogues, 1-methyl-L-tryptophan (MLT) and 3-(Thianaphthen-3-yl)-L-alanine (S-Trp) and D-Trp. MLT is considered to be one of the most promising inhibitors. In 2009, it was shown to be slowly converted by hIDO-O<sub>2</sub> ( $k_{\text{cat}}$  (MLT)  $\approx 0.027 \text{ s}^{-1}$  and  $k_{\text{cat}}$  (L-Trp) =  $3.1 \text{ s}^{-1}$ )<sup>[54,122]</sup>. In rabbit IDO, the analogue S-Trp was reported to be a potent competitive inhibitor with respect to the substrate D-Trp<sup>[53]</sup>. In this analogue, the indolic nitrogen is replaced by a sulfur atom. The stereoisomer of L-Trp, D-Trp, is known to be converted by hIDO in the presence of oxygen. However, activity measurements showed a 170-fold larger  $K_{\text{m}}$  of D-Trp (2.6 mM) than for L-Trp in hIDO-O<sub>2</sub><sup>[54]</sup>. The structures of the analogues are shown in Appendix B.

The UV/Vis spectra collected at ambient temperature and the 4-K FTIR photolysis difference spectra of hIDO-CO without substrate and with L-Trp, MLT, S-Trp or D-Trp obtained after slow cool illumination are shown in Figure 3.9. The FTIR photolysis spectra might differ from the FTIR absorbance spectra with respect to the band amplitudes due to incomplete photolysis but reveal the band positions. The samples were prepared by adding the solid substrate to hIDO-CO to achieve the highest possible concentration. However, the solubilities of the substrates differ so that the highest achievable substrate concentration might still be too low to fully saturate the protein.

Binding of L-Trp to wt hIDO-CO is seen from a shift in the Soret band from 420 to 416 nm and from a red-shift of the IR bands to  $\approx 1891 \text{ cm}^{-1}$ . The UV/Vis spectra (Figure 3.9 a) of wt hIDO-CO in the presence of various substrates with MLT (cyan), S-Trp (blue) and D-Trp (green) show that only in the spectrum of hIDO-CO with MLT, the Soret band is shifted to an extent comparable to that achieved with L-Trp. The addition of S-Trp to hIDO-CO causes a small Soret band shift from 420 to 419 nm, whereas the addition of D-Trp does not induce any changes in the spectrum of hIDO-CO.

These observations are supported by the FTIR spectra shown in (Figure 3.9 b). The FTIR spectrum of hIDO-CO/MLT (cyan), featuring a band at  $1894 \text{ cm}^{-1}$ , demonstrates that MLT binding is similar to L-Trp binding. The spectrum of hIDO-CO/S-Trp (blue) shows three distinct bands at 1924, 1936 and  $1951 \text{ cm}^{-1}$ , similar to the A<sub>SF</sub> bands of hIDO-CO. In contrast to hIDO-CO the bands are of equal intensity. D-Trp generates only slight changes in the band positions of heme-bound CO (green), and it also generates changes in the amplitudes of the bands. Fitting the spectrum of hIDO-CO/D-Trp with the Gaussian peak function (Appendix C) reveals two major bands at 1922 and  $1930 \text{ cm}^{-1}$  and two only weakly populated conformational states with bands at 1900 and  $1945 \text{ cm}^{-1}$ .

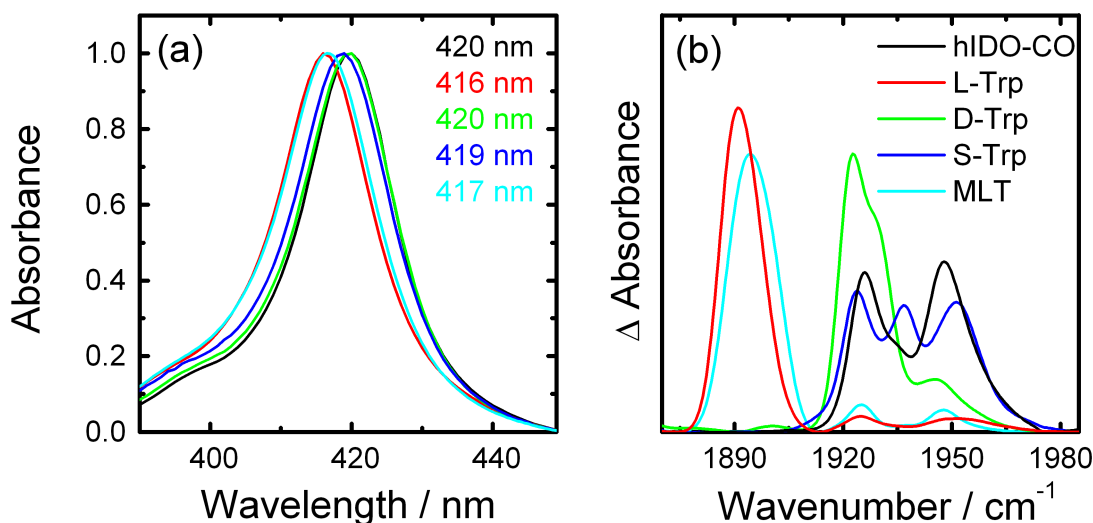


Figure 3.9: (a) UV/Vis spectra at ambient temperature and (b) 4-K FTIR photolysis difference spectra of hIDO-CO (black), hIDO-CO/L-Trp (red), hIDO-CO/D-Trp (green), hIDO-CO/S-Trp (blue) and hIDO-CO/MLT (cyan) measured after cooling the sample from 160 K to 4 K under continuous illumination (IP No.2; Chapter 2.5.7). UV/Vis spectra were normalized to amplitude 1 at the Soret band maximum. The peak maxima of the Soret bands are noted. For better comparison, the FTIR spectra were normalized to equal areas.

The Vis and FTIR spectra of hIDO-CO/MLT show that the methyl substitution of MLT does not hinder the binding of the molecule. The interactions of MLT with the heme group and the CO ligand must be almost identical as with L-Trp. The extraordinary low stretching frequency of CO upon L-Trp and MLT binding to hIDO-CO indicates formation of a hydrogen bond between the ligand and a positive partial charge. These results exclude formation of a hydrogen bond between the ligand and the NH of the indole moiety and favor hydrogen bond formation between the CO and the amino group of the substrate backbone.

On the basis of the results obtained with MLT, we expected S-Trp to behave similarly to L-Trp. The replacement of the NH by a sulfur atom in the indole moiety of the inhibitor does not form any steric hindrance. The binding of the amino acid backbone to the protein was expected to be comparable to the binding of L-Trp and MLT. However, the FTIR spectrum of hIDO-CO/S-Trp does not exhibit any  $A_L$ -like band as seen for hIDO-CO/MLT. The free electron pairs of the sulfur in the 'indole' moiety might render the S-Trp unsuitable as a substrate in the hydrophobic heme-pocket of hIDO. Possibly, the binding of S-Trp in an L-Trp-like manner is hindered electrostatically.

Both, Vis and FTIR absorbance spectra of hIDO-CO/D-Trp reveal that D-Trp does not bind in an L-Trp-like way to hIDO-CO. We assume that hydrogen bond formation cannot be realized between the backbone of D-Trp and the heme group as well as between the backbone and the ligand. It is, however, possible that the small band at  $1900\text{ cm}^{-1}$  represents the substrate conformation in which D-Trp binds similar to L-Trp and is converted.

### 3.6 Binding of D-Trp in hIDO Variants

In contrast to hIDO-CO/L-Trp, the Vis spectrum of hIDO-CO/D-Trp does not exhibit any blue shift of the Soret band. The FTIR spectra revealed that binding of D-Trp does not induce strong changes in the stretching frequency of heme-bound CO. To further investigate D-Trp binding in hIDO-CO, the 4-K FTIR photolysis difference spectra of the two variants R231A and T379A hIDO-CO are compared with the spectra of wt hIDO-CO upon addition of excess D-Trp (Figure 3.10).

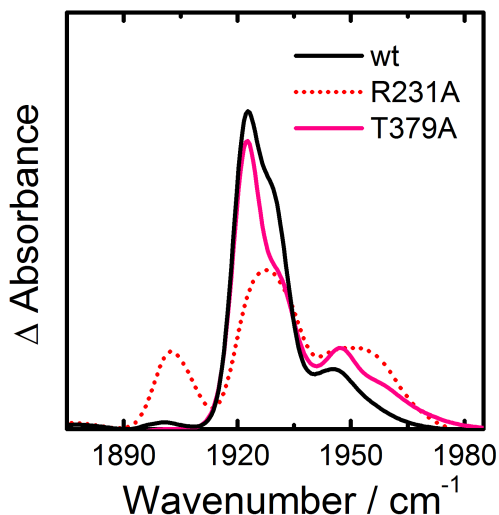


Figure 3.10: 4-K FTIR photolysis difference spectra of wt hIDO-CO (black solid line), R231A hIDO-CO (red dotted line) and T379A hIDO-CO (magenta solid line) in the presence of D-Trp.

The absorbance spectra of wt (black solid line) and T379A (pink solid line) hIDO-CO in the presence of D-Trp are very similar suggesting that replacement of the T in the outside loop does not influence the binding of D-Trp to the protein. Most likely, T379 is not involved in the binding of D-Trp in the wt protein. Only the tiny band at  $1900\text{ cm}^{-1}$  is missing in this mutant, indicating that the small fraction of D-Trp binding in an L-Trp-like matter is not present. In contrast, a new band at

1902  $\text{cm}^{-1}$  is generated in the mutant R231A upon addition of D-Trp to the sample (red dotted line). A larger fraction of D-Trp than in the wt protein is able to bind in a similar orientation as L-Trp. Presumably, the missing interaction between R231 and D-Trp enables an L-Trp-like binding of D-Trp.

### 3.7 Conclusions

At least three distinct active site conformations can be identified in hIDO-CO, namely  $A_1$ ,  $A_2$ , and  $A_3$ . The fraction of  $A_4$ , observed in some protein samples, is assumed to represent a partly denatured protein conformation.  $A_2$  is the favored state under physiological conditions, whereas the states  $A_1$  and  $A_3$  gain at the expense of the  $A_2$  conformation at cryogenic temperatures. Variant G261A gives some insight into the structural differences of the three active site conformations. As a result of the small change in the evolutionarily conserved loop (residues 260-265), the two states  $A_1$  and  $A_2$  are deleted. The strong aggregation tendency and the low expression rates of mutants G261W and G261V suggest that the flexibility of the loop that is limited by any mutation of the glycine, is of utmost importance in the folding process of hIDO. This flexibility leads to the formation of at least three conformational substates. Estrin and coworkers have predicted a hydrogen bond formation between the ligand CO and the backbone NH group of G265 in the flexible loop<sup>[123]</sup>. An interaction between the CO and the NH moiety would be in good agreement with the CO stretching frequency of state  $A_1$  (1926  $\text{cm}^{-1}$ ) indicating a positive partial charge in the CO vicinity. The band position is similar to that of the active site conformation  $A_3$  of Mb, where the  $N_\epsilon$ -H of the H64 is in close vicinity to the CO ligand<sup>[120]</sup>. Furthermore, the example of Mb has impressively demonstrated that only minor changes in the active site structure can alter the CO stretching vibration<sup>[96]</sup>. Hence, the A states of hIDO-CO may result from only small structural changes at the active site, possibly by different orientations of the flexible loop.

Binding of L-Trp changes the stretching frequency of the heme-bound CO rather drastically. Most likely, the strong shift in frequency is due to formation of a hydrogen bond between the ligand and the L-Trp, either between the NH of the indole moiety and the ligand or between the amino end of L-Trp and the ligand. The striking similarity of the FTIR spectra of hIDO-CO/MLT and hIDO-CO/L-Trp excludes that formation of a hydrogen bond between the CO and the NH of the indole moiety is responsible for the change in the CO stretching vibration. Therefore, an interaction between the amino group of the L-Trp and the CO is likely. But although the FTIR spectra reveal that MLT is binding analogously to L-Trp at the active site, the conversion of the substrate is significantly slower<sup>[122]</sup>.

The proper geometry between the iron-bound ligand and the substrate is most likely required for a highly efficient catalytic reaction. Therefore, not only substrate binding itself but also the exact positioning of the substrate is of importance. This positioning is realized by interactions between the protein matrix and the substrate. Changes in the optical spectrum reveal interactions between the heme and the L-Trp, most likely between the 7-propionate and the amino group of L-Trp (Chapter 3.1). Mutagenesis studies have demonstrated the importance of R231 (Chapter 3.4). In both hIDO variants, R231A and R231E, no  $A_L$ -like band is observed upon addition of L-Trp to the sample, indicating that L-Trp does not bind at the active site. We suggest that the affinity for L-Trp is markedly decreased in R231A hIDO-CO and R231E hIDO-CO. Activity measurements with mutant R231A by Sugimoto et al. [55] revealed a significant decrease in activity towards L-Trp. Simulations by Estrin and coworkers have predicted the formation of a salt bridge between the side chain of the R231 and the carboxylate of the L-Trp in hIDO- $O_2$  [123]. Additionally, the mutation of T379 changes the affinity of hIDO-CO towards L-Trp. The backbone amid of this residue is thought to interact with the carboxylate group of the L-Trp, similar to interactions in xcTDO [24]. Identified interactions of the L-Trp with the amino acids in the distal pocket, the heme group and the heme-bound CO are visualized in Figure 3.11 a.

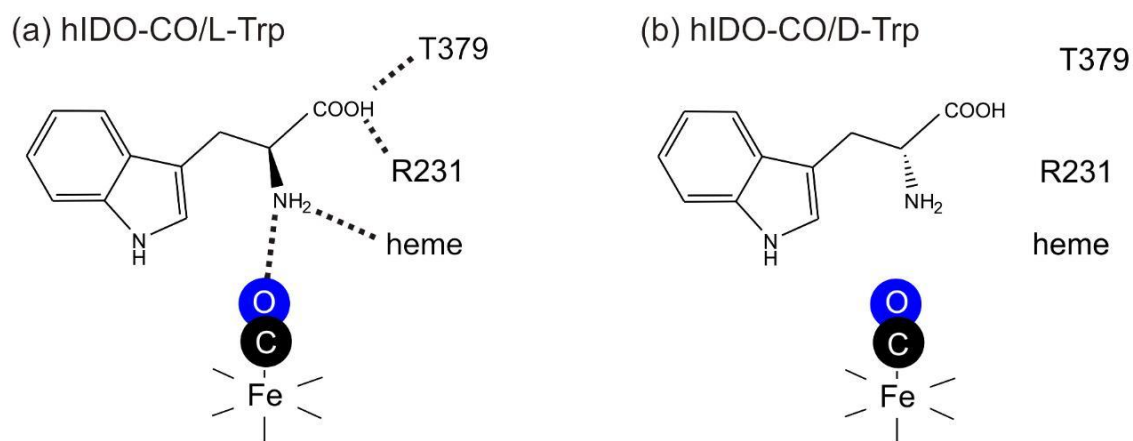


Figure 3.11: Scheme of interactions between the (a) L-Trp and (b) D-Trp with the ligand CO, the heme group and the protein matrix of hIDO.

The FTIR absorbance spectra of hIDO-CO/MLT underline that the substituent at the nitrogen of the indole moiety changes the CO stretching vibration only slightly, indicating that the influence of the methyl substitution on the position of the substrate is negligible. Based on the similar CO stretching band we assume that all interactions between the MLT backbone, the ligand and protein matrix are implemented.

The measurements with D-Trp and S-Trp are in contrast to these results. In hIDO-CO/D-Trp, only a tiny fraction of protein was observed with a band at  $\approx 1900 \text{ cm}^{-1}$ . This fraction might display the population where the D-Trp backbone interacts with the protein matrix similar to L-Trp. The major fraction of hIDO-CO/D-Trp displays  $A_{\text{SF}}$ -like bands. We assume that the interactions between the 7-propionate, R231, T379 and ligand with D-Trp are not present and D-Trp does not bind in a L-Trp like manner. Hence, the hydrogen bond cannot be formed between the D-Trp and the CO and the CO stretching frequency appears similar to that of hIDO-CO. The 4-K FTIR photolysis difference spectra of the variants T379A and R231A with D-Trp support this hypothesis. No differences are observed between the spectra of wt hIDO-CO and the variant T379A hIDO-CO. However, the tiny band at  $1900 \text{ cm}^{-1}$  is missing in T379A hIDO-CO/D-Trp, indicating that the fraction of protein binding D-Trp similar to L-Trp does not exist in the mutant. This observation confirms that amino acid T379 is necessary to bind D-Trp in the L-Trp-like way. However, T379 is not involved to bind D-Trp in its major conformation in wt hIDO. An A band similar to the  $A_{\text{L}}$  band is observed in the mutant R231A upon D-Trp addition. Possibly, R231 spatially hinders the binding of D-Trp in the same position as L-Trp. The exchange of R231 to a smaller A residue might allow the formation of a hydrogen bond between the ligand and the D-Trp. Interactions between the protein matrix and the D-Trp are shown in Figure 3.11 b.

Both the amino and carboxyl ends of S-Trp are identical to those of amino acids L-Trp and MLT. Therefore, we had expected S-Trp to bind to hIDO-CO in a similar manner. However, after addition of S-Trp to the sample, the CO stretching bands appear similar to the  $A_{\text{SF}}$  bands of hIDO-CO. Based on the crystal structure and simulations, hydrophobic interactions of the aromatic indole region of L-Trp with the amino acids F163 and F226 are supposed<sup>[55,123]</sup>. S-Trp displays a free electron pair and is, therefore, partially negatively charged. This might result in the distortion of the 'indole' moiety by changed interactions between F226 and F163 with the 'indole' and simultaneously in the disruption of the backbone interactions. In consequence, the spectra only displays bands similar to substrate free protein as seen for D-Trp.

## Chapter 4

# Probing the Protein Matrix

The last 50 years of heme protein research have focused mainly on small transporter globins such as Mb and hemoglobin. Intensive studies were carried out on the interplay of function, structure and dynamics in Mb<sup>[73,124,125]</sup>, which serves as an excellent model system. Mb binds ligands such as O<sub>2</sub>, NO or CO reversibly at the heme iron. Binding and release of ligands in Mb were studied in detail. Upon photolysis at cryogenic temperatures, ligands were shown to reside in cavities inside the protein matrix, so-called ligand docking sites<sup>[63,65]</sup>. In wt Mb, a primary docking site B, located in close vicinity to the heme iron, and secondary docking sites C and D were observed<sup>[67-69]</sup>. Already in 1997, Lim et al.<sup>[126]</sup> underlined the essential role of site B in the ligand binding process. It is thought to mediate the accessibility of the ligand to the heme iron. In particular mutagenesis studies showed that the docking sites facilitate the regulation of the capture and release of ligands in Mb<sup>[64]</sup>.

In dioxygenases such as hIDO, the diatomic ligand O<sub>2</sub> is consumed during the catalytic reaction. Ligand release is thus not necessary. The regulation of ligand binding must be ensured, whereas the regulation of ligand release from the protein does not seem that important. This difference to a typical ligand storage protein raises the question if transient ligand docking sites exist in hIDO and if they are influenced by the binding of L-Trp.

In the following, CO was utilized to probe the protein matrices of hIDO-CO and hIDO-CO/L-Trp for internal cavities and to explore ligand migration within the protein. By applying well-designed IPs, the iron-ligand bond was cleaved and different photolysis intermediates were generated with the ligands trapped at different transient docking sites. The TDS technique was applied to sort the ligands according to their rebinding barriers and, thereby, differentiate between the docking sites.

## 4.1 Existence of Ligand Docking Sites in hIDO-CO and hIDO-CO/L-Trp

To scan hIDO-CO and hIDO-CO/L-Trp for primary and secondary docking sites, carefully selected illumination protocols were applied. Experience has shown that short-time photolysis at 4 K preferentially traps ligands at the primary docking site B. In CO-ligated Mb, 1-s illumination at 4 K is sufficient to completely photolyze the sample and trap the ligands at site B<sup>[127]</sup>. Upon prolonged illumination at higher temperatures, the ligands migrate into more remote docking sites. Cooling the sample from 160 to 4 K under light enables the ligands to explore both the B site as well as the secondary docking sites (C site, D site, etc.).

Figure 4.1 shows 4-K FTIR absorbance difference spectra (dotted lines), representing the total fraction of CO bound to the protein, and 4-K FTIR photolysis spectra of hIDO-CO and hIDO-CO/L-Trp. The latter spectra recorded after 10-s illumination at 4 K (thin solid lines)(IP No.1; Chapter 2.5.7) and after slow cooling from 160 to 4 K under light (thick solid lines) (IP No.2) reveal the fraction of CO molecules that were photolyzed by the applied illumination protocol.

The IR absorbance difference spectrum of hIDO-CO (black) displays the ensemble of the  $A_{SF}$  bands, primarily consisting of the  $A_1$  and  $A_3$  bands. In conformation  $A_1$ , all CO ligands become trapped at transient docking sites, whereas in  $A_3$ , the photoproduct yield is  $\approx 70\%$  after short time illumination at low temperature and  $\approx 90\%$  after extended illumination. In hIDO-CO/L-Trp, the photoproduct yield after slow cool illumination is only  $\approx 75\%$ . Merely 15% of hIDO-CO/L-Trp is photolyzed after short-time illumination at 4 K.

If well defined docking sites exist, we may expect narrow stretching bands of photolyzed CO. Indeed, the photodissociated CO displays photoproduct bands in the spectral region between 2090 and 2160  $\text{cm}^{-1}$  (Figure 4.1). The FTIR photolysis spectra of hIDO-CO display several photoproduct bands after brief illumination at 4 K (thin black line). This illumination is expected to only populate docking sites in close vicinity to the heme. In the following, we will refer to these bands as B bands. Interestingly, no distinct photoproduct bands appear in hIDO-CO/L-Trp after the same illumination procedure (thin red line). Note that the yield of photolyzed CO is very low under these conditions. The FTIR photolysis spectra recorded after cooling the samples from 160 to 4 K under light display new photoproduct bands in both samples, hIDO-CO (thick black line) and hIDO-CO/L-Trp (thick red line).

In summary, the photoproduct bands in hIDO-CO clearly indicate that primary and secondary docking sites exist in hIDO. The binding of L-Trp to the protein significantly changes the corresponding photoproduct bands. Therefore, binding of L-Trp obviously induces changes in the electric field at the CO docking sites. At the same time, binding of L-Trp changes the photoproduct yield.

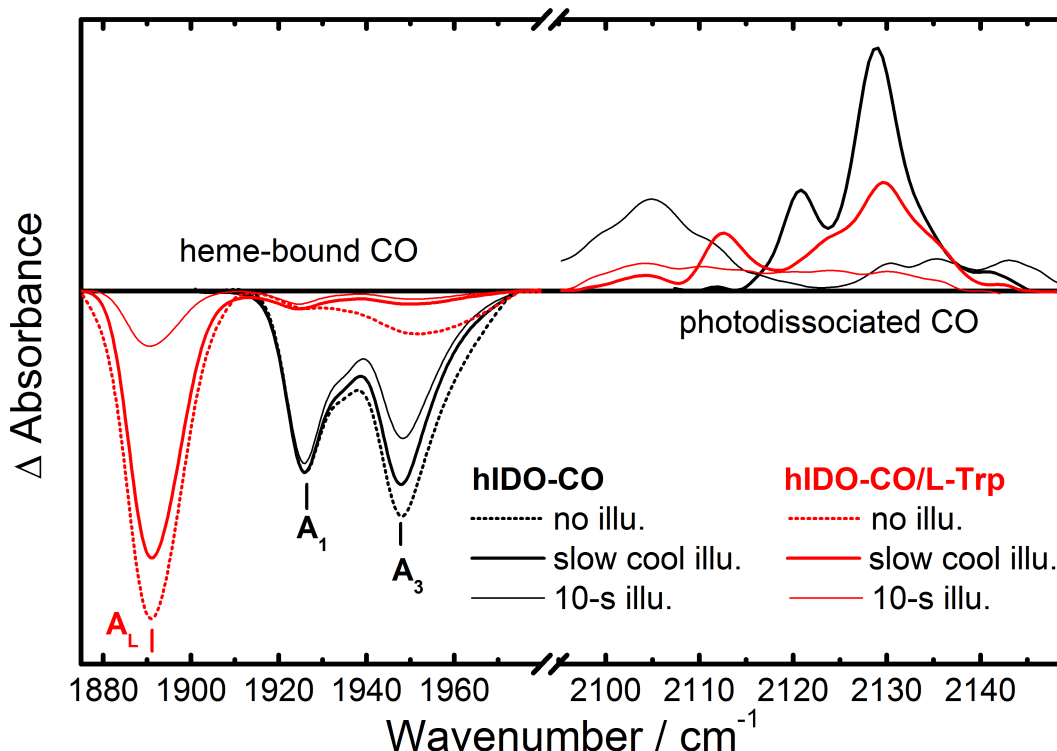


Figure 4.1: Photolysis Difference Spectra of hIDO-CO and hIDO-CO/L-Trp. 4-K FTIR absorbance difference spectra of hIDO-CO (black) and hIDO-CO/L-Trp (red) are plotted with dashed lines. 4-K FTIR photolysis spectra after 10-s illumination at 4 K (IP No. 1) (thin lines) and after slow cooling from 160 to 4 K under light (IP No. 2) (thick line) are shown as solid lines. The spectral areas were all normalized to the FTIR absorbance difference spectrum.

## 4.2 Ligand Dynamics in the Docking Sites

Figure 4.2 presents TDS contour maps of hIDO-CO after slow cool illumination (IP No.2). Figure 4.2a and b show absorbance changes in the bands of heme-bound and photodissociated CO, respectively. The red contours indicate an absorbance decrease, whereas the black ones represent an absorbance increase. The amplitudes of the A state bands increase in two steps, at  $\approx 20$  K and  $\approx 170$  K, indicating rebinding of CO at the heme iron (Figure 4.2a). Surprisingly, these features are not visible in the photoproduct map (Figure 4.2b). Instead, we note a gradual loss in the photoproduct bands starting at 50 K and extending up to 180 K. Obviously, in the present sample, the pronounced changes in the absorbance of the photoproduct bands cannot be ascribed to ligand rebinding.

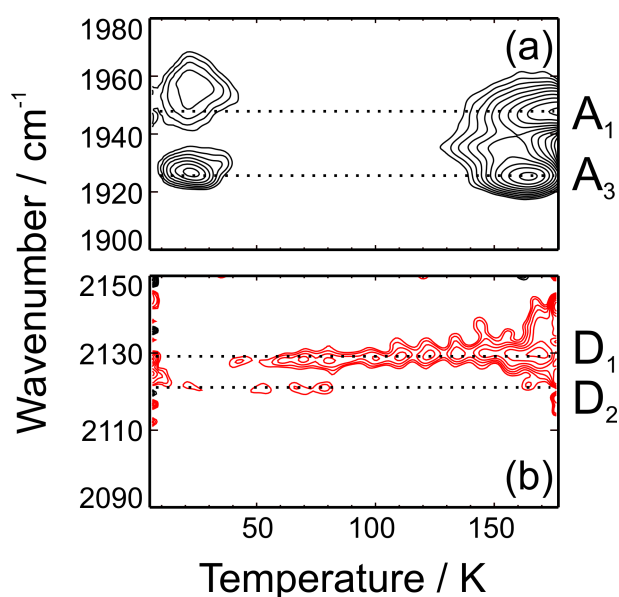


Figure 4.2: TDS contour plots of substrate-free hIDO-CO after continuous illumination from 160 to 4 K (IP No. 2). Absorbance changes are shown for the bands of (a) heme-bound CO and (b) photodissociated CO. Black and red lines indicate an absorbance increase and decrease, respectively. Contours are spaced logarithmically.

The extent of the absorbance decrease in the photoproduct bands is even more obvious from the data shown in Figure 4.3. After 15,000-s illumination at 160 K, the hIDO-CO and hIDO-CO/L-Trp samples were cooled to 7 K in the dark (IP No. 3; Chapter 2.5.7). During the cooling process, transmission spectra were taken every kelvin. FTIR photolysis spectra were calculated by using transmission spectra recorded before illumination as reference spectra.

To demonstrate the spectral changes, absorbance spectra in the temperature range from 140 to 7 K are plotted every 10 K. Between 140 and 7 K, the A bands in hIDO-CO remain constant (Figure 4.3 a). Concomitantly, a marked increase in the photoproduct bands is obvious. In the photoproduct bands of hIDO-CO/L-Trp, similar effects are observed (Figure 4.3 b). Again, the photoproduct bands show a temperature-dependent change in amplitude. Interestingly, the increase in band intensities with decreasing temperature differs in each of the bands.

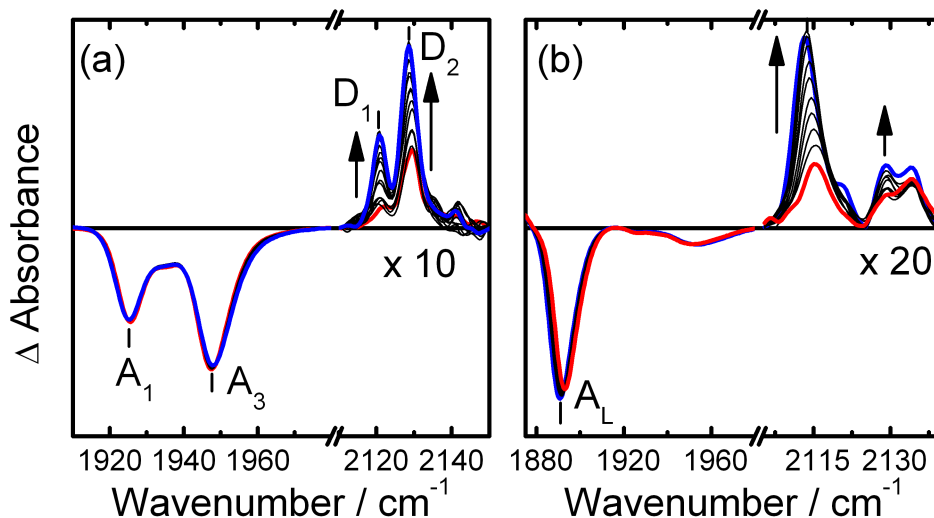


Figure 4.3: Effect of ligand dynamic in docking sites on the photoproduct bands. FTIR photolysis difference spectra of (a) hIDO-CO and (b) hIDO-CO/L-Trp. After 15,000-s illumination at 160 K, the samples were cooled to 7 K (IP No.3). Spectra were taken every kelvin from 160 to 7 K. Absorbance spectra from 140 (red spectra) to 7 K (blue spectra) are plotted (every 10 K).

Figure 4.4 gives a closer insight into the development a particular set of photoproduct bands,  $D_1$  ( $2120 \text{ cm}^{-1}$ ) and  $D_2$  ( $2129 \text{ cm}^{-1}$ ), of hIDO-CO (Figure 4.3 a). (Nomenclature will be discussed in Chapter 4.3.) Between 7 and 140 K, the photoproduct spectra were fitted with Gaussians (Appendix C). To improve the data quality, 10 absorbance spectra were averaged for each data point. In Figure 4.4, the relative areas, referenced to the band areas at 7 K (panel a), positions (panel b) and widths (full width at half maximum, FWHM) (panel c) of the photoproduct bands are plotted as a function of temperature. The areas of the photoproduct bands  $D_1$  and  $D_2$  decrease by  $\approx 75\%$  and  $\approx 50\%$  from 7 to 140 K. Simultaneously, the peak maximum of  $D_2$  band blue-shifts by  $1 \text{ cm}^{-1}$  towards  $2130 \text{ cm}^{-1}$  with increasing temperature, whereas the peak position of  $D_1$  band is scattered around a mean value of  $2121 \text{ cm}^{-1}$ . A band broadening is clearly observed in the  $D_1$  band above 100 K. In contrast, there is only a moderate increase in the band width of the  $D_2$  band.

The data show that the area of the photoproduct bands changes strongly with temperature. However, the area decrease seen in the samples of hIDO-CO and hIDO-CO/L-Trp is not based on the recombination of CO to the heme iron and, therefore, the area cannot be taken as a measure of the photolyzed population. Instead, the pronounced decay in absorbance intensity and the broadening of the photoproduct bands with temperature indicate thermal activation of CO librations

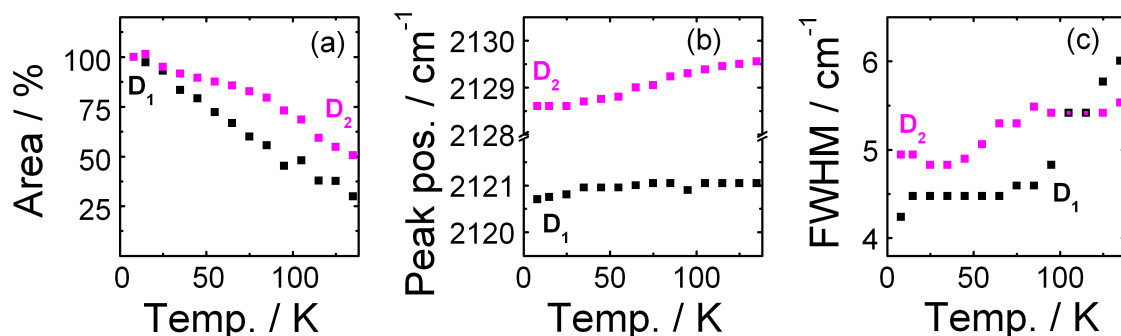


Figure 4.4: Development of the photoproduct bands D<sub>1</sub> (black squares) and D<sub>2</sub> (magenta squares) of hIDO-CO with temperature. (a) Relative areas with respect to the band areas at 7 K as a function of temperature. (b) Peak position of the D<sub>1</sub> and D<sub>2</sub> bands. (c) Peak width (FWHM) of D<sub>1</sub> and D<sub>2</sub> bands.

in the docking site(s). Similar effects were observed in the double mutant Mb L29W-S108L<sup>[105,106]</sup>. Kriegl et al.<sup>[106]</sup> presented experiments on the Mb mutant that illustrated the effect of temperature on the stretching bands of a CO molecule trapped in opposite orientations in a transient docking site<sup>[106,127]</sup>. Due to the local electric field in the docking site, the two CO orientations are associated with two distinct IR stretching bands. With increasing temperature, the two bands approach each other. Our data show a peak shift in the D<sub>2</sub> band but only a minor shift in the D<sub>1</sub> band. Moreover, in both bands, a peak shift to higher stretching frequencies is observed. These results suggest that the two bands D<sub>1</sub> and D<sub>2</sub> do not represent the CO molecule in opposite orientations in a particular docking site. In Chapter 4.3, we focus on the assignment of the photoproduct bands.

The dynamics of CO in the secondary docking sites in hIDO-CO and hIDO-CO/L-Trp complicates the comparison of photoproduct bands at different temperatures. We showed that band positions and areas change with temperature. To avoid incorrect interpretation of the data, all discussions about photoproduct bands will be based on FTIR absorbance spectra measured at 4 K.

### 4.3 hIDO-CO: Docking Sites and Ligand Migration

In Chapter 4.1, we have shown that transient ligand docking sites exist in hIDO-CO. TDS experiments can help to assign the corresponding photoproduct bands to particular CO rebinding processes. Carefully selected illumination protocols allow to distinguish between docking sites in close vicinity to the heme-iron and more remote docking sites. Figure 4.5 presents TDS contour plots of hIDO-CO recorded following three different illumination protocols.

The TDS map of heme-bound CO obtained after 10-s illumination at 4 K (IP No. 2; Chapter 2.5.7) displays maximal ligand recombination to the heme iron in  $A_1$  and  $A_3$  at 23 and 20 K, respectively (Figure 4.5 a). The shoulder above  $1950\text{ cm}^{-1}$  is due to recombination in  $A_4$ . The weakly populated  $A_2$  conformation recombines at  $\approx 110$  K. Due to the low rebinding temperatures, we assume that these recombination processes in  $A_1$  and  $A_3$  represent CO rebinding from a docking site located in close vicinity to the heme iron, the primary docking site B.

Cooling the sample under continuous illumination populates both primary and remote docking sites (IP No. 2; Chapter 2.5.7)(Figure 4.5 b). Absorbance changes at 23 K in substate  $A_1$  correspond to recombination from the primary docking site. The absorbance changes observed at  $\approx 20$  K at CO stretch frequencies above  $1950\text{ cm}^{-1}$  display recombination in conformational substate  $A_4$ . This substate does not feature any further recombination processes. Therefore, we suggest that the substate mirrors a partly denatured protein conformation (see also Chapter 3.3). Additionally, the TDS contour map displays CO rebinding at 164 K in  $A_1$  and at  $\approx 180$  K in  $A_3$ . Minor recombination in  $A_1$  is observed at  $\approx 98$  K.

To selectively populate this photoproduct intermediate, the hIDO-CO sample was illuminated for 15,000 s at 60 K and cooled to 4 K in the dark (IP No. 4; Chapter 2.5.7). Figure 4.5 c displays the TDS data recorded after the described illumination. By applying this IP we ensure that CO is only trapped at secondary docking sites. Any CO ligands trapped at site B rebind during cooling. In  $A_1$ , recombination extends from 80 to 110 K, with a maximum at  $\approx 98$  K. In  $A_2$ , ligand recombination is still maximal at  $\approx 110$  K and, hence, the two illumination procedures (IP No. 1 and No. 4) populate the same docking site in  $A_2$ -type proteins. CO recombination in  $A_3$  is still maximal at  $\approx 180$  K, as observed after slow cool illumination (Figure 4.5 b).

Figure 4.5 d presents FTIR photolysis spectra at 60 (black line) and 120 K (red line) recorded during the TDS experiment shown in Figure 4.5 c. The difference between these spectra is solely related to rebinding in  $A_1$ . The corresponding photoproduct band, inserted as a blue line, represents CO ligands trapped at a docking site we will denote as site C in the following.

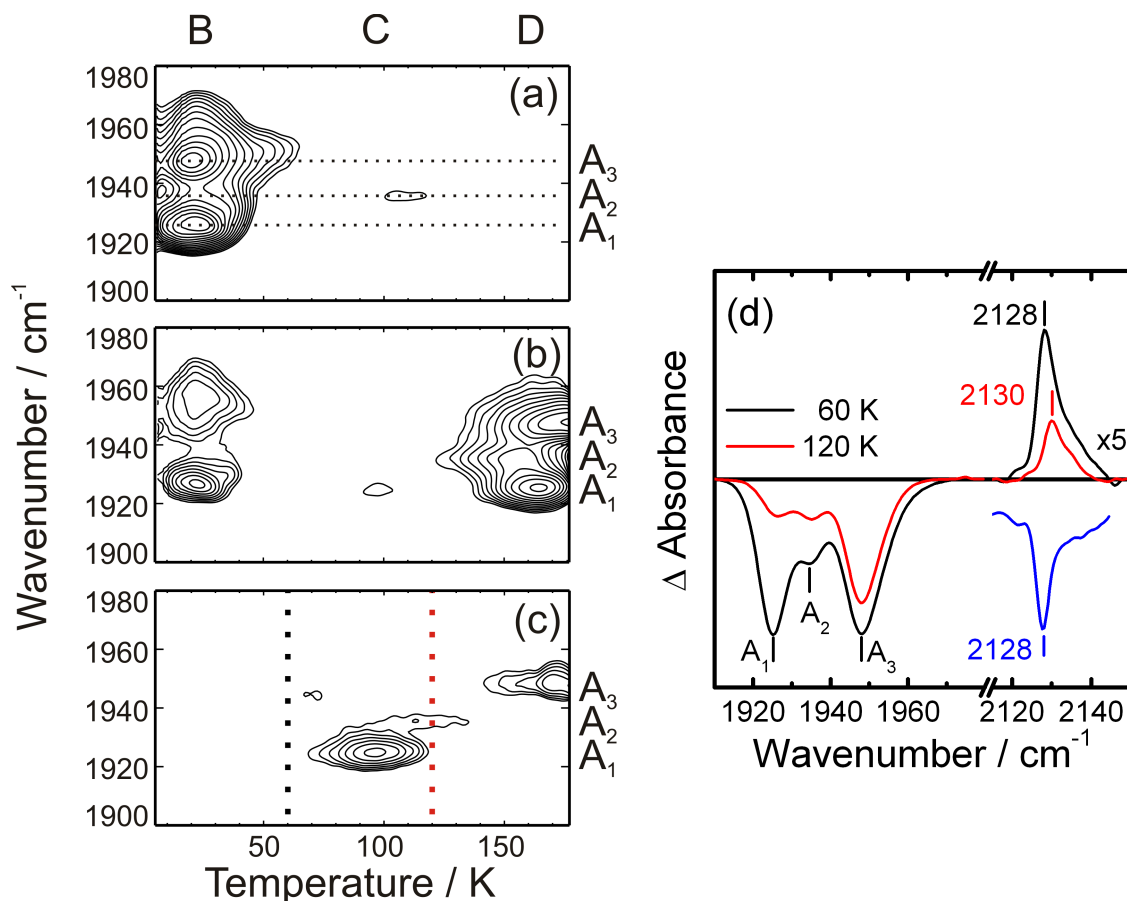


Figure 4.5: Geminate recombination of CO in hIDO-CO. TDS maps of hIDO-CO after (a) 10 s of illumination at 4 K (IP No.1), (b) after cooling from 160 to 4 K under light (IP No.2) and (c) after cooling the sample to 4 K after 15,000 s of illumination at 60 K (IP No.4). Solid lines indicate an absorbance increase. Contours are spaced logarithmically. (d) FTIR photolysis difference spectra of IDO-CO at 60 K (black line) and 120 K (red line) taken after 15,000 s of illumination at 60 K (IP No.4). The temperatures of the spectra are marked in the respective color in panel c. The difference of the photoproduct spectra is plotted in blue.

The 4-K FTIR photolysis difference spectra recorded after the described illumination protocols are shown in Figure 4.6. To populate the primary docking site B, the hIDO-CO sample was illuminated for 10 s at 4 K (red line) (IP No.1; Chapter 2.5.7). The spectrum exhibits broad photoproduct bands. We applied the identical illumination protocol to several hIDO-CO samples. All samples showed significant differences in the B bands. Three bands at 2105, 2112 and 2144  $\text{cm}^{-1}$  were always present in all samples, but the relative band intensities changed significantly from sample to sample.

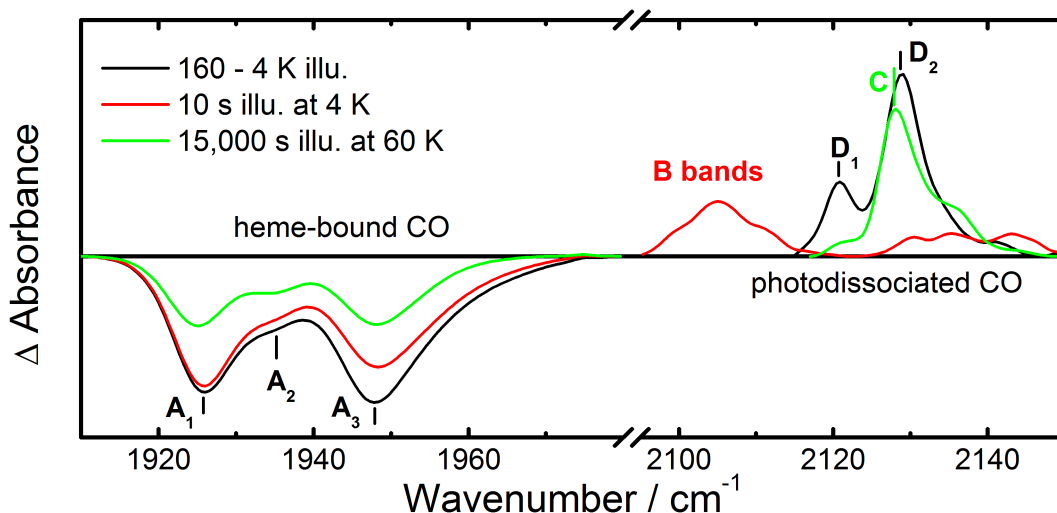


Figure 4.6: Assignment of photoproduct bands in hIDO-CO. 4-K FTIR photolysis difference spectra of hIDO-CO after 10-s illumination at 4 K (red line) (IP No.1), after cooling the sample to 4 K after 15,000-s illumination at 60 K (green line) (IP No.4) and after slow cooling from 160 to 4 K under light (IP No.2) (black line).

Several experiments were performed to assign the B bands (Figure 4.6) to the different A substates. With our experimental setup, kinetic studies could not achieve the necessary temporal resolution to observe the photolysis processes at 4 K in the photoproduct bands. In contrast, recombination kinetics at 4 K did not reveal any ligand rebinding from the B site to the heme iron within 15,000 s. Furthermore, we investigated the correlation between the band areas of heme-bound CO and photodissociated CO. However, any significant assignment of the major B bands to the A state bands could not be achieved.

The spectrum recorded after 15,000-s illumination at 60 K and cooling to 4 K in the dark shows photoproduct bands at 2120, 2128 and 2137  $\text{cm}^{-1}$  (Figure 4.6, green line) (IP No.4). The band at 2128  $\text{cm}^{-1}$  corresponds to the C band associated with rebinding in  $A_1$  at  $\approx 98$  K (Figure 4.5).

Cooling the sample from 160 to 4 K under light generates two photoproduct bands at 2120 and 2129  $\text{cm}^{-1}$  (Figure 4.6 a, black line) (IP No.2). The corresponding TDS contour map (Figure 4.5) revealed two major recombination processes in  $A_1$  and  $A_3$  at 160 and 180 K. Therefore, we assume that the two bands are associated with these recombination processes. In the following, we will refer to the two bands as  $D_1$  (2120  $\text{cm}^{-1}$ ) and  $D_2$  (2129  $\text{cm}^{-1}$ ) bands.

Mutant G261A adopts only substate  $A_3$  and may help to assign the bands of  $D_1$  and  $D_2$  to the substates  $A_1$  and  $A_3$ . Figure 4.7a shows the 4-K FTIR photolysis difference spectra of wt hIDO-CO (black) and G261A hIDO-CO (green) after cooling the sample from 160 to 4 K under light (IP No.2). The bands of heme-bound CO of variant G261A have been discussed in detail (Chapter 3.4). The photoproduct bands of mutant G261A obtained after prolonged illumination at higher temperatures do not differ from the ones in the wt protein. Both bands, termed as  $D_1$  and  $D_2$  in wt hIDO-CO, occur in the mutant G261A. The recorded TDS contour map of G261A hIDO-CO after prolonged illumination displays a CO recombination pattern as seen in substate  $A_3$  of the wt protein (Figure 4.7 b). The major ligand recombination process to the heme iron in the variant occurs at  $\approx 170$  K. Only a minor fraction of CO rebinds below 50 K, indicating a weak population at the primary docking site B after this illumination protocol.

The results with variant G261A demonstrate clearly that, in the  $A_3$  substate, both photoproduct bands  $D_1$  and  $D_2$  exist. Recombination from the corresponding docking site(s) is observed at  $\approx 170$  K.

The conformational substates of hIDO-CO,  $A_1$ ,  $A_2$  and  $A_3$ , feature significantly different recombination characteristics. Using different illumination procedures, we have proven the existence of site C in conformation  $A_1$ . Whereas this cavity C is highly populated after illumination at 60 K, its population is small after slow cool illumination. In contrast to protein conformation  $A_1$ , no population of a site C is observed in substate  $A_3$  (Figure 4.5 b). The TDS experiments revealed recombination above 160 K in  $A_1$  and  $A_3$ . We assign this rebinding process to recombination from docking site(s) D. After illumination at 60 K, ligand recombination to  $A_3$  is maximal at  $\approx 180$  K. Applying slow cool illumination does not change the recombination temperature (Figure 4.5 c). However, the same TDS contour plot demonstrates that, in substate  $A_1$ , the maximal absorbance change then occurs at  $\approx 164$  K, indicating a recombination process that was not observed after illumination at 60 K. The 4-K FTIR photolysis difference spectra show that the two bands  $D_1$  (2120  $\text{cm}^{-1}$ ) and  $D_2$  (2129  $\text{cm}^{-1}$ ) are associated with these recombination processes in  $A_1$  and

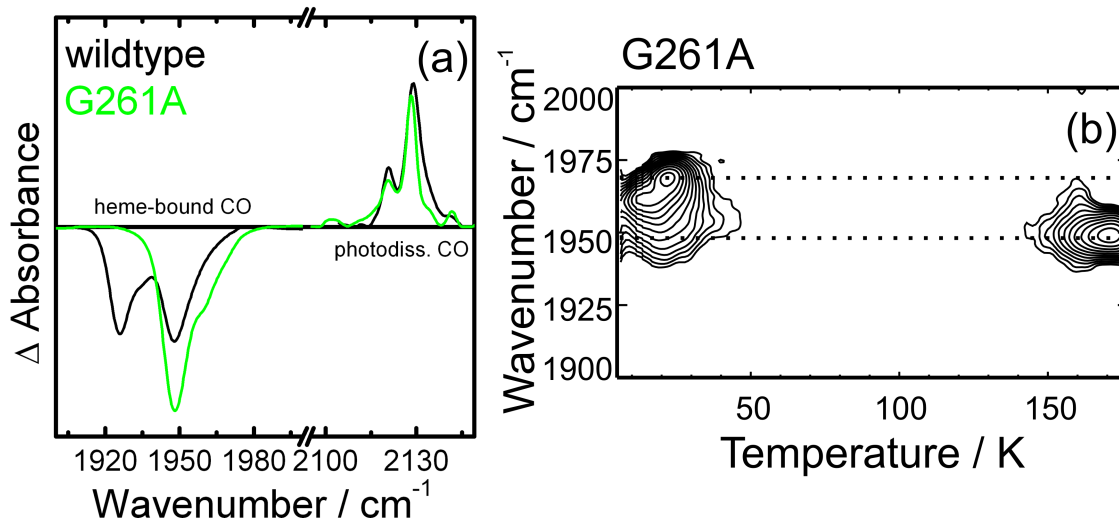


Figure 4.7: Variant G261A hIDO-CO: Assignment of photoproduct bands  $D_1$  and  $D_2$ . (a) 6-K FTIR photolysis spectra of G261A (green) and wt hIDO-CO (black) after cooling the sample from 160 to 4 K under illumination (IP No.2). (b) TDS contour map of G261A after continuous illumination from 160 to 4 K (IP No.2). Absorbance changes are shown for the bands of heme-bound CO. Black lines indicate an absorbance increase. Contours are spaced logarithmically.

$A_3$  (Figure 4.6). Any interference of the D bands with the identified C band is negligible due to the weak intensity of the C band after slow cool illumination. The assignment of the photoproduct bands  $D_1$  and  $D_2$  is not trivial. Different scenarios are possible.

(1) If photodissociated CO is trapped in a docking site in opposite orientations (C-O or O-C)<sup>[106]</sup>, the local electric field in the docking site gives rise to a doublet of CO stretching bands. Kriegl et al.<sup>[106]</sup> presented the effect of increasing temperature on the stretching vibration bands of a CO molecule in opposite orientations trapped in one docking site. The bands approach each other with increasing temperature. We have demonstrated that no opposite peak shift of the two bands occurs (Figure 4.4b). This observation disfavors the hypothesis of  $D_1$  and  $D_2$  representing CO in two orientations in one docking site.

(2) If we assume that the two bands  $D_1$  and  $D_2$  are associated with the dominant substates  $A_1$  and  $A_3$ , respectively, a protein with only one of the two protein conformations should only exhibit a single photoproduct band. This interpretation is not consistent with the results seen in the hIDO variant G261A (Figure 4.7). In

this mutant, only substate  $A_3$  with a CO stretching vibration peaking at  $1948\text{ cm}^{-1}$  exists. However, the FTIR photolysis spectrum still displays both photoproduct bands,  $D_1$  and  $D_2$ .

(3) Two docking sites might be present in both protein conformations. Each photoproduct band represents CO in one of these docking sites independent of the protein conformation. This scenario is imaginable if we assume that the recombination temperature of CO from these sites is determined by the protein conformation at the active site. In state  $A_1$ , recombination is maximal at 164 K whereas CO rebinding is maximal at 180 K in  $A_3$ .

In summary, the experiments presented here suggest that, in addition to a primary docking site B three remote docking sites (C,  $D_1$  and  $D_2$ ) exist in substate  $A_1$ . In substate  $A_3$ , site C either does not exist or could not be populated by our illumination protocols; only docking sites B,  $D_1$  and  $D_2$  could be identified. Substate  $A_2$  is only a minority species at cryogenic temperatures. Therefore, most photoproduct bands of this species may be too small to be detected, especially if they are superimposed by the photoproduct bands associated with  $A_1$  and  $A_3$ . Table 4.1 summarizes the band positions of the photoproduct bands in the distinct protein conformations.

Table 4.1: Assignment of photoproduct bands. Band positions were determined with an estimated error of  $\pm 1\text{ cm}^{-1}$ .

		A states			
		$A_1$	$A_2$	$A_3$	$A_4$
	band position ( $\text{cm}^{-1}$ )	1926	1936	1948	1956
B	band position ( $\text{cm}^{-1}$ )	2105, 2112, 2044			
	recombination temp. (K)	23		20	$\approx 20$
C	band position ( $\text{cm}^{-1}$ )	2128			
	recombination temp. (K)	97	$\approx 110$		
$D_1$	band position ( $\text{cm}^{-1}$ )	2120			
$D_2$	band position ( $\text{cm}^{-1}$ )	2129			
	recombination temp. (K)	164		$\approx 180$	

## 4.4 hIDO-CO/L-Trp: Docking Sites and Ligand Migration

In the following, changes in the photolysis yield and in geminate ligand recombination induced by L-Trp binding are discussed in detail. A first comparison of the photoproduct bands of the hIDO-CO (black curves) and hIDO-CO/L-Trp (red curves) proteins was shown in Figure 4.1. Upon L-Trp addition to the sample, photoproduct bands associated with site B could no longer be identified. However, bands at 2112, 2123, 2130 and 2136  $\text{cm}^{-1}$  were produced under slow cool illumination. These bands will be named  $D_{L1}$ ,  $D_{L2}$ ,  $D_{L3}$  and  $D_{L4}$ , respectively.

Figure 4.1 also revealed significant changes in the photolysis yield after L-Trp binding. Both hIDO-CO and hIDO-CO/L-Trp were illuminated for 10 s at 4 K. While the photolysis yield was almost 100% in hIDO-CO, only a small fraction of hIDO-CO/L-Trp could be photolyzed.

To get more detailed information on the photolysis kinetics, samples of hIDO-CO and hIDO-CO/L-Trp were cooled to 4 K and illuminated for 15,000 s (Figure 4.8). Using a neutral density filter (3-OD), the laser intensity was attenuated 1,000-fold in comparison to the standard laser intensity (150 mW). Transmission spectra were collected continuously during illumination. FTIR photolysis difference spectra were calculated according to Equation 2.6. Figure 4.8 a shows the evolution of the FTIR photolysis difference spectra of hIDO-CO (black lines) and hIDO-CO/L-Trp (red lines) with time. The absorbance changes in the bands of  $A_1$  (black filled squares),  $A_3$  (black empty squares) of hIDO-CO and  $A_L$  (red cycles) are plotted as a function of time (Figure 4.8 b). For comparison, we added the temporal development of the amplitudes at the position of the  $A_1$  (red filled squares) and  $A_3$  (red empty squares) bands of hIDO-CO/L-Trp. In both A states of hIDO-CO, trapping of CO at the primary docking site after photodissociation is much more efficient than in the proteins that have L-Trp bound at the active site. It takes  $\approx 4,000$  s and hence 4 s without the density filter, to photolyse almost all CO in hIDO-CO. However, illumination of 15,000 s at 4 K photolyzes only a small fraction of CO in proteins with L-Trp bound at the active site ( $\approx 20\%$ ). The development in the  $A_{SF}$  bands of hIDO-CO/L-Trp is similar to the evolution in the  $A_{SF}$  bands of hIDO-CO.

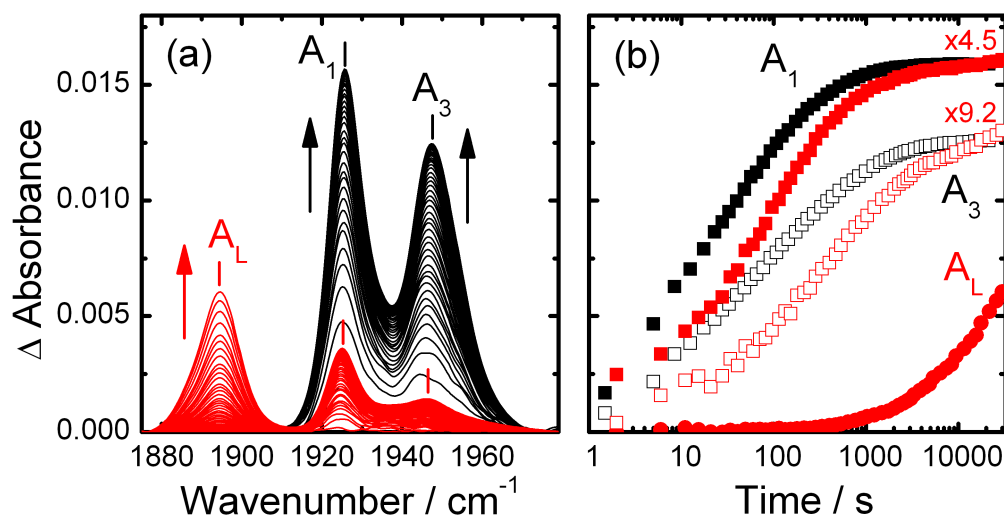


Figure 4.8: Comparison of photolysis yield in hIDO-CO and hIDO-CO/L-Trp. Development of 4-K FTIR photolysis spectra collected during laser illumination through a 3-OD neutral density filter at 4 K (laser power 150 mW). (a) Evolution of the FTIR absorbance spectra of hIDO-CO (black lines) and hIDO-CO/L-Trp (red lines) upon light exposure. (b) Amplitudes of the  $A_1$  (filled squares),  $A_3$  (empty squares) and  $A_L$  (circles) bands of hIDO-CO (black) and hIDO-CO/L-Trp (red). For better comparison, the absorbances of hIDO-CO/L-Trp at the positions of  $A_1$  and  $A_3$  were scaled to match those of hIDO-CO.

To investigate ligand recombination in hIDO-CO/L-Trp, TDS experiments were performed (Figure 4.9). TDS data after 10-s illumination at 4 K are plotted as contour maps in Figure 4.9 a (IP No.1). Selected FTIR photolysis difference spectra of this experiment are shown in Figure 4.9 b. Recombination of CO in  $A_L$  is maximal at 35 K. The pronounced wavenumber shift with temperature in the absorbance change might be caused by kinetic hole burning<sup>[128,129]</sup>. This effect is ascribed to the structural heterogeneity of the CO environment and the linear relation between an energy barrier and the stretching frequency. Kinetic hole burning was observed earlier in the A bands of CO-ligated neuroglobin<sup>[106]</sup> or in the Soret band of Mb<sup>[129]</sup>. The corresponding absorbance spectra shown in Figure 4.9 b demonstrate that CO recombination in  $A_L$  is almost complete at 60 K.

The TDS plot in Figure 4.9 a shows that CO recombination in the  $A_{SF'}$  states occurs at  $\approx 20$  K, similar to recombination in hIDO-CO (compare Figure 4.5). The TDS contour plot in Figure 4.9 c displays absorbance changes in the bands of heme-bound CO recorded after cooling the sample from 160 to 4 K under light (IP No. 2). Maximal recombination in  $A_L$  occurs at  $\approx 45$  K.

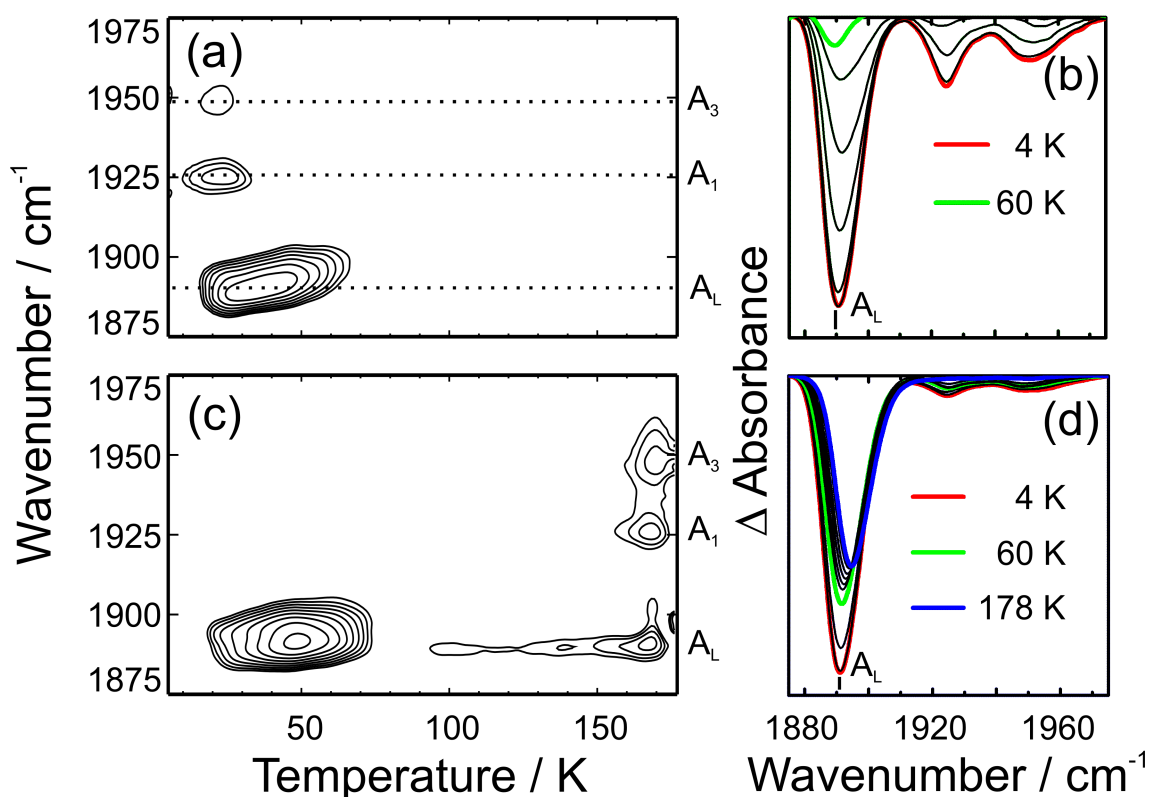


Figure 4.9: Geminate rebinding of CO in hIDO-CO/L-Trp. (a, c) TDS maps of hIDO-CO/L-Trp (a) after 10-s illumination at 4 K (IP No.1) and (c) after slow cooling from 160 K to 4 K under light (IP No.2)(b, d) FTIR photolysis difference spectra collected during the TDS measurements. Data were published previously<sup>[130]</sup>

Small absorbance changes in the  $A_L$  band of hIDO-CO/L-Trp extend from 90 to 178 K. Recombination of CO to the protein fraction  $A_{SF}$  is complete at 180 K. Selected FTIR photolysis spectra of this measurement are plotted in Figure 4.9d. The decrease in the band intensity of  $A_L$  between 4 and 60 K represents recombination from the primary docking site B. The intensity change in the band of heme-bound CO between 60 and 178 K is significantly smaller. Additionally, a band shift from 1892 to 1894  $\text{cm}^{-1}$  due to an intrinsic temperature dependence of the band is observed. The spectra reveal that, at 178 K, only about 50% of the total protein population has rebound the ligand.

To examine rebinding of CO from the secondary docking sites, hIDO-CO/L-Trp was illuminated at 160 K for 15,000 s. Subsequently, the sample was cooled to 4 K in the dark to populate only the remote docking sites D. A transmission spectrum was recorded at 4 K and referenced against the transmission spectrum recorded before illumination according to Equation 2.6. This 4-K FTIR photolysis difference spectrum displays the overall photolyzed CO. To determine the extent of CO recombination between 160 K and after a temperature cycle to 180 K, the sample temperature was increased to 180 K and, subsequently, decreased back to 4 K. A spectrum was measured again and referenced against the transmission spectrum recorded before illumination. Comparison of 4-K FTIR photolysis spectra ensures that the changes between the spectra measured after illumination at 160 and 180 K are solely caused by CO rebinding. Changes due to intrinsic temperature effects are excluded. The temperature cycling was repeated several times with increasing maximal temperatures. The spectra collected after the different temperature cycles are compiled in Figure 4.10. Immediately after illumination at 160 K, the 4-K FTIR photolysis spectrum depicts a dominant  $A_L$  band and weak  $A_{SF}$  bands (black line). Four photoproduct bands are observed,  $D_{L1}$ ,  $D_{L2}$ ,  $D_{L3}$  and  $D_{L4}$ .

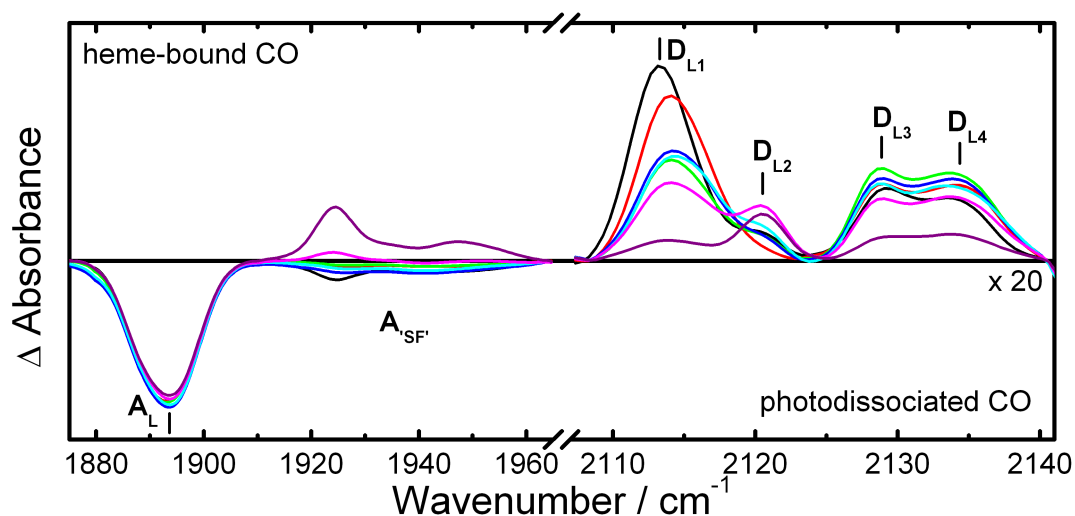


Figure 4.10: Recombination of CO in hIDO-CO/L-Trp at  $T > 160$  K. The sample was illuminated for 15,000 s at 160 K and subsequently cooled to 4 K in the dark. A cycle of heating and cooling was performed. 4-K FTIR photolysis spectra recorded after a temperature increase to 160 K (black), 180 K (red), 190 K (green), 200 K (blue), 210 K (cyan), 220 K (magenta) and 230 K (violet) are plotted.

In the  $A_L$  bands, no absorbance change is observed upon cycling up to 230 K. In the minor fraction  $A_{SF'}$ , recombination of CO is complete at 190 K; the  $A_{SF'}$  bands have decayed to zero. After a temperature excursion to 230 K,  $A_{SF'}$  bands with a positive amplitude develop, implying that an excess fraction of  $A_{SF'}$  has evolved. This phenomenon will be discussed in detail in Chapter 6.

Because the  $A_L$  band does not show rebinding for the temperature cycles reaching 220 K as maximal temperature, we do not expect changes in the bands of photodissociated CO. Accordingly, the intensities of the bands  $D_{L3}$  and  $D_{L4}$  are sufficiently stable. However, the bands  $D_{L1}$  and  $D_{L2}$  reveal changes between 160 and 190 K. Whereas  $D_{L2}$  decreases to zero amplitude,  $D_{L1}$  exhibits a blue shift to  $2114\text{ cm}^{-1}$  and, simultaneously, a loss of intensity ( $\approx 40\%$ ). We assume that the decay of the  $D_{L2}$  band represents recombination of CO in the small fraction of  $A_{SF'}$ . However, the significant intensity decrease in band  $D_{L1}$  cannot be explained by CO recombination to  $A_L$  or  $A_{SF'}$ . No interconversion between the photoproduct bands is observed. Possibly, some CO ligands escape into the solvent and give rise to a broad absorbance band that cannot be distinguished from the background.

Upon a temperature increase to 200 and 210 K, the intensity of the bands is constant. Only after the temperature cycles reached 220 K, a decrease in the photoproduct bands was observed, representing the onset of CO rebinding. Simultaneously, the amplitude of the  $A_{SF'}$  bands turns positive indicating CO recombination to an L-Trp-free-like protein (see Chapter 5).

In summary: After brief illumination at low temperatures, several B bands appear in the photoproduct spectrum of hIDO-CO, indicating that primary docking sites become populated. Upon addition of L-Trp, these definite B bands are no longer present (Figure 4.1). Simultaneously, the CO photolysis yield is significantly lower in L-Trp-bound proteins. Whereas 10-s illumination at 4 K is sufficient to photolyze almost 100% of CO in hIDO-CO, only about 20% of CO is photolyzed in hIDO-CO/L-Trp (Figure 4.8). L-Trp at the active site also influences ligand recombination. Rebinding from the primary docking site in hIDO-CO to the heme iron peaks at about 20 K. Binding of L-Trp shifts the maximal recombination temperature to 35 K (Figure 4.9). On the basis of these results, we conclude that the B site is at least partly blocked by L-Trp bound at the active site or hinders the access to that site. At the same time, this results in a resistance to CO recombination to the heme iron. Upon L-Trp addition to hIDO-CO, new photoproduct bands are observed after slow cool illumination (Figure 4.1). The TDS plot recorded after this illumination procedure revealed no significant recombination of CO below 180 K with the exception of minor CO rebinding at  $\approx 100\text{ K}$  (Figure 4.9). This process might be associated with recombination of a small fraction of photolyzed CO in site C similar to hIDO-CO where the C site is only weakly populated by a slow cool illumination. Due to the low population, a C band cannot be resolved. Therefore, the photoproduct bands observed after slow cool illumination belong to

photolyzed CO hosted in the remote docking sites D. The shift of the photoproduct band suggests either that these sites are newly generated by L-Trp binding or that L-Trp binding changes the electric field in the docking sites D. Recombination from these sites does not occur below 220 K.

## 4.5 L-Trp Analogues

In Chapter 3.5 we have shown that the active site structure determines the binding affinity and variability of the position of substrate analogues at the active site of hIDO-CO. The individual modes of binding might also affect the accessibility of the CO docking sites and geminate recombination of the ligand after photolysis. Changes in the photoproduct bands and the recombination of CO after binding of D-Trp, S-Trp and MLT to hIDO-CO may, in return, provide information on the substrate position. The structures of the L-Trp analogues are shown in Appendix B.

Figure 4.11 shows 6-K FTIR photolysis spectra of hIDO-CO/D-Trp (green), hIDO-CO/S-Trp (blue) and hIDO-CO/MLT (cyan) after 10-s illumination at 6 K (IP No.1) and after cooling the samples from 160 to 6 K under light (IP No.2) (left panels: a, c, e). Immediately after the slow cooling illumination procedure (IP No.2), a TDS experiment was started, recording FTIR spectra every kelvin from 6 to  $\approx 170$  K. Figure 4.11 b, d and f shows the absorbance changes at the peak maxima in the A state bands as a function of temperature. The peak absorbance changes indicate the major CO recombination temperatures.

Figure 4.11 a displays 6-K FTIR photolysis spectra of hIDO-CO/D-Trp (green) and hIDO-CO (black) recorded after 10-s illumination at 6 K (dotted lines) (IP No.1) and after cooling the sample from 160 K to 4 K under light (solid lines) (IP No.2). The spectra of heme-bound CO have already been discussed in detail (Chapter 3.5). In comparison to the photoproduct bands of hIDO-CO, the bands of hIDO-CO/D-Trp do not display significant differences, indicating that the binding of D-Trp does not affect the nature and accessibility of the docking sites. The absorbance changes (Figure 4.11 b) show that recombination occurs in two steps in hIDO-CO/D-Trp, at  $\approx 20$  K and at temperatures  $> 160$  K. These results are again very similar to hIDO-CO (Figure 4.5). Obviously, D-Trp bound to hIDO-CO does not influence CO geminate recombination.

In Figure 4.11 c, 6-K FTIR photolysis spectra of hIDO-CO/S-Trp (blue) are plotted. S-Trp addition to the sample has only a small influence on the photoproduct bands. After 10-s illumination at 6 K, two distinct B bands are observed at 2106 and 2145  $\text{cm}^{-1}$ . These band positions are similar to the B band positions seen in hIDO-CO, but the relative amplitudes of the bands have changed. The photoproduct bands obtained after prolonged illumination have identical positions as the

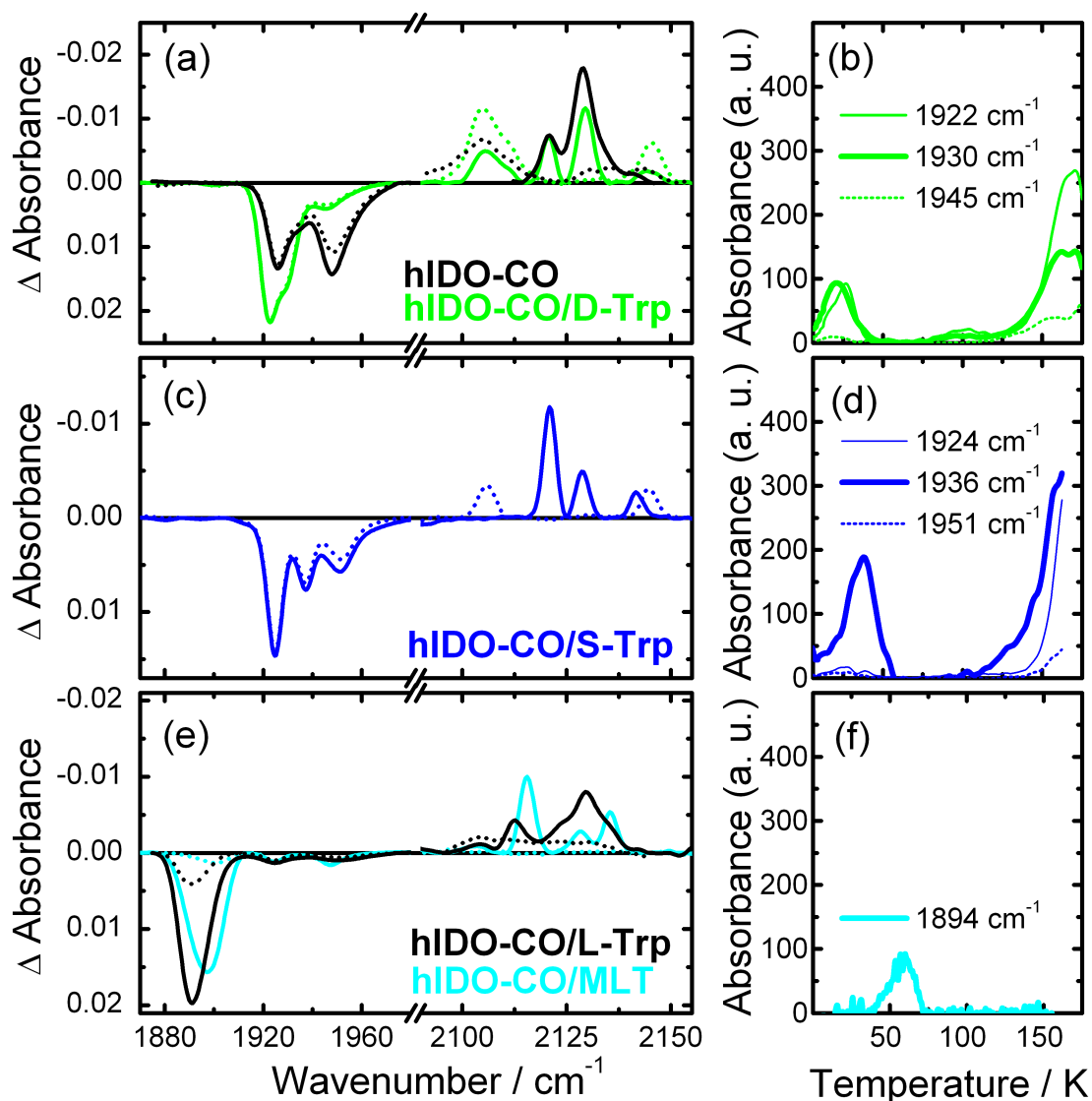


Figure 4.11: FTIR photolysis difference spectra and integrated absorbance changes as a function of temperature of (a,b) hIDO-CO/D-Trp (green), (c,d) hIDO-CO/S-Trp (blue) and (e,f) hIDO-CO/MLT (cyan). Left panels: 6-K FTIR photolysis difference spectra after 10-s illumination at 6 K (dotted lines) (IP No.1) and after continuous illumination while cooling from 160 to 6 K (solid lines) (IP No.2). For comparison, the spectra of hIDO-CO and hIDO-CO/L-Trp recorded after identical illumination protocols were added in (a) and (e), respectively (black lines). Right panels: Absorbance changes as a function of the temperature determined at selected wavenumbers. Data was recorded after continuous illumination while cooling from 160 to 6 K (IP No.2).

D bands observed in substrate-free hIDO. However, the relative intensities differ, indicating that the relative CO populations in the docking sites are influenced. Apparently, the S-Trp molecule in the distal pocket does not change the electric field in the existing docking sites but affects the relative populations within the sites. In Figure 4.11d, we plot the absorbance changes as a function of temperature at 1924, 1936 and 1951  $\text{cm}^{-1}$  recorded after cooling the sample from 160 to 6 K under light. Absorbance changes in the bands 1924 and 1951  $\text{cm}^{-1}$  occur only above 160 K, indicating that CO recombines exclusively from remote docking sites. Recombination in the A state with a band at 1936  $\text{cm}^{-1}$  is maximal at 38 K. A further maximum in the absorbance change is observed at temperatures above 160 K. In comparison to hIDO-CO, in the A state band at 1936  $\text{cm}^{-1}$ , rebinding from site B is affected whereas recombination of CO from remote docking sites is similar.

The FTIR photolysis spectra of hIDO-CO/MLT (cyan) and hIDO-CO/L-Trp (black) are compared in Figure 4.11e. The spectra show similarities in both the bands of heme-bound and photodissociated CO. The 6-K FTIR photolysis spectra of heme-bound CO of hIDO-CO/MLT reveal that the binding position of this L-Trp analogue must be almost identical to the one of L-Trp (Chapter 3.5). After 10-s illumination at 4 K, only a minute fraction of the CO is photolyzed in hIDO-CO/L-MLT (IP No.1). Consequently, B bands are absent in the photoproduct spectrum. Prolonged illumination traps ligands at more remote docking sites (IP No.2). As observed for hIDO-CO/L-Trp, the photoproduct bands representing CO at secondary sites are different from those in hIDO-CO. The spectrum displays three photoproduct bands. Compared to hIDO-CO/L-Trp, the band positions differ slightly. In Figure 4.11f absorbance changes at 1894  $\text{cm}^{-1}$ , recorded after slow cool illumination, are plotted as a function of temperature. The results demonstrates that binding of MLT to hIDO-CO influences CO recombination significantly. The absorbance changes display a weak recombination process of CO at  $\approx 58$  K. No further recombination is observed below 160 K. These results indicate that geminate recombination from remote docking sites is hindered by binding of MLT at the active site. We assume that MLT also blocks the B site similar to L-Trp and, therefore, prohibits CO release from and CO recombination to the binding site.

Summarizing the results, we have shown that D-Trp neither changes the photoproduct bands nor the geminate recombination process. Interference of the substrate with the accessibility of the ligand docking sites is unlikely. Upon addition of S-Trp, the positions of the photoproduct bands are not significantly changed. However, the band intensities are changed from substrate-free protein, indicating a change in the population equilibria of the docking sites. Additionally, differences in CO recombination are observed in the A state associated with a band at 1936  $\text{cm}^{-1}$ .

Recombination from the B site at  $\approx 38$  K is markedly increased with respect to hIDO-CO. Because the photoproduct bands are not significantly changed, we presume that access to the B site is blocked by S-Trp binding.

MLT changes the photoproduct bands and CO recombination. The changes are very similar to the ones seen upon L-Trp addition, confirming again that binding of MLT and L-Trp at the active site is identical. The slight changes in the photoproduct bands are likely based on the additional methyl group. This is a first hint that the methyl group of the MLT side chain may be positioned in the vicinity of the docking sites.

## 4.6 Conclusions

Many years of research on Mb have proven that ligand binding and release are mediated by the primary and secondary docking sites in the protein matrix. Especially the B site is of utmost importance. Immediately after photodissociation, the ligand occupies this site close to the heme iron. From there, it either rebinds to the heme iron, escapes to secondary docking sites or exits into the solvent. The actual rebinding step can only occur from site B. Rebinding from either the solvent or the secondary docking sites, the ligand settles at site B again and has the choice to rebind or escape into the protein matrix or the solvent. For Mb at physiological temperatures, it is known that the CO returns to the solvent about 40 times before, finally, the covalent bond between the CO and the heme iron is formed<sup>[124]</sup>.

We could show that in hIDO-CO, in addition to a primary docking site close to the ligand binding site, additional secondary docking sites exist. Interestingly, the number of docking sites differs for the analyzed A states of hIDO-CO, indicating that structural differences exist between the protein matrices of these substates.

After addition of L-Trp to hIDO-CO, no B photoproduct bands are observed anymore. Moreover, binding of L-Trp at the active site changes the CO release from and the CO recombination to the heme iron significantly, as indicated by the low photolysis yield upon photolysis at 4 K and the increased recombination temperature of CO after photolysis. We suggest that L-Trp binding at the active site occupies the B site or that L-Trp binding blocks access to that site.

However, new photoproduct bands appear in the spectrum of hIDO-CO/L-Trp after slow cool illumination. This result shows that L-Trp either changes the electric field in the existing docking sites or gives rise to new docking sites. CO recombination from these remote docking sites D does not occur below 220 K. At this temperature, large scale motions of the protein are facilitated and L-Trp can exit the active site (see also Chapter 5).

Upon addition of MLT to hIDO-CO, we again observed changes in the photoproduct bands. Because of the very similar  $A_L$  band, the L-Trp analogue is expected

to bind in an almost identical position as L-Trp and, therefore, differences in the photoproduct band positions are most likely based on the methyl group at the 'indole' moiety. The methyl group might change the electric field at the secondary docking site. Similar to L-Trp, binding of MLT to hIDO-CO changes geminate recombination of the ligand to the heme iron.

The photoproduct spectra of hIDO-CO/D-Trp and hIDO-CO/S-Trp are highly similar to those of hIDO-CO. Binding of these analogous does not significantly modify the electric field at the primary and secondary docking sites. Changes in the CO recombination are only observed in hIDO-CO/S-Trp. Whereas rebinding of CO from the secondary docking sites occurs at similar temperatures as in hIDO-CO, maximal recombination from the primary docking site shifts to higher temperatures, indicating that S-Trp influences the accessibility of the primary docking site.

Our experiments have shown that L-Trp binding almost completely blocks geminate recombination of CO to the heme iron after photolysis. The hIDO-Fe<sup>2+</sup>/L-Trp complex inhibits binding of the ligand at the active site of the protein; formation of a ternary complex is hindered. Hence, we assume that the enzyme activity is influenced by the order of ligand and substrate binding. L-Trp binding studies revealed that the affinity of L-Trp towards the deoxy protein ( $K_d = 400 \mu\text{M}$ ) is much lower than towards ligated protein<sup>[131]</sup>. The  $K_m$  of L-Trp towards hIDO-O<sub>2</sub> was determined as  $15 \mu\text{M}$ <sup>[54]</sup>. The L-Trp dissociation coefficient of hIDO-CO is  $K_d = 95 \mu\text{M}$  (compare Chapter 6). The results of binding studies and our experiments clarify the discussed order about the binding of ligand and substrate: The ligand must bind before the substrate occupies the active site and, thereby, blocks access to the B site. As soon as the ternary complex is formed, the ligand is trapped at the active site by L-Trp. The probability of the ligand to leave the L-Trp bound protein is low. At the same time, the binding affinity of L-Trp to the ligated hIDO is high. A strong complex of protein, substrate and ligand is formed that is only broken by the catalytic reaction.

# Chapter 5

## L-Trp Migration

It was shown in Chapter 4.4 that CO recombination from remote docking sites in hIDO-CO/L-Trp is significant only above 220 K. The presence of L-Trp at the active site prevents rebinding of the photodissociated ligand to the heme iron.

In this chapter we investigate the recombination process of CO in L-Trp-bound protein applying isothermal kinetic measurements. We elucidate the escape of L-Trp from the active site required for CO rebinding to the heme iron. Kinetic experiments and FTIR photolysis difference spectroscopy were used to track L-Trp within the protein matrix.

### 5.1 Photolysis at $T \geq 200$ K

To obtain further insight into CO recombination in hIDO-CO/L-Trp, CO photodissociation and relaxation experiments were performed on both hIDO-CO and hIDO-CO/L-Trp between 200 and 260 K. Initially, a 'dark' transmission spectrum was recorded. Then, the samples were illuminated for 100 s. Subsequently, the samples were kept in the dark for 5,000 s to allow CO recombination. In this time period, transmission spectra were collected in logarithmically spaced time intervals. FTIR photolysis difference spectra were calculated as described in Chapter 2.5.4.

In Figure 5.1, we plot the spectra collected at two selected temperatures, 200 K (panels a and b) and 240 K (panel c). The photolysis difference spectra of hIDO-CO and hIDO-CO/L-Trp at 200 K are shown in Figure 5.1 a and b, respectively. The  $A_{SF}$  bands of hIDO-CO plotted with negative amplitudes represent CO missing at the heme iron due to photolysis. These bands disappear over time (thin black lines) (Figure 5.1 a), indicating recombination of the ligands at the heme iron. The process is finished after  $\approx 300$  s. Figure 5.1 b shows the development of FTIR photolysis difference spectra of hIDO-CO/L-Trp over time (thick black lines). In the  $A_{SF}$

bands, similar kinetics are seen as in the  $A_{\text{SF}}$  bands of hIDO-CO (compare Figure 5.1 d, black filled squares ( $A_{\text{SF}'}$ ) and black empty squares ( $A_{\text{SF}}$ )). Within 300 s, all CO ligands rebind to the small fraction of presumably substrate-free hIDO-CO. In contrast, the  $A_{\text{L}}$  band, representing L-Trp-bound proteins, remains constant. No CO rebinds to the substrate-bound enzyme to form hIDO-CO/L-Trp.

Figure 5.1 c shows 240-K FTIR photolysis difference spectra of hIDO-CO/L-Trp (thick red lines). The band  $A_{\text{L}}$  remains essentially constant for 100 s after photolysis, indicating that CO does not rebind in L-Trp-bound hIDO (top panel in Figure 5.1 c). In the same time period, however, the  $A_{\text{SF}'}$  bands change significantly. In a first step (1),  $A_{\text{SF}'}$  decays to zero, implying that all molecules accounting for these bands rebind CO. This process is complete within  $\approx 1$  s. Similar kinetics were obtained in a control experiment with hIDO-CO (data not shown). Surprisingly, the amplitude of  $A_{\text{SF}'}$  turns positive with  $t_{1/2} \approx 15$  s (Figure 5.1, step 2). Therefore, additional, apparently L-Trp-free hIDO-CO molecules must have been generated. In the following, we will refer to these molecules as hIDO-CO/--L-Trp.

Obviously, CO photodissociation has led to escape of L-Trp from the active site to yield a protein conformation that is spectrally identical to  $A_{\text{SF}}$ . CO recombination to hIDO-CO/--L-Trp, is significantly slower compared to  $A_{\text{SF}'}$  molecules, implying that L-Trp is still bound in the protein matrix and affects the CO rebinding kinetics. We denote this newly occupied site as the secondary, inhibitory binding site.

In a last step (step 3, Figure 5.1 c), the initial equilibrium state is restored. Both the excess  $A_{\text{SF}}$  and  $A_{\text{L}}$  bands decay to zero. The crisp isosbestic point at  $1917 \text{ cm}^{-1}$  suggests a two-state transition with  $t_{1/2} \approx 300$  s. This transition is not associated with rebinding but rather represents the return of L-Trp to its primary binding site at the fully CO-ligated hIDO active sites.

Figure 5.1 shows the temporal development in the  $A_{\text{SF}}$  (panel d) and  $A_{\text{L}}$  (panel e) bands at different temperatures between 200 K and 260 K. The data were normalized by their peak areas. The numbers correspond to the steps shown in Figure 5.1 c.

The experiments demonstrate impressively that L-Trp has to leave the active site before CO can rebind to the heme iron. Only then, the protein returns to its equilibrium state, hIDO-CO/L-Trp.

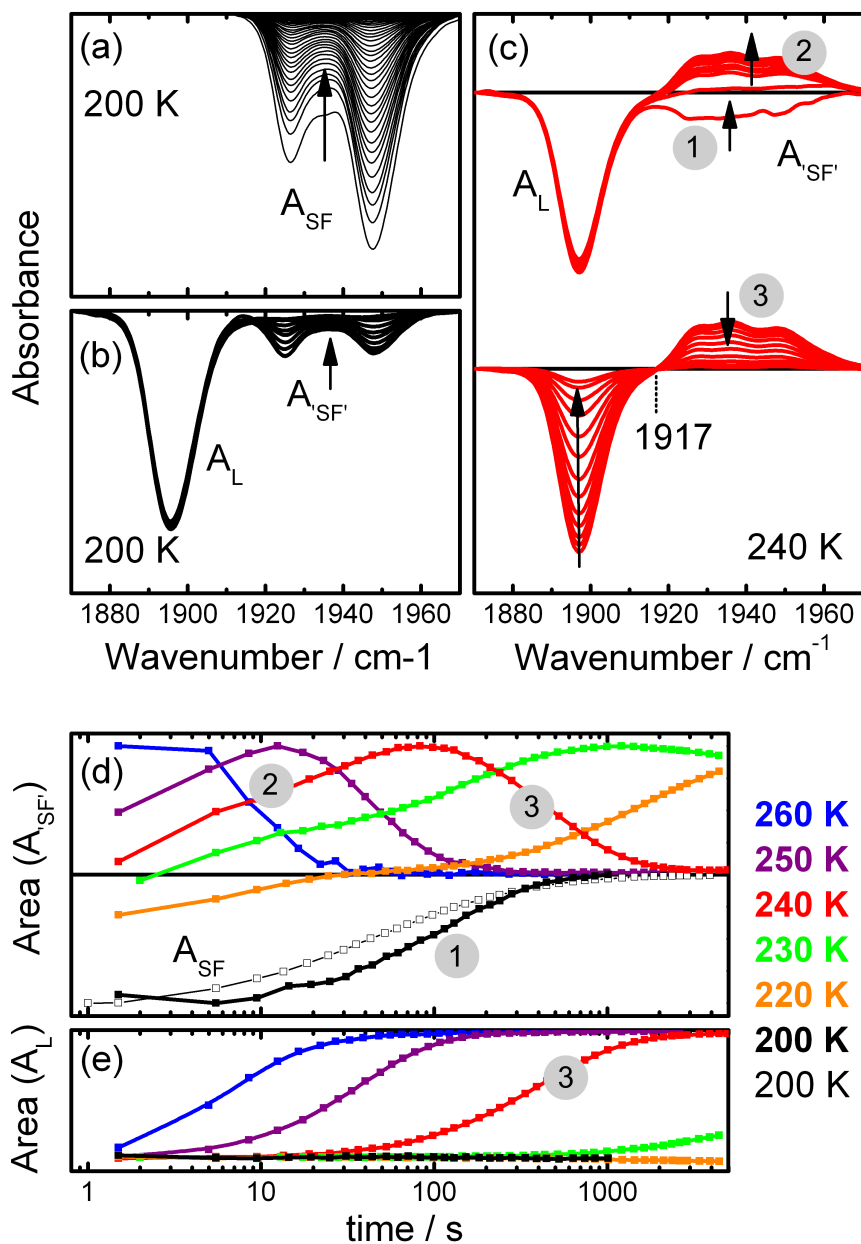


Figure 5.1: CO recombination kinetics in hIDO-CO/L-Trp. (a - c) Temporal development of FTIR photolysis difference spectra. (a) hIDO-CO (200 K), (b, c) hIDO-CO/L-Trp at 200 (b) and 240 K (c). Processes in time are indicated by arrows. (d, e) Temporal development of the normalized  $A_{SF'}$  and  $A_L$  band areas of hIDO-CO/L-Trp at 260 K (blue symbols), 250 K (violet), 240 K (red), 230 K (green), 220 K (orange), 200 K (black), and hIDO-CO at 200 K (black open symbols). Numbers refer to reaction steps. Data were published previously<sup>[132]</sup>.

## 5.2 Photolysis at $T < 200$ K

The isothermal kinetic measurements described in Chapter 5.1 have shown that L-Trp exits the active site after photodissociation of CO at  $T \geq 200$  K. In this temperature region, large scale motions are present that most likely are required for L-Trp escape. We assume that the CO ligands escape into the solvent upon photolysis. The following experiment was performed to elucidate whether L-Trp migration also occurs when CO is trapped at transient docking sites within the protein.

To this end, a hIDO-CO/L-Trp sample was illuminated at 100 K for 15,000 s (Figure 5.2). At this temperature, the CO is trapped in the protein matrix. Large-scale motions are arrested. The FTIR photolysis difference spectrum recorded immediately after illumination (thick black line) shows the  $A_L$  and  $A_{SF}$  bands, indicating the fractions of photolyzed hIDO-CO/L-Trp and hIDO-CO in the sample. Afterwards, the sample temperature was increased to 237 K and another spectrum was measured (black thin line). We observe a shift in the  $A_L$  band caused by the temperature increase. Simultaneously,  $A_{SF}$  bands with positive amplitudes occur, indicating a L-Trp-free hIDO-CO species. The experiment was repeated, illuminating the sample at 120, 140 and 160 K. With increasing temperature, the amplitude of the  $A_L$  band and thus the fraction of photolyzed hIDO-CO/L-Trp as well as the fraction of hIDO-CO/--L-Trp increase, indicating that the photoproduct yield correlates directly with the amount of hIDO-CO/--L-Trp molecules.

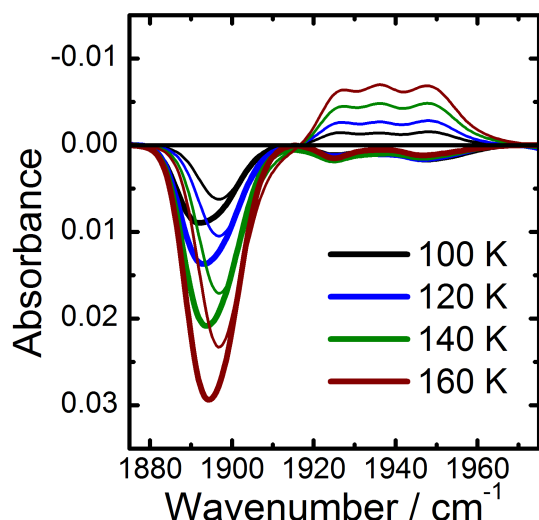


Figure 5.2: Formation of hIDO-CO/--L-Trp after photolysis at  $T < 200$  K. FTIR photolysis difference spectra of hIDO-CO/L-Trp after 15,000-s illumination at 100 K (black), 120 K (blue), 140 K (green) and 160 K (dark red). Spectra drawn with thin lines were measured after illumination plus temperature excursion to 237 K.

Obviously, it is the absence of CO at the binding site that triggers L-Trp migration away from the active site. It is not important for L-Trp escape whether the CO leaves into the solvent or whether the ligand is trapped at secondary docking sites.

### 5.3 Tracking L-Trp in the Enzyme

We have shown that CO photodissociation induces escape of L-Trp from the active site. The observation that ligand recombination in the newly generated hIDO-CO/--L-Trp molecules is slower than in substrate-free hIDO-CO indicates that the L-Trp does not leave the protein matrix and, at its new secondary docking site, slows CO rebinding. If the new L-Trp position is close to or even coincide with a CO docking site, we should expect changes in the photoproduct spectra.

Figure 5.3 shows the 4-K FTIR photolysis difference spectra of hIDO-CO (black thick line) and hIDO-CO/L-Trp (red thick line), recorded after continuous illumination from 160 K to 4 K. To generate the hIDO-CO/--L-Trp species, the hIDO-CO/L-Trp sample was illuminated for 100 s at 230 K to photodissociate the CO and to prompt L-Trp to exit the active site. Subsequently, the sample was kept in the dark at 230 K for 1,000 s to ensure complete CO rebinding (compare Figure 5.1 e). Within this time interval, L-Trp does not return to the active site. Subsequently, the sample was cooled to 4 K to trap this non-equilibrium conformation, with the CO bound to the heme iron and the L-Trp populating the secondary binding site. After measuring a transmission spectrum at 4 K, the CO was photodissociated by applying the slow cool illumination protocol (IP No.2). The 4-K FTIR photolysis difference spectrum determined afterwards is shown as a red thin line in Figure 5.3.

The A bands in the spectrum are similar to those of hIDO-CO (Figure 5.3; black thick line), verifying that L-Trp is no longer present at the active site. The small  $A_L$  band represents a minor fraction of hIDO-CO/L-Trp that reformed during cooling. The photoproduct spectrum is essentially indistinguishable from that of hIDO-CO. Thus, L-Trp at the secondary binding site does not affect the vibrational bands of the photodissociated CO, indicating that L-Trp has no contribution to the electric fields sensed by the CO ligands in the docking sites. L-Trp at the inhibitory docking site is spectroscopically silent.

### 5.4 Monitoring the Heme

The binding of L-Trp changes the Soret band position of CO-ligated hIDO. Therefore, we expect the process of L-Trp migration to affect this band as well. Figure 5.4a presents the Vis spectra of hIDO-CO (black dashed line) and hIDO-CO/L-Trp (red line) at 240 K, displaying Soret bands at 420 and 416 nm. Both samples were illuminated for 3 min at 240 K. In the substrate-free protein, CO recombination was complete within 1 s after switching off the laser (data not shown). In contrast, the spectrum of hIDO-CO/L-Trp displayed two Soret bands at 438 nm and 420 nm immediately after illumination, indicating a mixture of deoxy

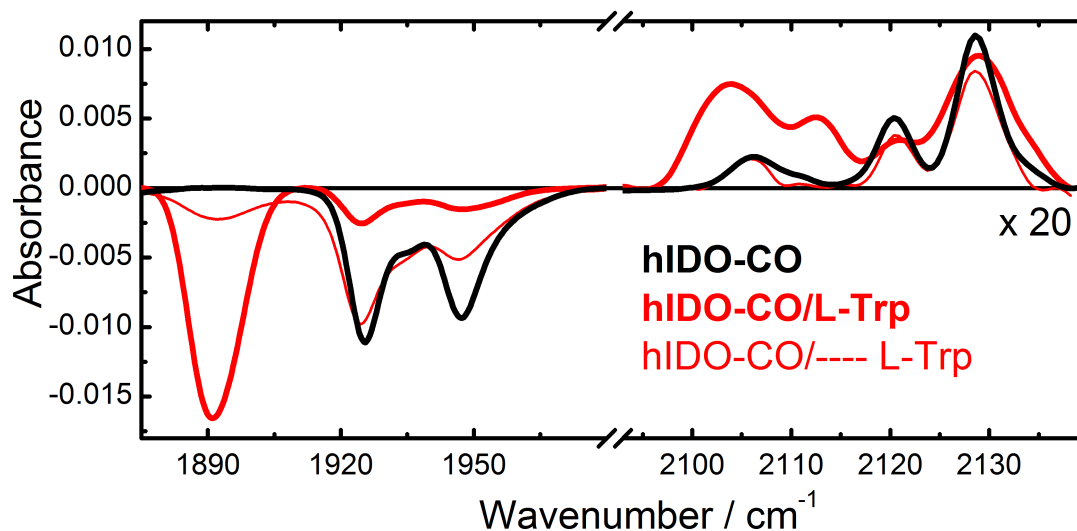


Figure 5.3: Tracking L-Trp in the protein matrix. 4-K FTIR photolysis difference spectra. Red thick line: hIDO-CO/L-Trp, L-Trp at the active site. Red thin line: hIDO-CO/L-Trp, L-Trp removed from the active site. Black thick line: hIDO-CO. Adapted from Reference<sup>[132]</sup>.

hIDO and hIDO-CO (green line). A band at 415 nm was absent, suggesting that there is no significant fraction of CO-ligated protein with L-Trp at the active site in the sample. Subsequently, the sample was kept in the dark and the development of the Soret bands was observed over time by collecting spectra continuously. The spectrum recorded 30 min after illumination is marked in blue. Within the 30-min interval, the intensity of the Soret band at 420 nm increased, indicating that CO rebound to a hIDO conformation with the spectral signature of hIDO-CO. Relaxation to the hIDO-CO/L-Trp conformation was not observed within 30 min. The CO recombination kinetics are slower than for hIDO-CO, suggesting that L-Trp is at the secondary binding site and hinders rebinding. The isosbestic point at 427 nm indicates a two-state transition between the deoxy hIDO and hIDO-CO states.

These results support the conclusion that L-Trp exits the active site after photodissociation of CO and, subsequently, positioned at a secondary docking site, slows the CO recombination as drawn from the FTIR experiments (Chapter 5.1). The differences in the CO and L-Trp relaxation times in the two experiments result from the different glycerol concentrations.

The experiment was repeated at 245 K and 250 K (Figure 5.4 b and c). At 245 K, the intensity increase of the Soret band at 420 nm was accompanied by a peak shift toward 416 nm, which shows that L-Trp migrates back to its initial position at the active site. At 250 K, the intensity increase and the band shift occur simultaneously on the experimental time scale.

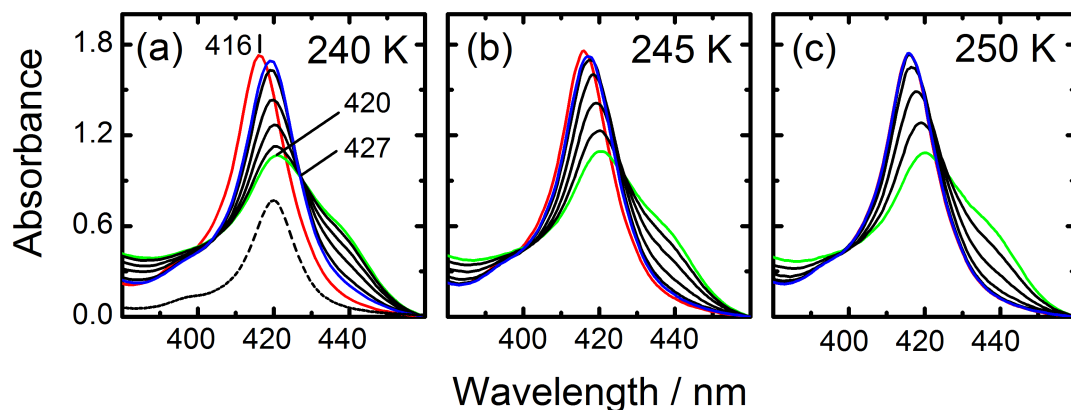


Figure 5.4: Vis absorption spectra of hIDO-CO/L-Trp measured before (red lines) and after photolysis at (a) 240 K, (b) 245 K and (c) 250 K. Spectra plotted as green lines were recorded immediately after illumination. The blue line represents the spectrum collected 30 min after photolysis. As a reference, the spectrum of hIDO-CO was added in (a) (dashed black line). The samples were prepared in 75%/25% (vol/vol) glycerol/100 mM KPb, pH 8). Data were published previously<sup>[132]</sup>.

The experiment was repeated with samples prepared with different L-Trp concentrations (Figure 5.5). Each sample was cooled to 240 K and illuminated for 3 min. Subsequently, spectra were recorded for 40 min. Selected spectra of three different samples with L-Trp concentrations of 20 mM, 4.8 mM and 0.64 mM are shown in Figure 5.5 a, b and c, respectively. From the absorbance spectra collected before illumination (red lines), we have analyzed the dependence of the Soret peak position on the L-Trp concentration (Figure 5.6 a). Binding of L-Trp at the active site of hIDO-CO can be described by a dissociation coefficient,  $K_d = 1.5 \pm 0.5$  mM. Note that this value was determined at 240 K for hIDO in 70% glycerol.

The absorbance spectra measured immediately after photolysis (green lines) show Soret bands at 420 and 438 nm, indicating a mixture of deoxy hIDO and hIDO-CO. With increasing concentrations of L-Trp, the intensity of the Soret band at 420 nm decreases and hence the fraction of hIDO-CO characterized by fast CO rebinding. The Vis spectra marked in blue were recorded 40 min after illumination (Figure 5.5). The grey area in Figure 5.5a represents the fraction of proteins that slowly rebind CO. The absorbance increase is observed at 420 nm at low L-Trp

concentrations. Thus these proteins appear as apparently substrate-free proteins, hIDO-CO/--L-Trp, with CO recombination hindered by L-Trp at the inhibitory docking site.

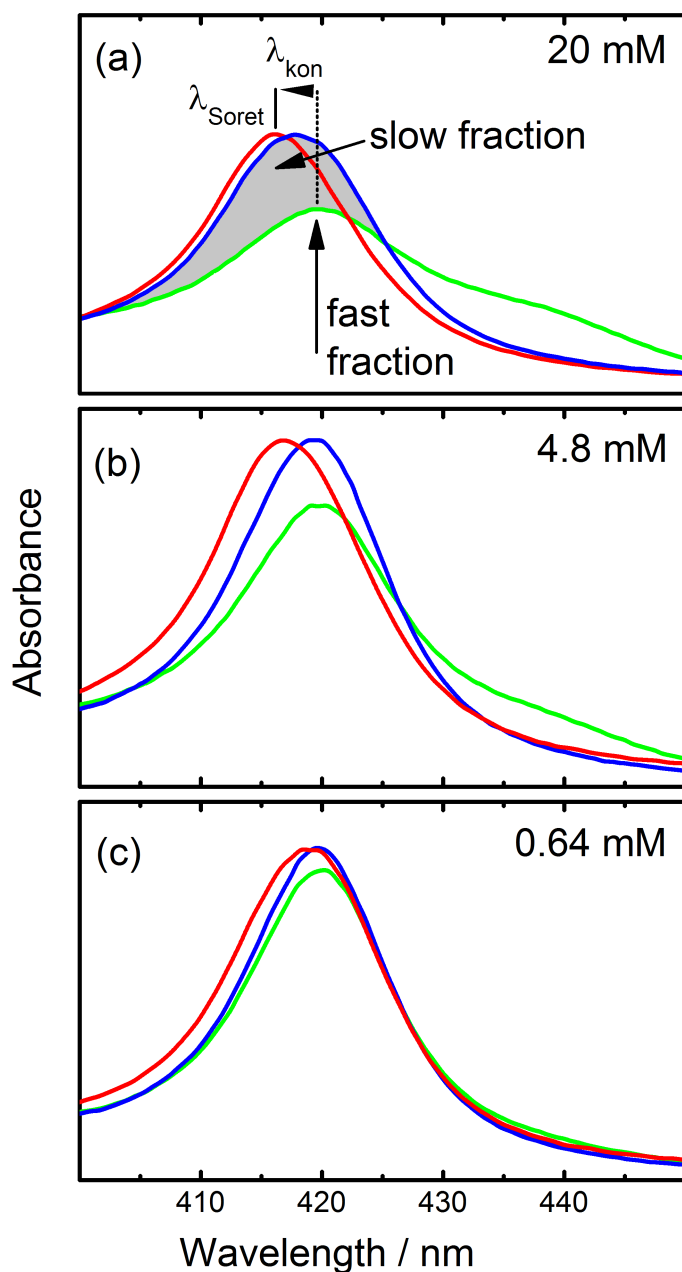


Figure 5.5: CO recombination at different L-Trp concentrations. Vis spectra of hIDO-CO/L-Trp measured before photolysis (red line), immediately after photolysis (green line) and 40 min after photolysis (blue line) at 240 K. The L-Trp concentrations of the samples were (a) 20 mM, (b) 4.8 mM and (c) 0.64 mM. The samples were prepared in 70%/30% (vol/vol) glycerol/100 mM KPB, pH 8). Data were published previously<sup>[132]</sup>.

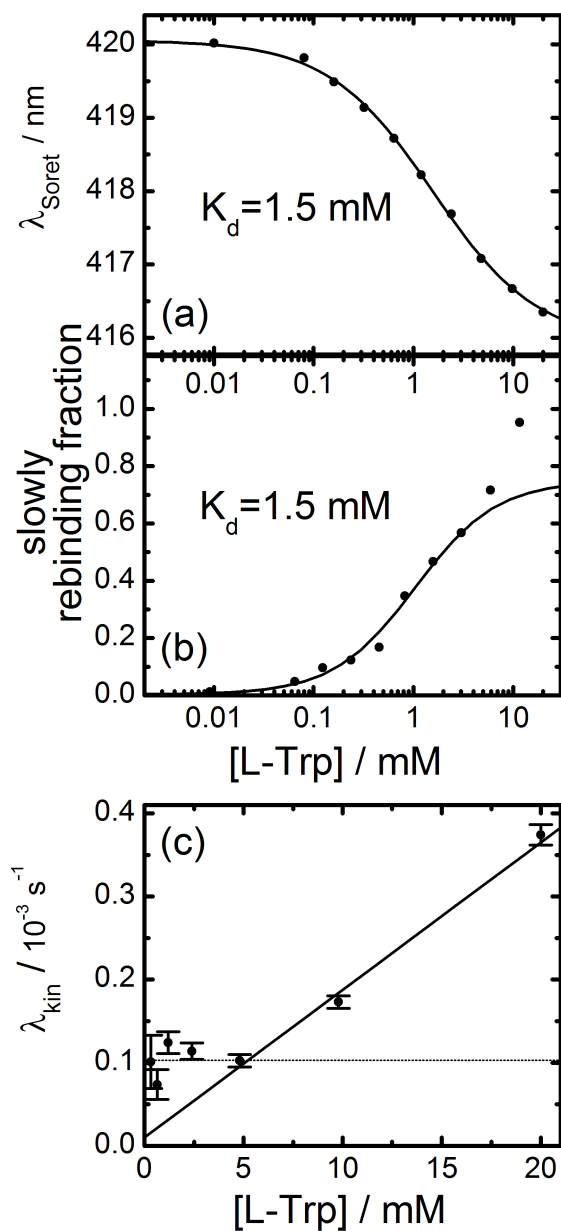


Figure 5.6: Analysis of CO and L-Trp binding to hIDO-CO/L-Trp at different L-Trp concentrations. (a) Peak position of the hIDO-CO Soret band as a function of the L-Trp concentration. (b) Fraction of hIDO molecules that slowly rebinds CO, as a function of the L-Trp concentration. (c) Apparent rate coefficient of L-Trp relaxation into the active site as a function of the L-Trp concentration. Solid line: Linear fit to the data points at L-Trp concentrations  $> 3 \text{ mM}$ . Dotted line: average  $\lambda_{\text{kin}}$  for L-Trp concentrations  $< 5 \text{ mM}$ . All data were taken at 240 K. The samples were prepared in 70%/30% (vol/vol) glycerol/100 mM KPB, pH 8. Data were published previously<sup>[132]</sup>.

The protein fraction exhibiting a slow CO rebinding kinetics was plotted as a function of the L-Trp concentration (Figure 5.6 b). Below  $\approx 3$  mM L-Trp, the concentration dependence can be described by an equilibrium dissociation coefficient  $K_d = 1.5$  mM. The value is identical to the dissociation coefficient determined from the Soret band shift (Figure 5.6 a). The more protein molecules have L-Trp bound at the active site before photolysis, the higher the fraction of proteins that rebind the CO ligand slowly after photolysis. This correlation indicates that the slowly rebinding molecules are generated by an intramolecular migration of L-Trp. At L-Trp concentrations above  $\approx 5$  mM, the fraction of slow rebinders is higher than predicted by the binding isotherm. Apparently, the L-Trp concentration in the solvent is high enough to partly populate the secondary docking site.

In Figure 5.6 c, we plot the apparent rate coefficient,  $\lambda_{\text{kin}}$ , describing the kinetics of L-Trp returning to the active site. The data were obtained from the time dependence of the Soret peak shift. As expected for an intramolecular migration of L-Trp, the kinetics of L-Trp returning to the active site is independent of the L-Trp concentration in the solvent for concentrations below  $\approx 5$  mM. At higher substrate concentrations, the L-Trp relaxation process shows a linear dependence on the L-Trp concentration in the solvent, indicating a bimolecular reaction.

## 5.5 Conclusions

The scheme in Figure 5.7 summarizes the findings described above, the process of L-Trp migration in hIDO upon CO photodissociation. The numbers given in black circles correspond to the processes observed in the isothermal kinetic measurements (Chapter 5.1). The different protein species are numbered from 1 to 8 in the upper left corner of each diagram. Species that were detected in the experiments are depicted in dark blue, whereas transient species are marked in light blue.

Photodissociation of CO in substrate-free hIDO-CO (species 1) generates deoxy hIDO (species 2). CO recombination to the heme iron is complete within 300 s at 200 K and within less than 1 s at 240 K (step 1) (Figure 5.1).

Illumination of hIDO-CO/L-Trp (species 3) results in photodissociation of the CO ligand (species 6) and, subsequently, in the escape of L-Trp from the active site (species 7). At low L-Trp concentrations, the substrate is expected to migrate to a secondary inhibitory L-Trp binding site (green oval). Here, L-Trp is spectroscopically silent but affects the CO recombination kinetics. Only after the L-Trp has left the active site, CO can rebind to the heme iron (species 4; hIDO-CO/--L-Trp). However, CO recombination is significantly slower than in substrate-free proteins (step 2). In a final step (3), L-Trp settles back in the active site, creating the initial

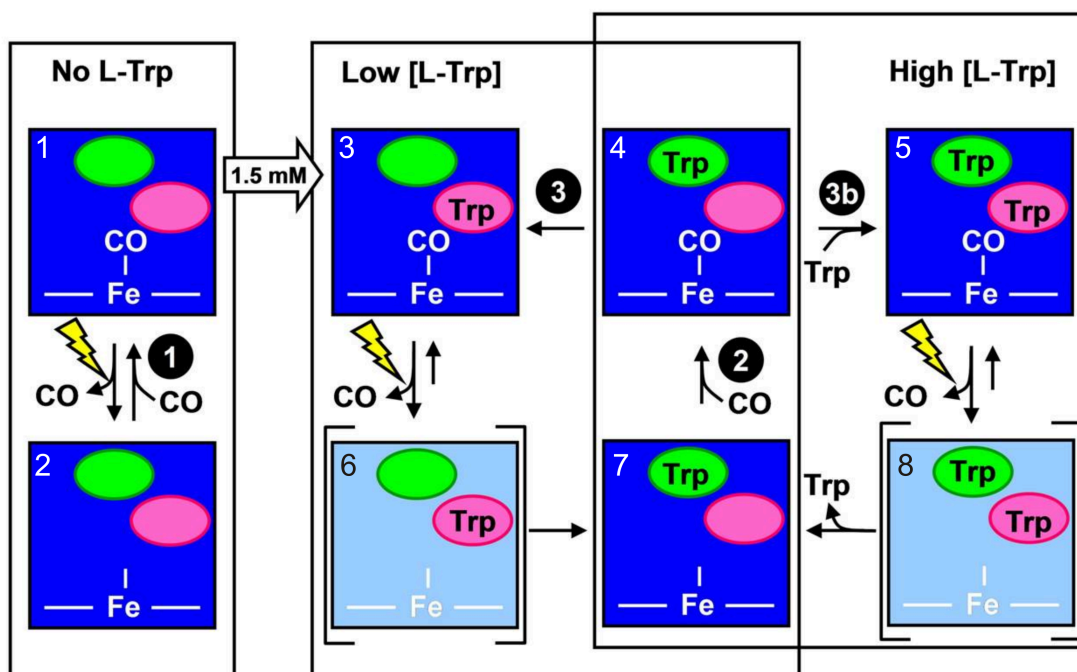


Figure 5.7: Scheme of L-Trp migration in hIDO. The data have been published in Reference<sup>[132]</sup>.

state (species 3). L-Trp migration at low substrate concentrations is independent on the L-Trp concentration in the sample solution, indicating an internal migration process as shown in the scheme.

At high L-Trp concentrations, L-Trp is also expected to populate the secondary binding site of the CO-ligated protein (species 5). Upon photodissociation, CO leaves the binding site (species 8) and, subsequently, L-Trp escapes from the active site. However, the molecule migrates into the solvent because the secondary site is already occupied and enables CO recombination (species 7). L-Trp relaxation back to the initial state depends on the L-Trp concentration (step 4), suggesting a bimolecular process, with L-Trp rebinding from the solvent.

In summary, the scheme elucidates the interplay between the protein, the ligand and the substrate, L-Trp. Photodissociation of CO prompts L-Trp to leave the active site of hIDO. The results also implicate the existence of a secondary binding site for L-Trp. L-Trp at this binding site is spectroscopically silent. However, CO recombination is significantly slower when the substrate occupies the secondary binding site. The data suggest that the site is occupied only at very high L-Trp concentrations.

For a long time, it was believed that, at high concentrations, the substrate binds to the ferric iron<sup>[31]</sup>. This binding of L-Trp was proposed to inhibit the reduction of the iron and, consequently, formation of the reactive ternary complex of reduced protein, substrate and ligand. However, a comparison of the equilibrium dissociation coefficient,  $K_d$ , for the binding of L-Trp to the ferric protein ( $K_d = 900 \mu\text{M}$ ) with the  $K_{si} = 170 \mu\text{M}$  excludes substrate inhibition is caused by the binding of L-Trp to the ferric enzyme<sup>[54]</sup>. An increasing number of studies suggests instead the existence of a second, an inhibitory binding site for L-Trp in hIDO, responsible for the substrate inhibition. Early binding studies in 1989, performed by Sono, gave first indications of an additional substrate binding site<sup>[133]</sup>. Further evidence for an inhibitory site was published by Lu et al.<sup>[131]</sup>. Performing equilibrium titration studies, two  $K_d$ s were determined for the binding of L-Trp to ferric hIDO-CN,  $K_{d_1} = 18 \mu\text{M}$  and  $K_{d_2} = 26 \text{mM}$ <sup>[131]</sup>.

Our data provide further, however indirect, evidence for the existence of a secondary inhibitory binding site for L-Trp.

## Chapter 6

# Ligand Binding at Ambient Temperature

Flash photolysis studies have shown that 4% of the photodissociated CO in wt Mb recombines from the protein interior at room temperature. This geminate recombination step is observed between 100 ns and 1  $\mu$ s<sup>[77]</sup>. The major fraction (96%) of CO rebinds to the heme iron in a bimolecular process from the solvent on the millisecond time scale<sup>[77]</sup>.

In Chapter 4, we have shown that, in hIDO-CO, both the release and the re-binding of CO is hindered by the presence of L-Trp. Photolysis experiments at 4 K demonstrated that the CO photoproduct yield is low when L-Trp is bound at the active site. Low temperature FTIR-TDS measurements revealed that geminate rebinding is also markedly influenced by L-Trp binding. With L-Trp located at the active site, CO cannot recombine from the remote docking sites. However, all experiments were performed at cryogenic temperatures.

In this chapter, the effect of L-Trp binding to hIDO-CO on the CO association and dissociation kinetics at physiological conditions was investigated using UV/Vis spectroscopy and flash photolysis. Additionally, L-Trp analogues were titrated to hIDO-CO to obtain further insight into the influence of substrate binding on the release and recombination of CO.

### 6.1 Spectroscopic and Kinetic Changes upon L-Trp Addition

The Soret band of heme proteins is sensitive to the ligation and oxidation states of the heme iron. Figure 6.1 shows spectra of the CO-bound and the deoxy states of hIDO-CO and hIDO-CO/L-Trp. Whereas the spectra of CO-ligated hIDO-CO (red dotted line) and hIDO-CO/L-Trp (red solid line) display a narrow band at 420 and

416 nm, respectively, the Soret bands of deoxy hIDO (black dotted line) and deoxy hIDO/L-Trp (black solid line) are broad, with the absorbance peaking at  $\approx 429$  and 427 nm.

In a flash photolysis experiment, a short laser flash cleaves the bond between the heme iron and the CO. Subsequently, the rebinding of the CO is monitored as a function of time. Typically, the absorbance changes at 436 nm are recorded in our laboratory because, at this wavelength, the difference between the spectra of the CO-ligated (pre-flash) and the deoxy (post-flash) species is maximal.

Preliminary tests revealed that, upon photolysis,  $\approx 76\%$  of CO in hIDO-CO can escape into the solvent under the applied conditions.

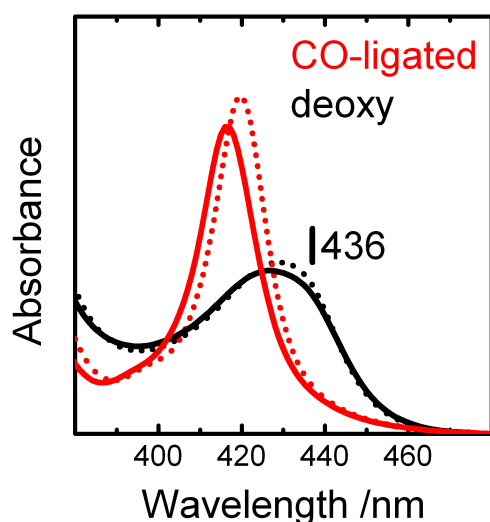


Figure 6.1: Visible Spectra of deoxy and CO-bound hIDO (dotted lines) and hIDO/L-Trp (straight lines). The spectra of deoxy and CO-bound protein are colored in black and red, respectively. The spectra of the deoxy proteins are normalized to equal areas. The spectra of the CO-ligated proteins are adjusted accordingly.

## 6.1. SPECTROSCOPIC AND KINETIC CHANGES UPON L-TRP ADDITION

---

In Figure 6.2, we present the visible spectra measured before flash photolysis (panel a) and the recorded time traces of CO rebinding to hIDO (panel c) at increasing L-Trp concentrations. The Soret band positions plotted as a function of the L-Trp concentration were determined by fitting the spectra with Gaussians (Appendix C). Note that the Soret band is a superposition of the Soret bands of hIDO-CO and hIDO-CO/L-Trp. In Figure 6.2b, the determined band position is plotted as a function of the L-Trp concentration.

Figure 6.2c displays the absorbance changes at 436 nm from  $10^{-4}$  to 10 s after the laser flash, which are related to bimolecular rebinding from the solvent. The initial amplitude of the kinetic trace indicates the fraction of proteins that have not rebound their ligand at time  $t$  after photolysis. As we want to concentrate on bimolecular rebinding, the kinetic trace of hIDO-CO was normalized to 1 at  $10^{-3}$  s where geminate rebinding is complete. The traces of hIDO-CO with L-Trp were scaled with respect to the time trace of hIDO-CO. With increasing L-Trp concentration, the absorbance difference at  $10^{-3}$  s after photolysis becomes smaller. Obviously, the presence of L-Trp at the active site hinders CO escape into the solvent. Interestingly, even at very high concentrations of L-Trp, where we expect to have only L-Trp-bound hIDO in the solution, the solvent process is not totally suppressed but has decreased to  $17 \pm 1\%$ .

To analyze the effect of L-Trp on the relative fraction that rebinds CO in a bimolecular process after photolysis, the amplitudes of the time traces at  $10^{-3}$  s are plotted as a function of the L-Trp concentration (Figure 6.2d). They represent the fraction of hIDO molecules that permit CO to escape into the solvent. In the following, we will refer to the absorbance amplitude at  $10^{-3}$  s as the level of the time trace.

To determine the  $K_d$  values associated with the Soret band shift and the changes in the absorbance amplitude, the experimental data were fitted by the Hill equation (Appendix C) assuming a Hill coefficient of  $n = 1$ . The fit yields  $K_d(\text{Soret}) = 117 \pm 2 \mu\text{M}$  and  $K_d(\text{Level}) = 95 \pm 4 \mu\text{M}$ , respectively. The two  $K_d$  values are very similar but not identical. It is possible that they represent the same process, which is the binding of L-Trp at the active site of hIDO-CO and, therefore, the formation of hIDO-CO/L-Trp.

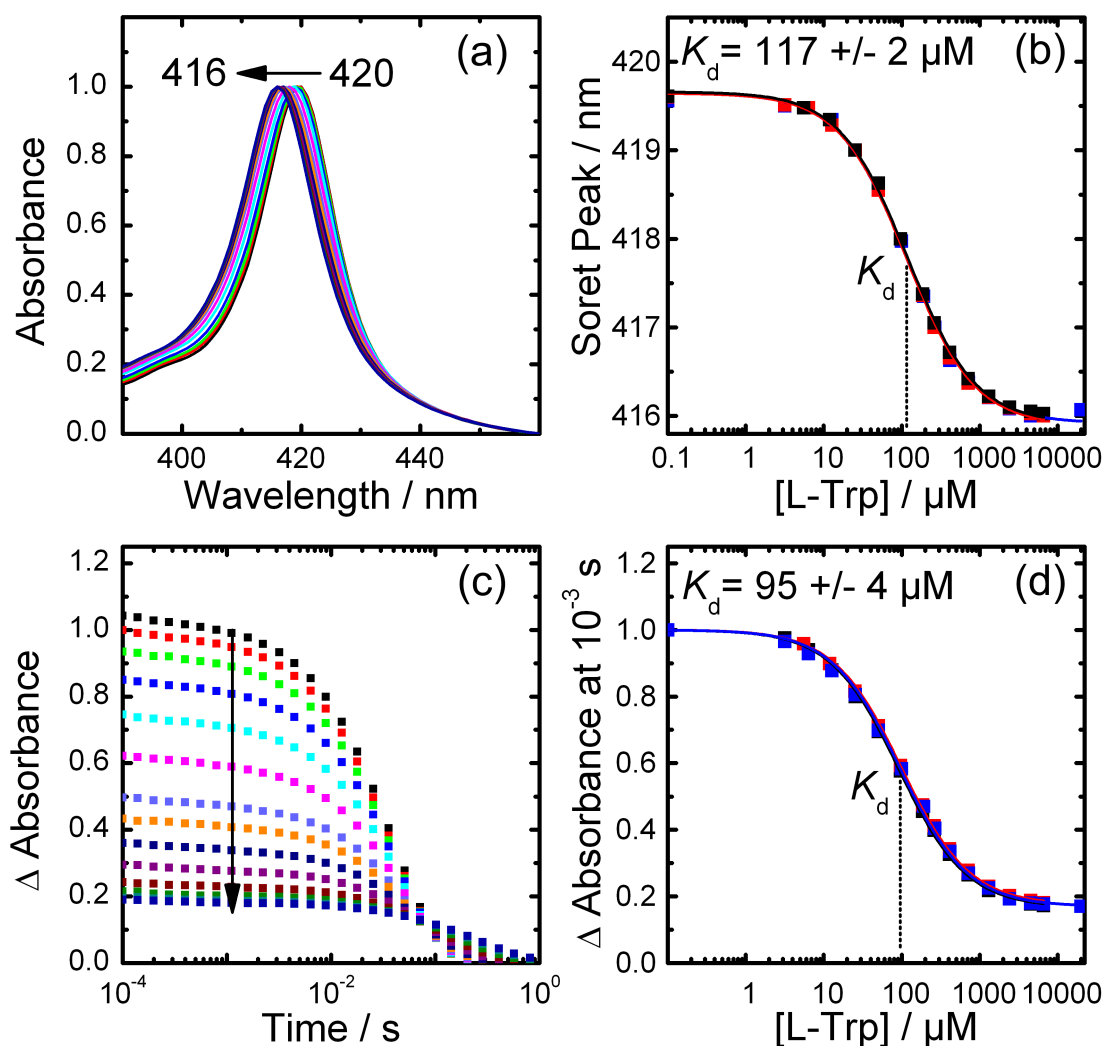


Figure 6.2: Development of visible spectra and time traces of hIDO-CO upon increasing L-Trp concentrations. (a) Shift of the Soret band. Spectra were scaled to 1 at the band maximum. Soret band positions were determined by a Gaussian fit (Appendix C). (b) Soret band position as a function of L-Trp concentration. (c) Time traces monitored at 436 nm. The amplitude of the time trace of hIDO-CO at  $10^{-3}$  s was set to 1. The levels of the time traces in hIDO-CO with different L-Trp concentrations were scaled accordingly. (d) Amplitudes as a function of L-Trp concentration. (b, d) Analysis of Soret band shift and changes in amplitude. The data sets of three experiments (plotted in red, blue and black) were fitted individually by the Hill equation (Appendix C). The given  $K_d$ s are the mean values of the three independent data sets.

## 6.1. SPECTROSCOPIC AND KINETIC CHANGES UPON L-TRP ADDITION

Figure 6.2c demonstrates that the fraction of CO escaping into the solvent after the photolysis decreases with increasing L-Trp concentration. However, even at the highest values, CO escape into the solvent is not completely suppressed. Bimolecular rebinding of this fraction was analyzed in detail (Figure 6.3). All time traces were normalized to 1 at  $10^{-3}$  s. The data sets were fitted with a biexponential and a triexponential decay because one exponential was not sufficient to fit the data. The results are plotted in Figure 6.3a and b, respectively. The non-normalized residuals are plotted in the panels below (Figure 6.3c and d). The attempts to fit the data with a biexponential decay show systematic deviations of the fit from the experimental data. The application of a triexponential decay decreases the deviations markedly. From fitting with three exponential decays, three rate coefficients were extracted,  $k'_{\text{SB}}(1) = 0.025 \text{ s}^{-1}\mu\text{M}^{-1}$ ,  $k'_{\text{SB}}(2) = 0.011 \text{ s}^{-1}\mu\text{M}^{-1}$  and  $k'_{\text{SB}}(3) = 0.003 \text{ s}^{-1}\mu\text{M}^{-1}$ .

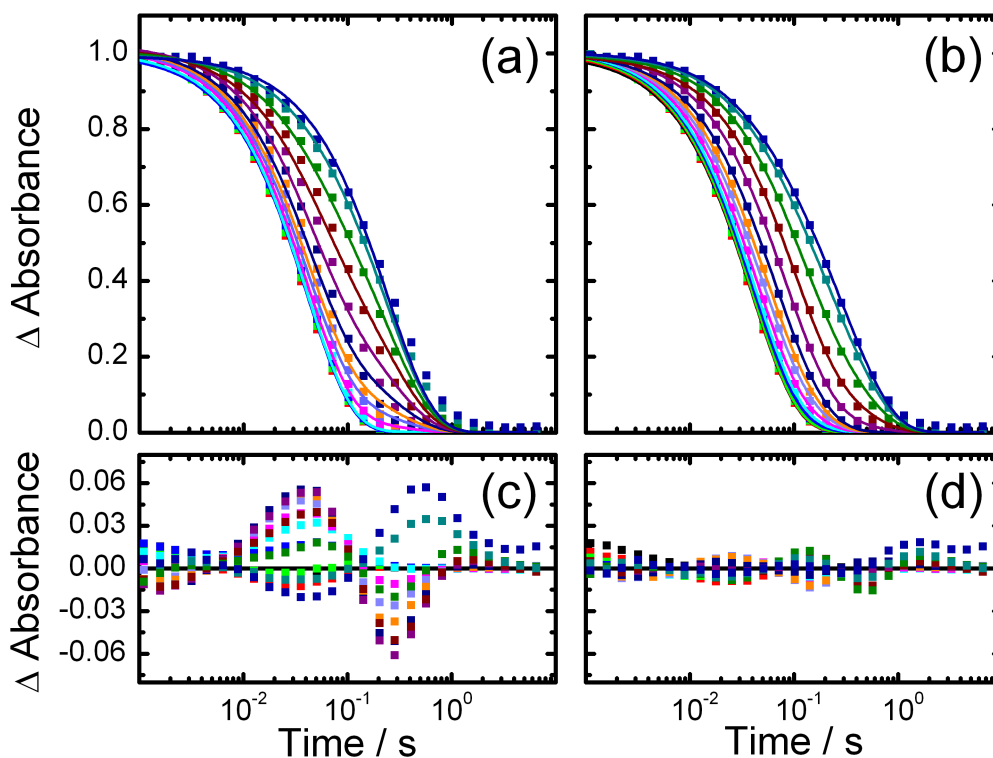
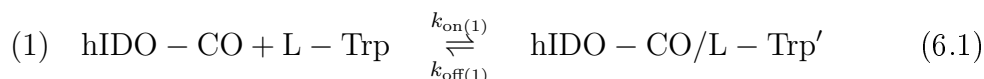
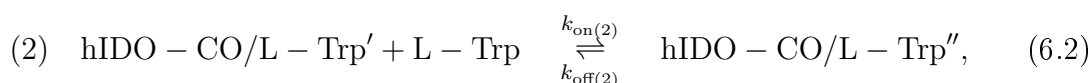


Figure 6.3: Analysis of the bimolecular recombination process of CO. The time traces of hIDO-CO with different L-Trp concentrations were approximated by (a) a biexponential and (b) a triexponential decay. (c, d) The non-normalized residuals of the two fits are plotted in the panels below.

Each exponential decay represents a distinct CO recombination process from the solvent. We suggest that the CO ligands rebind to three different protein states, with their relative populations varying as a function of the L-Trp concentration (Figure 6.4) and propose a sequential binding of two L-Trp molecules to hIDO-CO according to



and



where hIDO-CO, hIDO-CO/L-Trp' and hIDO-CO/L-Trp'' are the three states re-binding CO in a bimolecular process described by the rate coefficients  $k'_{\text{SB}}(1)$ ,  $k'_{\text{SB}}(2)$  and  $k'_{\text{SB}}(3)$ , respectively. The assumption that two L-Trp molecules bind sequentially to the protein implies that  $K_d(1) < K_d(2)$  with  $K_d = \frac{k_{\text{off}}}{k_{\text{on}}}$  and, at the same time, precludes the formation of hIDO-CO/L-Trp'' directly from hIDO-CO.

The relative fractions of the three protein states determined from the triexponential fit are plotted in Figure 6.4 as a function of the L-Trp concentration. The data from three independent experiments are marked with squares, circles and triangles. The fractions of the three states hIDO-CO, hIDO-CO/L-Trp' and hIDO-CO/L-Trp'' are colored in black, purple and pink, respectively. The graph demonstrates that the relative concentration of the intermediate state, hIDO-CO/L-Trp' grows at the expense of the initial state, hIDO-CO. The intermediate state reaches its maximal population at  $\approx 450 \mu\text{M}$  L-Trp. At even higher concentrations of L-Trp, the population of a third state, hIDO-CO/L-Trp'', increases.

## 6.1. SPECTROSCOPIC AND KINETIC CHANGES UPON L-TRP ADDITION

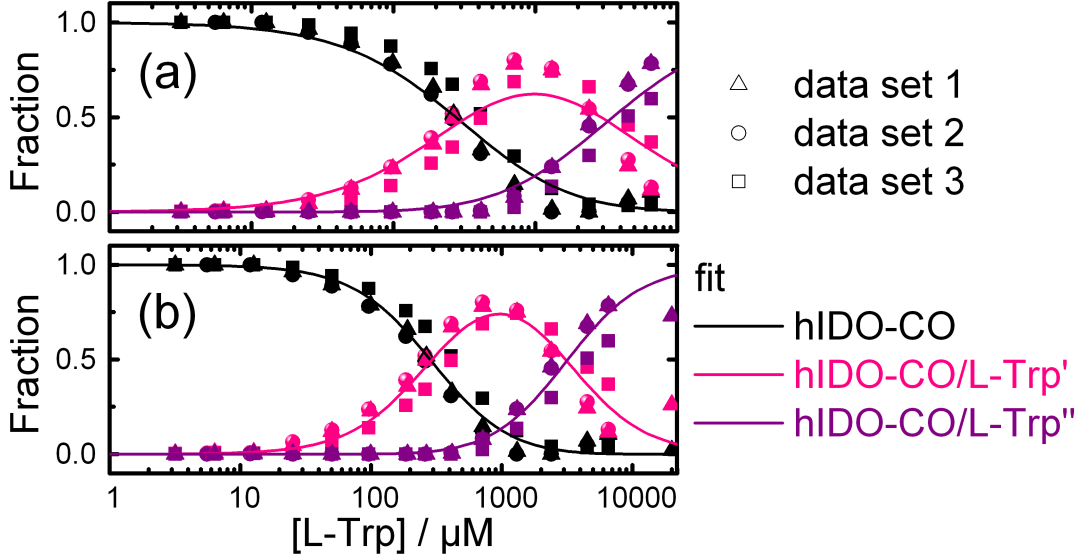


Figure 6.4: Development of the fractions of hIDO-CO, hIDO-CO/L-Trp' and hIDO-CO/L-Trp'' with increasing L-Trp concentration. The fractions obtained in three independent experiments are marked with squares, circles and triangles. The fractions hIDO-CO, hIDO-CO/L-Trp' and hIDO-CO/L-Trp'' are colored in black, pink and purple, respectively. Lines represent the obtained three-state fit curves with Hill coefficients  $n$  (a) set to 1 and (b) not fixed.

The fit function, used to model the data in Figure 6.4, is based on the global coupling of the state fractions. The sum of the three fractions is equal to 1 at all L-Trp concentrations,

$$hIDO - CO + hIDO - CO/L - Trp' + hIDO - CO/L - Trp'' = 1. \quad (6.3)$$

With  $K_d(1) = \frac{k_{\text{off}(1)}}{k_{\text{on}(1)}}$  and  $K_d(2) = \frac{k_{\text{off}(2)}}{k_{\text{on}(2)}}$ , the three fractions are coupled according to:

$$\begin{aligned} hIDO - CO \cdot k_{\text{on}(1)}^{n(1)} \cdot [L - Trp]^{n(1)} &= hIDO - CO/L - Trp' \cdot k_{\text{off}(1)}^{n(1)} \\ \Leftrightarrow \frac{hIDO - CO}{hIDO - CO/L - Trp'} &= \frac{k_{\text{off}(1)}^{n(1)}}{[L - Trp]^{n(1)} \cdot k_{\text{on}(1)}^{n(1)}} = \frac{K_d^{n(1)}}{[L - Trp]^{n(1)}} \end{aligned} \quad (6.4)$$

and

$$\begin{aligned}
 hIDO - CO/L - Trp' \cdot k_{\text{on}}^{n(2)} \cdot [L - Trp]^{n(2)} &= hIDO - CO/L - Trp'' \cdot k_{\text{off}}^{n(2)} \\
 \Leftrightarrow \frac{hIDO - CO/L - Trp'}{hIDO - CO/L - Trp''} &= \frac{k_{\text{off}}^{n(2)}}{[L - Trp]^{n(2)} \cdot k_{\text{on}}^{n(2)}} = \frac{K_{\text{d}}^{n(2)}}{[L - Trp]^{n(2)}},
 \end{aligned} \tag{6.5}$$

where  $[L - Trp]$  represents the L-Trp concentration.  $k_{\text{on}}$  and  $k_{\text{off}}$  describe the association and the dissociation rate coefficient of the L-Trp, respectively.  $n(1)$  and  $n(2)$  are Hill coefficients, describing the cooperativity of a reaction. With the Equations 6.3 to 6.5, the three fractions are given by:

$$hIDO - CO = \frac{1}{1 + \frac{[L-Trp]^{n(1)}}{K_{\text{d}}^{n(1)}} + \frac{[L-Trp]^{n(1)} \cdot [L-Trp]^{n(2)}}{K_{\text{d}}^{n(1)} \cdot K_{\text{d}}^{n(2)}}}, \tag{6.6}$$

$$hIDO - CO/L - Trp' = \frac{1}{\frac{K_{\text{d}}^{n(1)}}{[L-Trp]^{n(1)}} + 1 + \frac{[L-Trp]^{n(2)}}{K_{\text{d}}^{n(2)}}}, \tag{6.7}$$

$$hIDO - CO/L - Trp'' = \frac{1}{\frac{K_{\text{d}}^{n(1)} \cdot K_{\text{d}}^{n(2)}}{[L-Trp]^{n(1)} \cdot [L-Trp]^{n(2)}} + \frac{K_{\text{d}}^{n(2)}}{[L-Trp]^{n(2)}} + 1}. \tag{6.8}$$

To obtain the two dissociation coefficients associated with the sequential L-Trp binding processes,  $K_{\text{d}}(1)$  and  $K_{\text{d}}(2)$ , the data sets were fitted with the Equations 6.6 to 6.8. The fit curves are included in Figure 6.4. Assuming that the binding reactions are noncooperative, the Hill coefficients,  $n(1)$  and  $n(2)$ , were fixed to 1. The fit result is plotted in Figure 6.4 a. The two dissociation coefficients were determined as  $K_{\text{d}}(1) = 299 \pm 30 \mu\text{M}$  and  $K_{\text{d}}(2) = 3,245 \pm 379 \mu\text{M}$ . Especially for the transition between the states hIDO-CO and hIDO-CO/L-Trp', the fit does not sufficiently approximate the experimental data. A much better fit is achieved without fixing the Hill coefficient. It yields Hill coefficients  $n(1) = 1.4 \pm 0.1$  and  $n(2) = 1.5 \pm 0.2$ , indicating a cooperative binding behavior. The calculated dissociation constants are  $K_{\text{d}}(1) = 289 \pm 19 \mu\text{M}$  and  $K_{\text{d}}(2) = 3,150 \pm 222 \mu\text{M}$ .

## 6.1. SPECTROSCOPIC AND KINETIC CHANGES UPON L-TRP ADDITION

---

The analysis of the bimolecular recombination processes revealed that three states are involved in rebinding. We introduced the states hIDO-CO, hIDO-CO/L-Trp' and hIDO-CO/L-Trp". The state hIDO-CO is the substrate-free protein with a rate coefficient  $k'_{\text{SB}}(1) = 0.025 \text{ s}^{-1}\mu\text{M}^{-1}$ . The two equilibrium dissociation coefficients for the transitions between state hIDO-CO and hIDO-CO/L-Trp' as well as the transition between hIDO-CO/L-Trp' and hIDO-CO/L-Trp" are  $K_{\text{d}}(1) = 289 \pm 19 \mu\text{M}$  and  $K_{\text{d}}(2) = 3,150 \pm 222 \mu\text{M}$ , respectively.

$K_{\text{d}}(1)$ , describing the binding of L-Trp to hIDO-CO, does not equal the dissociation coefficients determined by the decrease of the absorbance amplitude at  $10^{-3} \text{ s}$ ,  $K_{\text{d}}(\text{Level})$ , or by the Soret band shift,  $K_{\text{d}}(\text{Soret})$ , that were expected to describe the binding of L-Trp at the active site of hIDO-CO. Therefore, the state hIDO-CO/L-Trp' must be different from the protein species with L-Trp bound at the active site of hIDO-CO, hIDO-CO/L-Trp.

These results give reason to reinvestigate the difference between  $K_{\text{d}}(\text{Level})$  and  $K_{\text{d}}(\text{Soret})$  of  $\approx 20 \mu\text{M}$ . Assuming that only protein species hIDO-CO/L-Trp contributes to the decrease in the absorbance amplitude but both species, hIDO-CO/L-Trp and hIDO-CO/L-Trp' contributes to the Soret band shift, the shift is a superposition of the shifts caused by the two species. Therefore, the development of the Soret band position has to be fitted with a weighted sum of two Hill functions, one describing the species hIDO-CO/L-Trp with  $K_{\text{d}}(\text{Level})$  and one representing the species hIDO-CO/L-Trp' with  $K_{\text{d}}(1)$ . The best result was achieved when the fraction of hIDO-CO/L-Trp contributed to the fit with 84% (Figure 6.5). This result is consistent with the relative fraction of hIDO-CO/L-Trp that contribute with the decrease in the absorbance amplitude (83%).

The third state, *hIDO-CO/L-Trp"*, exhibiting the slowest CO recombination process ( $k'_{\text{SB}}(3) = 0.003 \text{ s}^{-1}\mu\text{M}^{-1}$ ), appears only at high L-Trp concentrations, indicating the binding of a second L-Trp to the protein fraction of hIDO-CO/L-Trp'. The binding of a second L-Trp to hIDO-CO/L-Trp is not detectable in flash photolysis experiments because the first L-Trp hinders the CO to escape into the solvent.

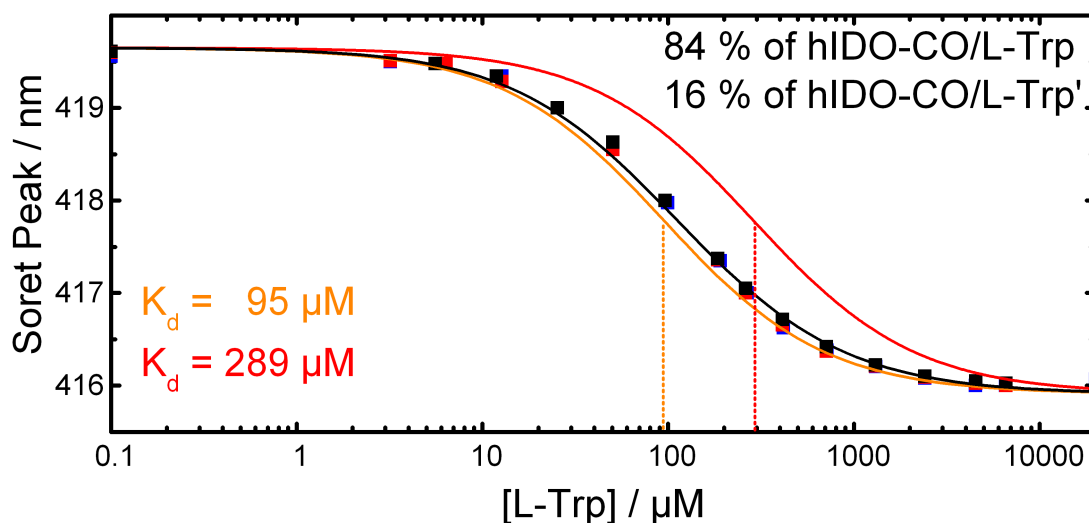


Figure 6.5: hIDO-CO/L-Trp and hIDO-CO/L-Trp' contribute to the Soret band shift. Fit of Soret band development with increasing L-Trp concentrations using a weighted sum of the Hill equation (Appendix C)(black line). For comparison, the Hill functions inserted in orange and red were simulated with equilibria dissociation coefficients of  $K_d(\text{Level}) = 95 \mu\text{M}$  and  $K_d(1) = 289 \mu\text{M}$ , respectively.

## 6.2 Spectroscopic and Kinetic Properties of MLT-, D-Trp- and S-Trp-bound hIDO

The flash photolysis experiments were also performed in their dependencies on concentrations of L-Trp analogues. Note that each analogue has a different solubility, resulting in different final concentrations in the experiments.

Figure 6.6 a displays the UV/Vis spectra of hIDO-CO in the presence of different L-Trp analogues at their maximal concentrations. The spectra of hIDO-CO (black) and hIDO-CO/L-Trp (red) are added for comparison. The Soret band positions upon addition of increasing concentrations of MLT (cyan), D-Trp (green) and S-Trp (blue) are shown in Figure 6.6 b. The changes in the Soret band position upon L-Trp titration are included in the graph (red line). The data were fitted with the Hill equation (Appendix C). Upon addition of MLT, a Soret band shift similar to the one in hIDO-CO/L-Trp is observed. The dissociation coefficient,  $K_d = 48 \pm 1 \mu\text{M}$ , is twofold lower than the one of L-Trp (Table 6.1). In contrast, addition of D-Trp does not affect the position of the Soret band. Consequently, no dissociation coefficient can be determined from these data. Only a slight blue shift to 419 nm is observed upon addition of S-Trp to hIDO-CO, with  $K_d \approx 388 \mu\text{M}$ .

6.2. SPECTROSCOPIC AND KINETIC PROPERTIES OF MLT-, D-TRP- AND S-TRP-BOUND HIDO

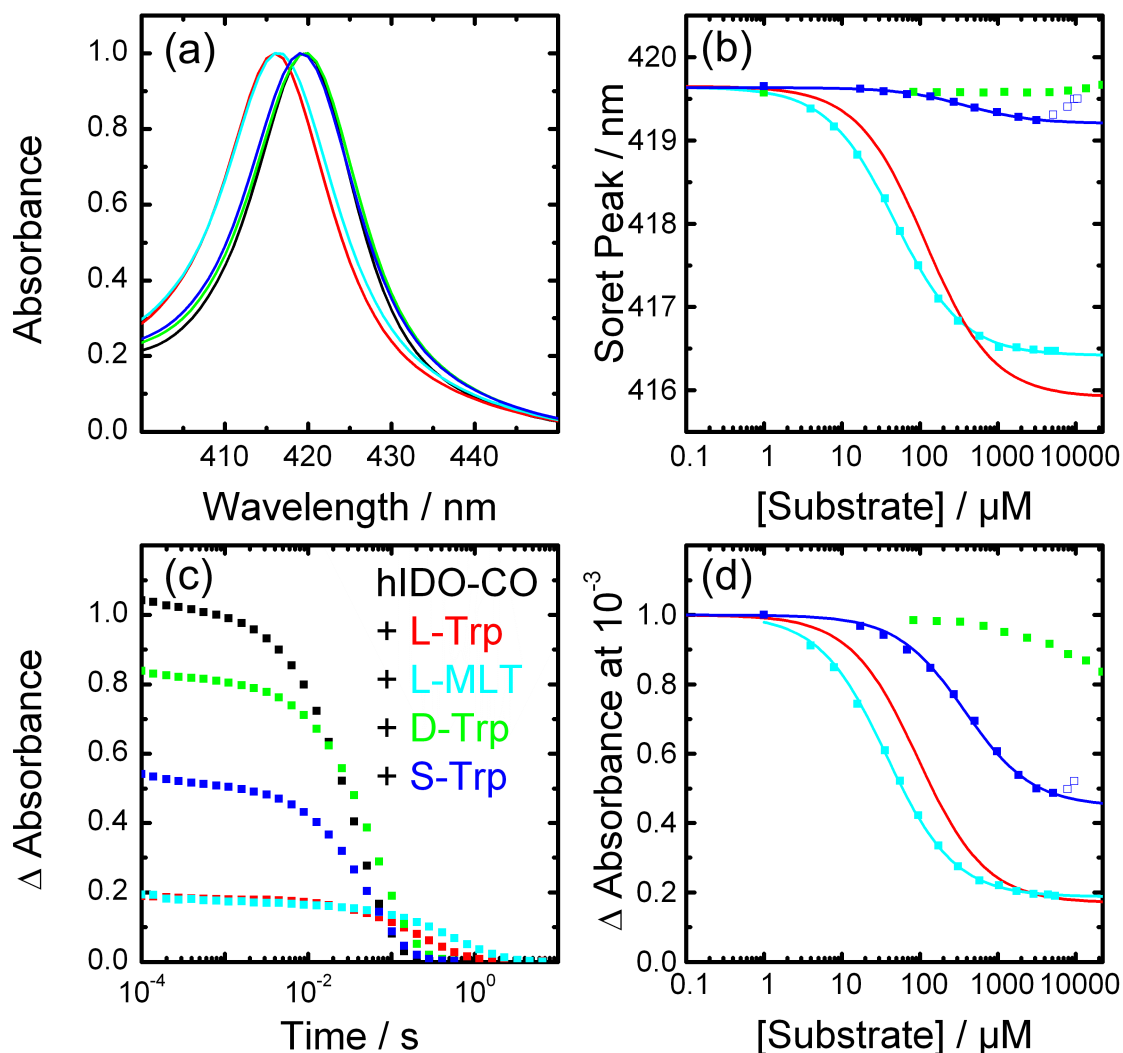


Figure 6.6: Development of visible spectra and kinetic traces upon addition of various substrates to hIDO-CO. (a, c) UV/Vis spectra and time traces of hIDO-CO without substrate (black), with 6.6 mM L-Trp (red), 5.5 mM MLT (cyan), 22.1 mM D-Trp (green) and 3.1 mM S-Trp (blue). (a) Spectra were scaled to 1 at the maximal amplitude. (b) Development of the Soret band position as a function of the substrate concentrations. For comparison, the titration curve of L-Trp is plotted in red. (c) Time traces monitored at 436 nm. The amplitude of the time trace of hIDO-CO at  $10^{-3}$  s was normalized to 1, and the time traces of hIDO-CO with L-Trp, MLT, D-Trp and S-Trp were scaled accordingly. (d) Levels as a function of the substrate concentrations. (b, d) Analysis of the Soret band shift and the relative amplitudes of the kinetic traces. The data sets of three experiments were averaged and fitted with the Hill equation (Appendix C).

The effect of the different substrates on the initial amplitude of the kinetic traces is depicted in Figure 6.6 c. The kinetic trace of hIDO-CO was normalized to 1 at  $10^{-3}$  s. The traces of hIDO-CO in the presence of the maximal concentrations of MLT (cyan), D-Trp (green) and S-Trp (blue) were scaled to the trace of hIDO-CO. In Figure 6.6 d, we present the amplitudes upon titration of hIDO-CO with the L-Trp analogues. The data were fitted with the Hill equation (Appendix C). Upon titration with MLT, the level of the traces of hIDO-CO/MLT decreases significantly as was also seen in hIDO-CO/L-Trp. We determined  $K_d = 38 \pm 1$   $\mu\text{M}$  for the association process of MLT to the active site of hIDO-CO that is slightly lower than the  $K_d$  determined by the Soret band shift. A less intense level decrease ( $\approx 50\%$ ) is observed for hIDO-CO/S-Trp that can be described by  $K_d \approx 374$   $\mu\text{M}$  (Table 6.1). For hIDO-CO/D-Trp, a level decrease of only  $\approx 15\%$  is observed. The data shown in Figure 6.6 d could not be reliably modeled with the Hill equation (Appendix C) because the achievable D-Trp concentrations are insufficient.

Figure 6.7 summarizes the changes in the bimolecular recombination process in hIDO-CO upon titration with L-Trp analogues. In Figure 6.7 a, the recorded time traces of hIDO-CO/MLT (cyan), hIDO-CO/D-Trp (green) and hIDO-CO/S-Trp (blue) are shown. Again, the traces of hIDO-CO (black) and hIDO-CO/L-Trp (red) are included for comparison. All traces were normalized to 1 at  $10^{-3}$  s. Whereas the kinetic traces of hIDO-CO with D-Trp and S-Trp exhibit only small differences compared to hIDO-CO, the relaxation of hIDO-CO/MLT to the equilibrium state is markedly changed. The time traces upon MLT addition were fitted with a triexponential decay as already described for hIDO-CO/L-Trp (Chapter 6.1). The corresponding rate coefficients were determined as  $k'_{\text{SB}}(1) = 0.026$   $\text{s}^{-1}\mu\text{M}^{-1}$ ,  $k'_{\text{SB}}(2) = 0.006$   $\text{s}^{-1}\mu\text{M}^{-1}$  and  $k'_{\text{SB}}(3) = 0.001$   $\text{s}^{-1}\mu\text{M}^{-1}$ . The development of the fractions hIDO-CO (squares), hIDO-CO/MLT' (circles) and hIDO-CO/MLT'' (triangles) are shown in Figure 6.7 b. The data set was fitted, applying the model including three protein fractions, introduced for hIDO-CO with L-Trp in Chapter 6.1. The two dissociation coefficients are  $K_d(1) = 282 \pm 15$   $\mu\text{M}$  and  $K_d(2) = 2,412 \pm 80$   $\mu\text{M}$ . The Hill coefficients were determined to be  $n(1) = 1.14 \pm 0.06$  and  $n(2) = 2.30 \pm 0.16$ , indicating cooperative binding reactions.

The time traces of hIDO-CO/D-Trp (green) and hIDO-CO/S-Trp (blue) could be fitted by single exponentials. The rate coefficients were determined as  $k'_{\text{SB}}(\text{D-Trp}) = 0.014$   $\text{s}^{-1}\mu\text{M}^{-1}$  and  $k'_{\text{SB}}(\text{S-Trp}) = 0.018$   $\text{s}^{-1}\mu\text{M}^{-1}$  (Figure 6.7). Table 6.1 compiles the  $K_d$ s determined for hIDO-CO/L-Trp, hIDO-CO/MLT, hIDO-CO/D-Trp and hIDO-CO/S-Trp.

6.2. SPECTROSCOPIC AND KINETIC PROPERTIES OF MLT-, D-TRP- AND S-TRP-BOUND hIDO

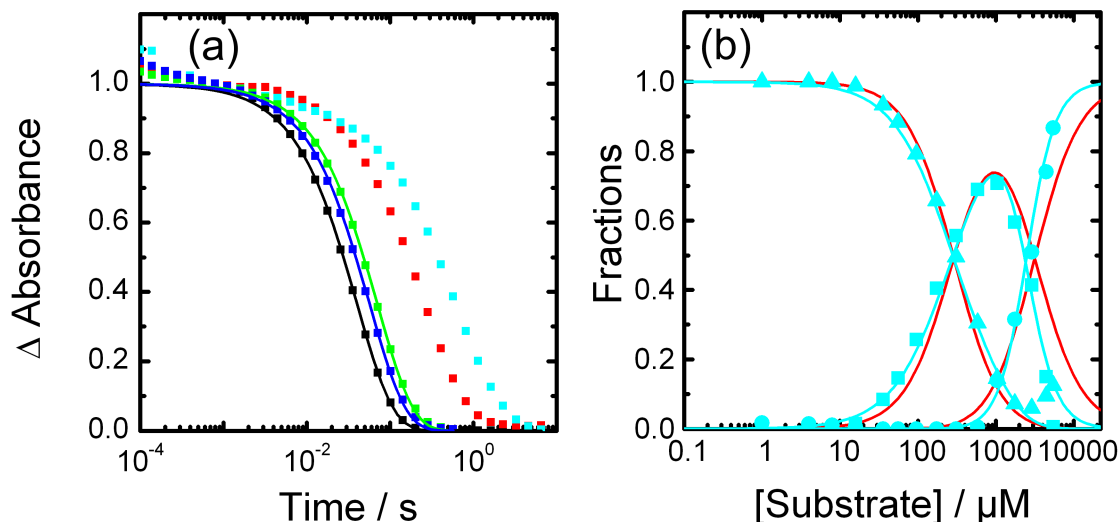


Figure 6.7: Analysis of bimolecular CO recombination in samples with different L-Trp analogues. (a) The time traces of hIDO-CO without substrate (black) and with 6.6 mM L-Trp (red), 5.5 mM MLT (cyan), 22.1 mM D-Trp (green) and 3.1 mM S-Trp (blue). All time traces were normalized to 1 at  $10^{-3}$  s. The time traces of hIDO-CO, hIDO-CO/S-Trp and hIDO-CO/D-Trp were fitted with single exponentials. (b) Development of the fractions hIDO-CO (squares), hIDO-CO/MLT' (cycles) and hIDO-CO/MLT'' (triangles) with increasing MLT concentration. The time traces of hIDO-CO with MLT were fitted with a triexponential decay (data not shown). The obtained three-state fit curves are plotted as cyan lines. For comparison the three-state fit curves obtained with hIDO-CO/L-Trp' are included as red lines (compare Figure 6.4).

The binding of L-Trp at the active site of hIDO hinders the release of CO into the solvent, as indicated by the decreasing amplitude of the kinetic trace. Additionally, L-Trp binding is accompanied by a significant shift in the Soret band, indicating an interaction between the heme moiety and the substrate. MLT exhibits a binding characteristics similar to L-Trp. Both the Soret band shift and the decreasing amplitude are observed with this L-Trp analogue. Interestingly, the binding affinity of MLT to hIDO-CO forming hIDO-CO/MLT is twofold higher than for the natural substrate L-Trp. Similar to L-Trp, MLT displays a protein state, hIDO-CO/MLT', in which CO is released to the solvent after photolysis, indicating the existence of a second binding conformation of MLT. The  $K_d = 282 \mu\text{M}$  is almost identical to the  $K_d$  obtained for hIDO-CO/L-Trp' suggesting that, in this position, the protein does not discriminate between L-Trp and MLT. The fraction of hIDO-CO molecules that bind MLT at the active site is  $\approx 85\%$ , as determined

from the decrease in the absorbance amplitude. Similar to hIDO-CO/L-Trp', a third, slow rebinding species is observed at high MLT concentrations that most likely reflects binding of another MLT molecule to a second, inhibitory binding site, hIDO-CO/MLT".

In contrast to MLT and L-Trp, the spectroscopic and the kinetic changes upon binding of D-Trp to hIDO-CO are small. Neither a Soret band shift nor a significant change in the amplitude of the solvent process ( $\approx 15\%$ ) is observed. A single exponential decay is sufficient to fit the kinetic trace (Figure 6.7 a, green line). The apparent rate coefficient,  $k'_{\text{SB}}(\text{D-Trp}) = 0.014 \text{ s}^{-1}\mu\text{M}^{-1}$ , determined from the recombination process of CO to hIDO-CO/D-Trp' reveals a slightly slower recombination process than observed in hIDO-CO, indicating that the protein has bound D-Trp at a position different from the active site of hIDO-CO.

Surprisingly, hIDO-CO/S-Trp features only a slight blue shift of the Soret band but displays a loss in amplitude of  $\approx 50\%$ , indicating that S-Trp blocks ligand escape into the solvent in this protein fraction but, at the same time, does not interact with the heme group as seen for L-Trp. The kinetic trace can be fitted by a single exponential decay (Figure 6.7 a, blue line). The rebinding from the solvent in the 'photolyzable' fraction, hIDO-CO/S-Trp', is slightly slower than in hIDO-CO ( $k'_{\text{SB}}(\text{S-Trp}) = 0.018 \text{ s}^{-1}\mu\text{M}^{-1}$ ).

Table 6.1: Equilibrium dissociation coefficients,  $K_{\text{d}}$ , describing the binding affinity of L-Trp and L-Trp analogues to hIDO-CO and hIDO-CO/L-Trp'.

experiment		$K_{\text{d}} / \mu\text{M}$			
		L-Trp	MLT	D-Trp	S-Trp
Soret band shift	$K_{\text{dSoret}}$	$117 \pm 2$	$48 \pm 1$	nd	$388 \pm 49$
Amplitude decrease	$K_{\text{dLevel}}$	$95 \pm 4$	$38 \pm 1$	nd	$374 \pm 19$
Bimolecular	$K_{\text{d}_1}$	$289 \pm 19$	$282 \pm 15$	nd	nd
recombination	$K_{\text{d}_2}$	$3,150 \pm 222$	$2,412 \pm 80$		

## 6.3 Conclusions

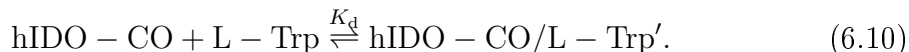
In summary, flash photolysis experiments support the following model of substrate binding to hIDO-CO:

hIDO-CO readily accommodates L-Trp;  $\approx 80\%$  of hIDO-CO molecules bind L-Trp at the active site forming hIDO-CO/L-Trp:



The binding of L-Trp at the active site causes a decrease of the amplitude of the kinetic traces of hIDO-CO measured after the laser flash, indicating that the CO cannot escape into the solvent if L-Trp is bound at the active site and, simultaneously, a Soret band shift by the interaction of the L-Trp with the heme group. The binding affinity of L-Trp to hIDO-CO is given by the decrease of the absorbance amplitude ( $K_d(\text{Level}) = 95 \mu\text{M}$ ).

In a fraction of  $\approx 20\%$  of hIDO-CO molecules, L-Trp does not bind at the active site of hIDO-CO but presumably in the heme pocket, forming hIDO-CO/L-Trp':



In this species, CO can escape into the solvent upon photolysis. Recombination of CO to hIDO-CO/L-Trp' is slightly slower than to hIDO-CO. The affinity of L-Trp to hIDO-CO is given by  $K_{d_1} \approx 289 \mu\text{M}$ . This species contributes to the Soret band shift and the L-Trp is, therefore, expected to interact with the heme group of hIDO-CO. Due to the slower rebinding kinetics of CO and the interaction with the heme, we assume that L-Trp binds in the heme pocket of the protein. However, we presume that the L-Trp at this binding site does not block the primary docking site. At increasing L-Trp concentrations, we have found evidence of a third species, hIDO-CO/L-Trp'', displaying an even slower CO recombination kinetics. As the fraction of this protein species increases with increasing L-Trp concentrations, a second L-Trp may bind to the protein. This second L-Trp is expected to bind at a second, inhibitory binding site.

The identification of the fraction of hIDO-CO/L-Trp' is based on a decreased CO association rate coefficient,  $k'_{\text{SB}}$ , in comparison to the substrate-free protein. Our experiments demonstrated that this protein fraction can most likely bind a second L-Trp molecule. At high concentrations of L-Trp, a third kinetic species is observed

with an even slower CO rebinding. CO recombination is only complete after  $\approx 10$  s. The equilibrium dissociation coefficient,  $K_d(2) = 3,150 \mu\text{M}$ , quantifies the affinity for the binding of a second L-Trp to hIDO-CO/L-Trp'. The binding of the second L-Trp causes an even slower CO recombination process. Therefore, the binding of L-Trp at this docking site inhibits the catalytic function of the protein. The existence of this secondary binding site of L-Trp can only be shown in the species hIDO-CO/L-Trp'. As the CO in hIDO-CO/L-Trp is trapped at the active site, no recombination process can be observed for this species and, therefore, we cannot obtain indications of a second binding site in the catalytically active species. However, the existence of this inhibitory binding site in the conformation hIDO-CO/L-Trp is likely, as high concentrations of L-Trp lead to an almost complete loss in activity<sup>[54]</sup> (Figure 1.2, Chapter 1.1.3).

As seen before, the behavior of the L-Trp analogue MLT is spectroscopically and kinetically very similar to L-Trp. The binding affinity of MLT to the active site of hIDO-CO is even higher than for L-Trp. It was shown that MLT is only slowly converted by hIDO<sup>[122]</sup>. These properties, the high binding affinity to hIDO and the slow conversion, make the molecule a perfect inhibitor for hIDO.

Only a slight loss in amplitude of the kinetic traces of 15% is observed after D-Trp addition to hIDO-CO. In this small fraction, the D-Trp might bind in a position similar to L-Trp at the active site of hIDO-CO. However, no Soret band shift is visible upon D-Trp addition, indicating that the formation of the hydrogen bond network, which is found for hIDO-CO with L-Trp at the active site, is not generated upon D-Trp binding. In the 'photolyzable' fraction, the recombination process is slightly slower than in substrate-free protein proving that D-Trp binds in the heme pocket.

# Chapter 7

## Conclusions and Discussion

### 7.1 Two Modes of L-Trp Binding

Based on our spectroscopical investigations we propose a model for L-Trp binding to hIDO-CO that distinguishes between two ways of L-Trp binding inside the heme pocket.

(1) In the dominant L-Trp bound species, hIDO-CO/L-Trp, L-Trp binds at the active site of hIDO-CO close to the heme-bound ligand. At ambient temperature,  $\approx 80\%$  of the proteins bind L-Trp in this conformation. Upon L-Trp binding at the active site, a pronounced network of interactions is formed between L-Trp, the protein matrix, the ligand and the heme group. The direct interaction between the L-Trp and the heme group is indicated by the Soret band shift. The formation of a hydrogen bond between the oxygen of the ligand and the substrate generates a significant red shift of the IR absorbance band of heme-bound CO,  $A_L$ . Mutagenesis studies suggest interactions between the substrate and amino acids R231 and T379.

In this binding mode, L-Trp either overlaps with the docking site B or, alternatively, blocks access to that site. Photoproduct bands of CO are absent in this species, indicating either that the B site is not populated by the ligand upon photolysis or that site B is structurally not well defined. In addition, the ligand cannot escape into the solvent upon photolysis at ambient temperature. The photolysis yield is also significantly decreased at very low temperatures. CO recombination to the heme iron does not occur as long as L-Trp is bound at the active site.

(2) In the second binding mode, hIDO-CO/L-Trp', L-Trp binds inside the protein but the CO can still escape into the solvent. The binding in this position slows the rebinding of CO with respect to substrate-free protein, as shown by the flash photolysis measurements. We assume that the ensemble of  $A_{SF'}$  bands in the IR spectra represents this protein species. Both the photolysis yield at 4 K as well as CO recombination at 200 K of the  $A_{SF'}$  states are slightly different from those observed in hIDO-CO. In contrast to the first binding mode, the heme-bound ligand does not interact with the L-Trp so that the CO stretching frequencies are similar to those of hIDO-CO. However, the species contributes to the blue shift of the Soret band upon L-Trp binding indicating an interaction between L-Trp and the heme group and, thereby, the binding of L-Trp inside the protein matrix.

We suppose that the L-Trp position in the dominant species, hIDO-CO/L-Trp, equals the position of L-Trp in the catalytically active ternary complex of hIDO-O<sub>2</sub>/L-Trp. But is the limited accessibility of the small gaseous ligand to docking site B upon L-Trp binding not detrimental for the hIDO activity? In Mb, the ligand docking site B was shown to be essential for the binding to and escape of the ligand from the binding site and, therefore, for the functionality of the protein.

We expect that the activity of hIDO is maintained as long as the ligand binds prior the substrate. Initially, in substrate-free hIDO, the docking site B can host the ligand and, therefore, ensures binding of the ligand to the heme iron. Subsequently, L-Trp binds at the active site and blocks site B. However, ligand release is not necessary under physiological conditions as the ligand O<sub>2</sub> is consumed during the catalytic reaction. Actually, the occupation of the docking site by L-Trp might even increase the stability of the ternary complex as the ligand cannot escape from the complex. Thereby, the probability of the enzymatic reaction to proceed is increased.

The group of Estrin performed a combination of classical molecular dynamics and hybrid quantum-classical methodologies to identify the L-Trp binding position in the heme pocket of hIDO<sup>[123]</sup>. They predicted two conformations of L-Trp, Cf1 and Cf2. Whereas in Cf1, hydrogen bond interactions between the L-Trp and the CO are absent, a hydrogen bond between the CO and the L-Trp was found in Cf2. However, they predicted a hydrogen bond between the NH in the indole moiety of L-Trp and the CO ligand, which is in disagreement with our results obtained by comparative measurements with the L-Trp analogue MLT. Although the two binding conformations are not consistent with the binding modes we propose, the results of Capece et al.<sup>[123]</sup> support the existence of multiple L-Trp positions and binding conformations.

## 7.2 Evidence of a Second Inhibitory Binding Site

For both rabbit IDO and hIDO, protein activity is inhibited at high concentrations of L-Trp, indicating the presence of a second L-Trp binding site<sup>[26,54]</sup>. Already in 1989, Sono published kinetic and spectroscopic studies on rabbit IDO suggesting the existence of a secondary effector binding site near to the substrate binding site<sup>[133]</sup>. Pellicciari and coworkers<sup>[108]</sup> were among the first performing molecular docking simulations on hIDO in 2007 based on the x-ray structure of hIDO/PI. They identified an enhancer binding site in the vicinity to the catalytic site, by fitting 3-indole-ethanol into the ternary complex of hIDO-Fe(II)/superoxide/L-Trp. Lu et al.<sup>[131]</sup> showed that the CN adduct of hIDO is capable of binding two L-Trp molecules and provided first experimental evidence of a second L-Trp binding site in hIDO.

Our spectroscopic data yield further evidence for the existence of a second, inhibitory L-Trp binding site in hIDO-CO/L-Trp'. Flash photolysis measurements at ambient temperature revealed binding of a second L-Trp to the protein fraction hIDO-CO/L-Trp' at high L-Trp concentrations, as was apparent from an even slower recombination of CO to the heme iron with respect to hIDO-CO/L-Trp'.

It is very likely that this inhibitory binding site exists as well in the major protein species hIDO-CO/L-Trp. The activity measurements by Yeh and coworkers showed that the activity of hIDO was almost totally inhibited at high L-Trp concentrations<sup>[54]</sup>. Therefore, we assume that both protein species are inhibited by a second L-Trp binding at an inhibitory site.

Our results provide further clear evidence of the existence of a second, inhibitory substrate binding site. This binding site is a potential drug target to control the activity of hIDO. As yet, its position inside the protein matrix as well as the mechanism by which binding of the second L-Trp decreases the protein activity remains unclear. Our results indicate that the second binding site is not located in hydrogen-bonding distance to the heme-bound ligand close to the active site or interferes with any of the docking sites, based on the finding that the L-Trp at the secondary docking site exhibits an IR spectrum of substrate-free protein. Therefore, we presume that binding of the second L-Trp does not disturb the L-Trp at the active site of hIDO-CO. The breakdown of the ternary complex for sterical reasons appears unlikely. Alternatively, the release of the product NFK could be hindered sterically, inhibiting a new conversion cycle.

### 7.3 Substrate Binding and Catalytic Activity

IDO converts a wide range of substrates, including L-Trp and D-Trp ( $K_m(\text{L-Trp}) = 15 \mu\text{M}$ ,  $k_{\text{cat}}(\text{L-Trp}) = 3 \text{ s}^{-1}$  and  $K_m(\text{D-Trp}) = 2,600 \mu\text{M}$ ,  $k_{\text{cat}}(\text{D-Trp}) = 6 \text{ s}^{-1}$ <sup>[23,54]</sup>) whereas S-Trp was shown to be an inhibitor<sup>[53]</sup>. A prominent inhibitor used in clinical trials is MLT with a  $K_m(\text{MLT})$  of  $62 \mu\text{M}$  but with a significantly decreased  $k_{\text{cat}}(\text{MLT})$  that is  $\approx 50$ -fold lower than that of L-Trp<sup>[54,122]</sup>.

As yet, the details of the catalytic reaction of hIDO are still under debate<sup>[14]</sup>. Several mechanisms have been proposed for the conversion of indoles in hIDO. Early proposals favored base-catalyzed abstraction mechanisms<sup>[55,107,134]</sup>. However, the finding that MLT is a substrate for hIDO<sup>[122]</sup> and that an active site base such as a histidine is absent at the active site of hIDO, intensified the search for alternative conversion mechanisms. Two mechanisms were proposed that considered the reactivity towards MLT and avoided the deprotonation of the indole NH group. The mechanisms suggest the initiation of the reaction by electrophilic addition<sup>[122]</sup> or radical addition<sup>[123,135,136]</sup>.

Both mechanisms require spatial proximity of the oxygen ligand to the  $\text{C}_2 = \text{C}_3$  double bond of L-Trp. Therefore, the exact positioning of the substrate at the active site is of utmost importance for the efficient activity of hIDO. The crystal structure and docking simulations show that an exquisite interaction network is established between the substrate, the protein matrix, the heme group and the ligand that ensures precise orientation of the substrate at the active site<sup>[55,123]</sup>. If this network is disrupted, e.g., by site directed mutagenesis, both the affinity for L-Trp and, concomitantly, the activity, are drastically reduced.

The binding of L-Trp at the active site causes a significant change in the stretching vibration of the heme-bound CO. The extraordinary low frequency of the  $A_L$  band indicates formation of a hydrogen bond between L-Trp and the CO oxygen atom. On the basis of our results we suggest that the  $A_L$  band is a perfect indicator for the binding of a substrate at the active site. Substrates that exhibit an  $A_L$ -like band establish a hydrogen bond to the ligand and thus bind at the active site in a L-Trp-like manner, which is likely a requirement for the conversion of the substrate. Our data on the L-Trp analogues D-Trp, S-Trp and MLT support this hypothesis.

The IR absorbance spectrum of hIDO-CO/D-Trp reveals only a weak  $A_L$ -like band. This is consistent with the low affinity of hIDO for D-Trp, as indicated by a  $K_m(\text{D-Trp})$  of  $2,600 \mu\text{M}$ . However, the  $k_{\text{cat}}(\text{D-Trp}) = 6 \text{ s}^{-1}$  equals the one of L-Trp, suggesting that the catalytic efficiency of the proteins binding D-Trp in a L-Trp-like way is similar to that of L-Trp<sup>[54]</sup>.

S-Trp is an inhibitor in rabbit IDO. The binding of S-Trp to hIDO-CO does not generate any shift in the band of heme-bound CO. We suggest that the binding position of S-Trp is at least slightly different from that of L-Trp and does not allow formation of a hydrogen bond between the ligand and the substrate.

The interactions established upon binding of MLT at the active site of hIDO-CO are identical to the ones in hIDO-CO/L-Trp, indicated by an  $A_L$ -like band and a significant Soret band shift. The binding affinity of MLT to hIDO-CO is even higher than for the natural substrate ( $K_d(\text{L-Trp}) \approx 95 \mu\text{M}$ ,  $K_d(\text{MLT}) \approx 38 \mu\text{M}$ <sup>[54]</sup>). However, the  $k_{\text{cat}}$  of MLT is significantly decreased compared to L-Trp<sup>[122]</sup>, demonstrating that the binding position of the substrate at the active site is an essential but not the only requirement for substrate conversion. Presumably, the methyl group at the nitrogen of the L-Trp indole moiety generates an inductive effect stabilizing a cation intermediate and, thereby, slows the electrophilic attack and, hence, the overall reaction<sup>[122]</sup>.

## 7.4 Inhibition of hIDO by 1-MT

The search for an efficient inhibitor for hIDO is still ongoing. Our experiments offer some ideas about the characteristics a competitive inhibitor should exhibit. (1) The inhibitor should have a high affinity towards hIDO-O<sub>2</sub>, (2) bind to the active site of hIDO-O<sub>2</sub> (not only within the heme pocket), and (3) block the B site of hIDO.

Although several inhibitors for hIDO were tested in recent years, the most promising inhibitor of hIDO is still 1-methyl-DL-tryptophan (1-ML), a racemate mixture of the two isoforms MLT and MDT. 1-ML acts as a competitive inhibitor of hIDO with a  $K_i(1\text{-ML})$  between 35 and 62  $\mu\text{M}$ <sup>[48,53,137]</sup>.

Our results suggest that MLT is an efficient inhibitor of hIDO because it binds in an L-Trp-like way. Thereby, it blocks the B site of hIDO, and we presume that the ternary complex is only broken down by conversion. This conversion, however, is very slow in the case of MLT<sup>[122]</sup>. According to our results obtained with D- and L-Trp, we expect the efficiency of inhibition of hIDO by MLT to be much higher than towards MDT. It seems of utmost importance to take the stereoselectivity of hIDO into account in the ongoing search for efficient and selective inhibitors.

## 7.5 hIDO, hIDO2 and TDO: Three Proteins Converting L-Trp

hIDO is only one out of three enzymes found to convert L-Trp in humans. The finding that the level of hIDO expression is increased in tumor cells, which promotes tumor growth by suppressing antitumor immune response, has intensified research on hIDO. The first results of inhibitory studies with 1-ML and the two isoforms, MLT and MDT, were puzzling because only in some cells the hIDO activity was inhibited by MDT<sup>[138]</sup>. These finding could be explained by the identification of a second gene encoding an IDO-like protein, hIDO2. The genes of hIDO and hIDO2 are situated adjacent to each other on one chromosome<sup>[139,140]</sup>. Both proteins share 43% similarity at the amino acid level<sup>[47]</sup>. However, they exhibit different expression patterns indicating different physiological functions<sup>[47,138]</sup>. Kinetic studies carried out by Meininger et al.<sup>[49]</sup>, showed that, despite great similarity in the structure including the active site, the  $K_m$  of hIDO2 for L-Trp is much higher than in hIDO (at least 290-fold). First studies have indicated that the two proteins do not share the same inhibition profiles<sup>[49]</sup>.

Just recently, TDO was found to be overexpressed in tumor cells demonstrating again the importance of selective inhibition of the three proteins<sup>[141]</sup>. For a successful identification of inhibitors and the understanding of the inhibitory mechanism(s), detailed studies of the kinetic and inhibitor profiles and the connection between protein structure and activity is required. This work gives a closer insight into the binding of the substrate L-Trp and the competitive inhibitor MLT. A comparative study with hIDO2 and TDO could be very helpful to identify the interplay between structure and activity. A 'targeted' identification of inhibitors requires a detailed understanding of the catalytic mechanism on a molecular basis.

## 7.6 Outlook

Our results expand the picture of ligand and substrate migration in hIDO and might help to advance in the search for more efficient inhibitors. However, a lot of questions remain unanswered and some topics need to be further elucidated.

As long as the crystal structure of L-Trp-bound hIDO is not solved, spectroscopic studies on the protein will help to obtain more information about the binding of L-Trp in hIDO. We have already identified some amino acids involved in binding of the substrate. Further site directed mutagenesis studies could elucidate if the affinity for the substrate is changed when the interactions between the indole moiety and the protein matrix is disturbed. Promising candidates for additional studies would be the amino acids F163 and F226.

We proved the existence of several ligand docking sites in substrate-free and L-Trp-bound hIDO. Combined with the tool of site directed mutagenesis, further FTIR spectroscopy measurements may be helpful to identify the positions of these docking sites within the protein matrix. The application of molecular dynamics simulations might also be very useful to assign the location of the ligand docking sites within the protein matrix.

Our experiments could only show the existence of an inhibitory site in the minor species hIDO-CO/L-Trp'. More elaborated flash photolysis experiments, e.g. pumping the ligand into the solvent by successive photolysis events, could give some insight into the ligand recombination in hIDO-CO/L-Trp and, therefore, into the existence of a second binding site in these species.

To selectively inhibit the three dioxygenases hIDO, TDO and hIDO2, a better knowledge of substrate binding in these proteins is needed. Comparative measurements with hIDO2 and TDO should be performed to gain a better understanding for the similarities and differences concerning the binding of substrates and inhibitors.



# Chapter 8

## Summary

In humans,  $\approx 95\%$  of the essential amino acid L-tryptophan (L-Trp) is metabolized in the kynurenine pathway. To date, three dioxygenases have been identified that catalyze the degradation of L-Trp to N-formylkynurenine by inserting dioxygen into the indole moiety of L-Trp which is the first and rate-limiting step of the pathway. The heme protein tryptophan 2,3-dioxygenase (TDO) is predominantly found in the liver whereas monomeric proteins, human indoleamine 2,3-dioxygenase (hIDO) and the only recently identified human indoleamine 2,3-dioxygenase 2, are distributed in different tissues of the body. Whereas the substrate specificity of TDO for L-Trp is high, hIDO is capable of binding and catalyzing a wider range of substrate such as D-tryptophan or Serotonin. However, the affinity for these substrates is decreased in respect to the L-Trp affinity. An increased expression of hIDO results in the depletion of L-Trp and the accumulation of its metabolites and was shown to be associated with several (patho)-physiological conditions. These findings set off an extensive search for selective inhibitors of hIDO. Although hIDO has been in the focus of intensive research, the details of ligand and substrate binding and conversion as well as protein inhibition at increased L-Trp concentration are not sufficiently elucidated yet.

This study focuses on the interactions between hIDO, ligand and substrate. Both, the relative orientation of the three components to each other as well as the complex formation were investigated. Replacing the physiological ligand dioxygen by carbon monoxide (CO) allowed the observation of the complex of hIDO, CO and L-Trp by visible and Fourier transform infrared (FTIR) spectroscopy. Heme-bound CO and photodissociated CO served to probe the active site structure and the protein matrix of hIDO. Temperature derivative spectroscopy (TDS) over a wide temperature range and flash photolysis measurements at ambient temperature were employed to study the kinetic of ligand and substrate binding in hIDO. The stretching vibration of heme-bound CO is very sensitive to changes in the electrostatic field

---

in its direct vicinity and can be used to probe already small changes at the active site of hIDO. The FTIR spectrum of hIDO-CO displayed at least three distinct absorbance bands of heme-bound CO representing different active site conformations, also denoted as conformational substates. The relative populations of the substates were shown to be strongly temperature dependent. Mutagenesis studies revealed that the different active site conformations might be based on structural changes in a flexible loop (residues amino acids 250 to 265) that is located close to the active site. TDS experiments showed that the protein substates exhibit differences in the number of transient ligand docking sites and in the internal ligand rebinding.

The incorporation of the physiological ligand O<sub>2</sub> into the indole moiety of the L-Trp requires the binding of L-Trp in close proximity to the heme-bound ligand. CO rebinding experiments at ambient temperature revealed that L-Trp binds in two different modes to hIDO-CO. The major fraction ( $\approx 80\%$ ) of L-Trp binds in close vicinity to the heme-bound ligand. FTIR and UV/Vis measurements showed that L-Trp in this binding mode establishes a network of interactions with the heme group, the CO ligand and the protein matrix. Mutagenesis studies verified that R231 and T379 are necessary for the binding of L-Trp in this orientation. The interaction network ensures the correct positioning of the substrate. The ternary complex with L-Trp in this binding mode is expected to be the catalytic active form. Additionally, the binding of L-Trp at the active site hinders the release from and the rebinding of the ligand to the heme iron. The results demonstrate that the ligand has to bind to the heme iron before the substrate to ensure the catalytic activity of the protein.

A smaller fraction of proteins also binds L-Trp but not at the active site. Upon photolysis, the ligand can escape into the solvent at ambient temperature. The rebinding of CO to the heme iron is slower than to hIDO-CO. L-Trp bound in this species interacts with the heme group but not with the CO ligand. In this protein fraction the binding of a second L-Trp to hIDO-CO at very high substrate concentration was observed, indicating the existence of a second substrate binding site. This second L-Trp binding site is presumably an inhibitory binding site causing the effect of hIDO activity inhibition at high substrate concentrations.

FTIR measurements demonstrated that the CO stretching vibration can be used to verify the binding of L-Trp and substrate analogous at the active site. Comparative measurements with different substrate analogous underline the stereoselectivity of hIDO for L-enantiomers. Structural variations in the indole moiety results in changes in the affinity of hIDO to the different substrates.

The results expand the picture of ligand and substrate migration in hIDO and might help in the search for more efficient inhibitors.

---

## Zusammenfassung

Im Menschen werden etwa 95% der essentiellen Aminosäure L-Tryptophan (L-Trp) im Kynurenin-Metabolismus umgesetzt. Bislang wurden drei Dioxygenasen entdeckt, die die Oxidation von L-Trp zu N-Formylkynurenin katalysieren. Hierbei werden die beiden Atome des am Häm gebundene Sauerstoffmoleküls auf die Indoleinheit des L-Trp übertragen. Das Hämprotein Tryptophan 2,3-Dioxygenase (TDO) wird fast ausschließlich in der Leber gefunden, während die monomere Indolamin 2,3-Dioxygenase (hIDO) und die erst kürzlich identifizierte Indolamin 2,3-Dioxygenase 2 in unterschiedlichen Gewebetypen des menschlichen Körpers produziert werden. Die Substratspezifität von TDO für L-Trp ist sehr hoch, während hIDO auch einige andere Substrate wie D-Tryptophan oder Serotonin mit eingeschränkter Affinität bindet und umsetzt. Eine erhöhte Expression von hIDO, die sowohl zu einem Mangel an L-Trp als auch zu einer Anhäufung von teilweise toxischen Zwischenprodukten führt, wird mit unterschiedlichen physiologischen Prozessen wie der Immuntoleranz gegenüber dem Fötus oder auch mit der durch Tumore hervorgerufene Immunsuppression in Verbindung gebracht. Daher ist das medizinische Interesse an hIDO und die Suche nach effektiven und gleichzeitig selektiven Inhibitoren groß. Trotz intensiver Forschung an hIDO in den letzten Jahren konnten viele Details der Substrat- und Ligandenbindung, der Substratumsatzung und der Proteininhibierung bei hohen Substratkonzentrationen, die vermutlich durch die Substratbindung an einer zweiten Bindestelle beruht, bislang nicht ausreichend erklärt werden.

Die vorliegende Arbeit beschäftigt sich mit der Wechselwirkung zwischen hIDO, Ligand und Substrat. Sowohl die relative Orientierung der einzelnen Komponenten zueinander als auch die Ausbildung des ternären Komplexes wurden untersucht. Der Austausch des physiologischen Liganden Sauerstoff durch Kohlenstoffmonoxid (CO) ermöglichte die Beobachtung des Komplexes mittels optischer sowie Fourier-Transform-Infrarot (FTIR) Spektroskopie. Häm-gebundenes und photodissoziiertes CO wurde als Sonde genutzt, um Änderungen an der aktive Stelle und in der Proteinmatrix zu untersuchen, die durch die Bindung von L-Trp auftreten. Temperatur-derivative Spektroskopie (TDS) über einen breiten Temperaturbereich und Blitzlichtphotolyse bei Raumtemperatur wurden zur Untersuchung der Kinetik der Liganden- und Substratbindung in hIDO genutzt.

Es konnte gezeigt werden, dass hIDO-CO in mindestens drei unterschiedlichen Konformationssubzustände vorliegt. Mutationsstudien wiesen darauf hin, dass die unterschiedlichen Subzustände auf strukturellen Unterschieden in einer flexiblen Aminosäurekette beruhen könnten. Die jeweiligen Subzustände unterscheiden sich durch ihre Anzahl an Kavitäten in der Proteinmatrix, die als transiente Ligandenandockstellen dienen, und in der Liganden-Rückbindung.

---

L-Trp bindet in zwei unterschiedlichen Arten in CO gebundenem hIDO. Etwa 80% der Proteine bindet L-Trp an der aktiven Stelle in nächster Nähe zum Liganden und bildet ein Netzwerk von Wechselwirkungen zu dem Liganden, dem Häm und der Proteinmatrix (Aminosäuren T379 und R231) aus. Vermutlich ist dieser Protein-Ligand-Substrat-Komplex katalytisch aktiv. Die Bindung von L-Trp hat zur Folge, dass die Freisetzung vom und die Bindung des Liganden am Hämeisen behindert wird. Unsere Experimente machen deutlich, dass für eine effiziente Funktionalität des Proteins die Bindung des Liganden an das Protein der Substratbindung vorangehen muss.

Eine kleinere Proteinfraction bindet ebenfalls L-Trp, jedoch nicht an der aktiven Stelle. In dieser Fraktion kann der Ligand nach Photolyse bei Raumtemperatur in das Lösungsmittel entweichen, zeigt aber im Vergleich zu hIDO-CO eine verlangsamte Rückbindung des Liganden. Das L-Trp in dieser Konformation wechselwirkt mit der Hämgruppe, jedoch nicht mit dem Liganden. Bei hohen Konzentrationen von L-Trp wird eine zweite Substratbindungsstelle besetzt, was die Rückbindung von CO weiter verlangsamt. Hierbei handelt es sich möglicherweise um die Bindestelle, die bei hohen Substratkonzentrationen für die Inhibierung des Proteins verantwortlich ist.

Die CO Streckschwingung kann zur Verifizierung der Bindung von L-Trp und Substratanaloga an der aktiven Stelle genutzt werden. Vergleichsstudien mit unterschiedlichen Substratanaloga heben die Stereoselektivität von hIDO für L-Enantiomere hervor.

Die Ergebnisse haben das derzeitige Bild der Liganden- und Substratbindung in hIDO erweitert und können helfen, die Suche nach Proteininhibitoren zielgerichteter zu gestalten.

# Appendix A

## List of Primers

Table A.1: Primer sequences. Bases encoding for the mutated amino acids are highlighted.

R231A	CATTTTTCAGTGTTCTT <b>GCC</b> ATATATTTGTCTGGC
R231E	CAGTGTTCTT <b>GAG</b> ATATATTTGTCTGGCTGG
G261A	CAAAGGAGTTTGCA <b>GCG</b> GGCAGTG
T367A	GGAGAATAAG <b>GCCT</b> CTGAAGACCCTTC
T379A	GAAGCCAAAGGA <b>GCT</b> GGAGGCACTG



## Appendix B

### Chemical Structures of L-Trp, D-Trp, S-Trp and MLT

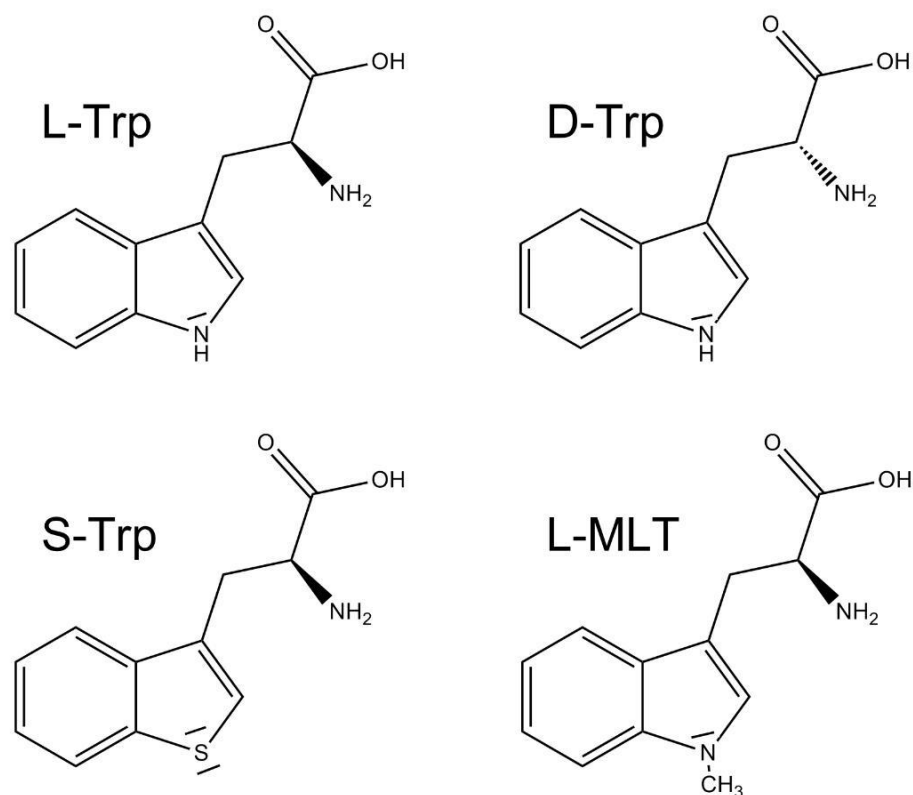


Figure B.1: Chemical structures of L-Trp, D-Trp, S-Trp and MLT.



# Appendix C

## List of Equations

### Gaussian

$$y = y_0 + A \cdot e^{-\frac{(x-x_c)^2}{2w^2}}$$

$A$ : amplitude

$y_0$ : offset

$x_c$ : center

$w$ : width

$2w$ : FWHM/ $\sqrt{\ln 4}$

### Exponential Decay

$$y = A \cdot e^{-x \cdot k}$$

$A$ : amplitude

$k$ : rate coefficient

### Hill Equation

$$y = y_0 + \left( \frac{A}{1 + \left( \frac{K_d}{x} \right)^n} \right)$$

$A$ : amplitude

$y_0$ : offset

$K_d$ : dissociation constant

$n$ : Hill coefficient



# Bibliography

- [1] Dawson, J. (1988) Probing structure-function relations in heme-containing oxygenases and peroxidases. *Science*, **240**, 433.
- [2] Antonini, E. and Brunori, M. (1971) *Hemoglobin and Myoglobin in their Reactions with Ligands*. North-Holland Publishing Co. Amsterdam.
- [3] Hsia, C. (1998) Respiratory function of hemoglobin. *New Engl. J. Med.*, **338**, 239.
- [4] Millikan, G. (1937) Experiments on muscle haemoglobin in vivo; the instantaneous measurement of muscle metabolism. *Proc. R. Soc. London. Biol.*, **123**, 218.
- [5] Hemmingsen, E. (1963) Enhancement of oxygen transport by myoglobin. *Comp. Biochem. Physiol.*, **10**, 239.
- [6] Wittenberg, J. and Wittenberg, B. (2003) Myoglobin function reassessed. *J. Exp. Biol.*, **206**, 2011.
- [7] Aono, S. and Nakajima, H. (1999) Structure and function of CooA, a novel transcriptional regulator containing a b-type heme as a CO sensor. *Coord. Chem. Rev.*, **190**, 267.
- [8] Chan, M. (2001) Recent advances in heme-protein sensors. *Curr. Opin. Chem. Biol.*, **5**, 216.
- [9] Lucas, M., Rousseau, D., and Guallar, V. (2011) Electron transfer pathways in cytochrome c oxidase. *Biochim. Biophys. Acta - Bioenerg.*, **1807**, 1305.
- [10] Brittain, T. (2008) Intra-molecular electron transfer in proteins. *Protein Pept. Lett.*, **15**, 556.
- [11] Mayo, S., Ellis, W., Crutchley, R., and Gray, H. (1986) Long-range electron transfer in heme proteins. *Science*, **233**, 948.

- 
- [12] Loew, G. and Harris, D. (2000) Role of the heme active site and protein environment in structure, spectra, and function of the cytochrome P450s. *Chem. Rev.*, **100**, 407.
- [13] Alderton, W., Cooper, C., and Knowles, R. (2001) Nitric oxide synthases: structure, function and inhibition. *Biochem. J.*, **357**, 593.
- [14] Efimov, I., Basran, J., Thackray, S., Handa, S., Mowat, C., and Raven, E. (2011) Structure and reaction mechanism in the heme-dioxygenases. *Biochemistry*, **50**, 2717.
- [15] Botting, N. (1995) Chemistry and neurochemistry of the kynurenine pathway of tryptophan metabolism. *Chem. Soc. Rev.*, **24**, 401.
- [16] Takikawa, O. (2005) Biochemical and medical aspects of the indoleamine 2,3-dioxygenase-initiated L-tryptophan metabolism. *Biochem. Biophys. Res. Commun.*, **338**, 12.
- [17] Vottero, E., Mitchell, D., Page, M., MacGillivray, R., Sadowski, I., Roberge, M., and Mauk, A. (2006) Cytochrome  $b_5$  is a major reductant in vivo of human indoleamine 2,3-dioxygenase expressed in yeast. *FEBS Lett.*, **580**, 2265.
- [18] Maghzal, G., Thomas, S., Hunt, N., and Stocker, R. (2008) Cytochrome  $b_5$ , not superoxide anion radical, is a major reductant of indoleamine 2,3-dioxygenase in human cells. *J. Biol. Chem.*, **283**, 12014.
- [19] Yuasa, H., Takubo, M., Takahashi, A., Hasegawa, T., Noma, H., and Suzuki, T. (2007) Evolution of vertebrate indoleamine 2,3-dioxygenases. *J. Mol. Evol.*, **65**, 705.
- [20] Yuasa, H. and Ball, H. (2011) Molecular evolution and characterization of fungal indoleamine 2,3-dioxygenases. *J. Mol. Evol.*, **72**, 160.
- [21] Zhu, X., Van Pee, K., and Naismith, J. (2010) The ternary complex of PrnB (the second enzyme in the pyrrolnitrin biosynthesis pathway), tryptophan, and cyanide yields new mechanistic insights into the indoleamine dioxygenase superfamily. *J. Biol. Chem.*, **285**, 21126.
- [22] Schutz, G. and Feigelson, P. (1972) Purification and properties of rat liver tryptophan oxygenase. *J. Biol. Chem.*, **247**, 5327.
- [23] Shimizu, T., Nomiya, S., Hirata, F., and Hayaishi, O. (1978) Indoleamine 2,3-dioxygenase. Purification and some properties. *J. Biol. Chem.*, **253**, 4700.

- 
- [24] Forouhar, F., et al. (2007) Molecular insights into substrate recognition and catalysis by tryptophan 2,3-dioxygenase. *Proc. Nat. Acad. Sci.*, **104**, 473.
- [25] Leeds, J., Brown, P., McGeehan, G., Brown, F., and Wiseman, J. (1993) Isotope effects and alternative substrate reactivities for tryptophan 2,3-dioxygenase. *J. Biol. Chem.*, **268**, 17781.
- [26] Yamamoto, S. and Hayaishi, O. (1967) Tryptophan pyrrolase of rabbit intestine. *J. Biol. Chem.*, **242**, 5260.
- [27] Uchida, K., Shimizu, T., Makino, R., Sakaguchi, K., Iizuka, T., Ishimura, Y., Nozawa, T., and Hatano, M. (1983) Magnetic and natural circular dichroism of L-tryptophan 2,3-dioxygenases and indoleamine 2,3-dioxygenase. I. Spectra of ferric and ferrous high spin forms. *J. Biol. Chem.*, **258**, 2519.
- [28] Uchida, K., Shimizu, T., Makino, R., Sakaguchi, K., Iizuka, T., Ishimura, Y., Nozawa, T., and Hatano, M. (1983) Magnetic and natural circular dichroism of L-tryptophan 2,3-dioxygenases and indoleamine 2,3-dioxygenase. II. Spectra of their ferric cyanide and ferrous carbon monoxide complexes and an oxygenated form. *J. Biol. Chem.*, **258**, 2526.
- [29] Taniguchi, T., Sono, M., Hirata, F., Hayaishi, O., Tamura, M., Hayashi, K., Iizuka, T., and Ishimura, Y. (1979) Indoleamine 2,3-dioxygenase. Kinetic studies on the binding of superoxide anion and molecular oxygen to enzyme. *J. Biol. Chem.*, **254**, 3288.
- [30] Takikawa, O., Kuroiwa, T., Yamazaki, F., and Kido, R. (1988) Mechanism of interferon-gamma action. Characterization of indoleamine 2,3-dioxygenase in cultured human cells induced by interferon-gamma and evaluation of the enzyme-mediated tryptophan degradation in its anticellular activity. *J. Biol. Chem.*, **263**, 2041.
- [31] Sono, M., Taniguchi, T., Watanabe, Y., and Hayaishi, O. (1980) Indoleamine 2,3-dioxygenase. Equilibrium studies of the tryptophan binding to the ferric, ferrous, and CO-bound enzymes. *J. Biol. Chem.*, **255**, 1339.
- [32] Sono, M. (1990) Spectroscopic and equilibrium studies of ligand and organic substrate binding to indoleamine 2,3-dioxygenase. *Biochemistry*, **29**, 1451.
- [33] Sono, M. (1986) Spectroscopic and equilibrium properties of the indoleamine 2,3-dioxygenase-tryptophan-oxygen ternary complex and of analogous enzyme derivatives. Tryptophan binding to ferrous enzyme adducts with dioxygen, nitric oxide, and carbon monoxide. *Biochemistry*, **25**, 6089.

- 
- [34] Tone, S., Takikawa, O., Habara-Ohkubo, A., Kadoya, A., Yoshida, R., and Kido, R. (1990) Primary structure of human indoleamine 2,3-dioxygenase deduced from the nucleotide sequence of its cDNA. *Nucleic Acids Res.*, **18**, 367.
- [35] Wichers, M. and Maes, M. (2004) The role of indoleamine 2,3-dioxygenase (IDO) in the pathophysiology of interferon- $\alpha$ -induced depression. *J. Psychiatry Neurosci.*, **29**, 11.
- [36] Uyttenhove, C., Pilotte, L., Théate, I., Stroobant, V., Colau, D., Parmentier, N., Boon, T., and Van den Eynde, B. (2003) Evidence for a tumoral immune resistance mechanism based on tryptophan degradation by indoleamine 2,3-dioxygenase. *Nat. Med.*, **9**, 1269.
- [37] Mellor, A. and Munn, D. (1999) Tryptophan catabolism and T-cell tolerance: immunosuppression by starvation? *Immunol. Today*, **20**, 469.
- [38] Munn, D., Mellor, A., et al. (2007) Indoleamine 2,3-dioxygenase and tumor-induced tolerance. *J. Clin. Invest.*, **117**, 1147.
- [39] Guillemin, G., Brew, B., Noonan, C., Takikawa, O., and Cullen, K. (2005) Indoleamine 2,3-dioxygenase and quinolinic acid immunoreactivity in Alzheimer's disease hippocampus. *Neuropath. Appl. Neuro.*, **31**, 395.
- [40] Macchiarulo, A., Camaioni, E., Nuti, R., and Pellicciari, R. (2009) Highlights at the gate of tryptophan catabolism: a review on the mechanisms of activation and regulation of indoleamine 2,3-dioxygenase (IDO), a novel target in cancer disease. *Amino acids*, **37**, 219.
- [41] Mailankot, M., Staniszewska, M., Butler, H., Caprara, M., Howell, S., Wang, B., Doller, C., Reneker, L., and Nagaraj, R. (2009) Indoleamine 2,3-dioxygenase overexpression causes kynurenine-modification of proteins, fiber cell apoptosis and cataract formation in the mouse lens. *Lab. Invest.*, **89**, 498.
- [42] Takikawa, O., Littlejohn, T., and Truscott, R. (2001) Indoleamine 2,3-dioxygenase in the human lens, the first enzyme in the synthesis of UV filters. *Exp. Eye Res.*, **72**, 271.
- [43] Schrotten, H., Spors, B., Hucke, C., Stins, M., Kim, K., Adam, R., and Däubener, W. (2001) Potential role of human brain microvascular endothelial cells in the pathogenesis of brain abscess: inhibition of *Staphylococcus aureus* by activation of indoleamine 2,3-dioxygenase. *Neuropediatrics*, **32**, 206.

- 
- [44] Mahon, B. and Mills, K. (1999) Interferon- $\gamma$  mediated immune effector mechanisms against *Bordetella pertussis*. *Immunol. Lett.*, **68**, 213.
- [45] Hwu, P., Du, M., Lapointe, R., Do, M., Taylor, M., and Young, H. (2000) Indoleamine 2,3-dioxygenase production by human dendritic cells results in the inhibition of T-cell proliferation. *J. Immunol.*, **164**, 3596.
- [46] Mellor, A. and Munn, D. (2004) IDO expression by dendritic cells: tolerance and tryptophan catabolism. *Nat. Rev. Immunol.*, **4**, 762.
- [47] Ball, H., Sanchez-Perez, A., Weiser, S., Austin, C., Astelbauer, F., Miu, J., McQuillan, J., Stocker, R., Jermini, L., and Hunt, N. (2007) Characterization of an indoleamine 2,3-dioxygenase-like protein found in humans and mice. *Gene*, **396**, 203.
- [48] Austin, C., et al. (2010) Biochemical characteristics and inhibitor selectivity of mouse indoleamine 2,3-dioxygenase-2. *Amino acids*, **39**, 565.
- [49] Meininger, D., Zalameda, L., Liu, Y., Stepan, L., Borges, L., McCarter, J., and Sutherland, C. (2011) Purification and kinetic characterization of human indoleamine 2,3-dioxygenases 1 and 2 (IDO1 and IDO2) and discovery of selective IDO1 inhibitors. *Biochim. Biophys. Acta - Proteins Proteomics*, **1814**, 1947.
- [50] Kumar, S., Jaller, D., Patel, B., LaLonde, J., DuHadaway, J., Malachowski, W., Prendergast, G., and Muller, A. (2008) Structure based development of phenylimidazole-derived inhibitors of indoleamine 2,3-dioxygenase. *J. Med. Chem.*, **51**, 4968.
- [51] Röhrig, U., et al. (2010) Rational design of indoleamine 2,3-dioxygenase inhibitors. *J. Med. Chem.*, **53**, 1172.
- [52] Sono, M. and Cady, S. (1989) Enzyme kinetic and spectroscopic studies of inhibitor and effector interactions with indoleamine 2,3-dioxygenase. 1. norharman and 4-phenylimidazole binding to the enzyme as inhibitors and heme ligands. *Biochemistry*, **28**, 5392.
- [53] Cady, S. and Sono, M. (1991) 1-Methyl-DL-tryptophan, beta-(3-benzofuranyl)-DL-alanine (the oxygen analog of tryptophan), and beta-[3-benzo(b)thienyl]-DL-alanine (the sulfur analog of tryptophan) are competitive inhibitors for indoleamine 2,3-dioxygenase. *Arch. Biochem. Biophys.*, **291**, 326.
- [54] Lu, C., Lin, Y., and Yeh, S. (2009) Inhibitory substrate binding site of human indoleamine 2,3-dioxygenase. *J. Am. Chem. Soc.*, **131**, 12866.

- 
- [55] Sugimoto, H., Oda, S., Otsuki, T., Hino, T., Yoshida, T., and Shiro, Y. (2006) Crystal structure of human indoleamine 2,3-dioxygenase: catalytic mechanism of O<sub>2</sub> incorporation by a heme-containing dioxygenase. *Proc. Natl. Acad. Sci. USA*, **103**, 2611.
- [56] Chauhan, N., Basran, J., Efimov, I., Svistunenko, D., Seward, H., Moody, P., and Raven, E. (2008) The role of serine 167 in human indoleamine 2,3-dioxygenase: a comparison with tryptophan 2,3-dioxygenase. *Biochemistry*, **47**, 4761.
- [57] DeLano, W. (2002) *The PyMOL Molecular Graphics System*. DeLano Scientific.
- [58] Gibson, Q. and Ainsworth, S. (1957) Photosensitivity of haem compounds. *Nature*, **180**, 1416.
- [59] Chance, M., Courtney, S., Chavez, M., Ondrias, M., and Friedman, J. (1990) Oxygen and carbon monoxide reactions with heme proteins: quantum yields and geminate recombination on picosecond time scales. *Biochemistry*, **29**, 5537.
- [60] Miller, L., Patel, M., and Chance, M. (1996) Identification of conformational substates in oxymyoglobin through the pH-dependence of the low-temperature photoproduct yield. *J. Am. Chem. Soc.*, **118**, 4511.
- [61] Austin, R., Beeson, K., Eisenstein, L., Frauenfelder, H., and Gunsalus, I. (1975) Dynamics of ligand binding to myoglobin. *Biochemistry*, **14**, 5355.
- [62] Brunori, M., Bonaventura, J., Bonaventura, C., Antonini, E., and Wyman, J. (1972) Carbon monoxide binding by hemoglobin and myoglobin under photodissociating conditions. *Proc. Natl. Acad. Sci.*, **69**, 868.
- [63] Ostermann, A., Waschipky, R., Parak, F., and Nienhaus, G. (2000) Ligand binding and conformational motions in myoglobin. *Nature*, **404**, 205.
- [64] Nienhaus, K., Deng, P., Kriegl, J., and Nienhaus, G. (2003) Structural dynamics of myoglobin: Spectroscopic and structural characterization of ligand docking sites in myoglobin mutant L29W. *Biochemistry*, **42**, 9633.
- [65] Chu, K., Vojtchovsky, J., McMahon, B., Sweet, R., Berendzen, J., and Schlichting, I. (2000) Structure of a ligand-binding intermediate in wild-type carbonmonoxy myoglobin. *Nature*, **403**, 921.

- 
- [66] Schotte, F., Lim, M., Jackson, T., Smirnov, A., Soman, J., Olson, J., Phillips, G., Wulff, M., and Anfinrud, P. (2003) Watching a protein as it functions with 150-ps time-resolved x-ray crystallography. *Science*, **300**, 1944.
- [67] Teng, T., Šrajer, V., and Moffat, K. (1994) Photolysis-induced structural changes in single crystals of carbonmonoxy myoglobin at 40 K. *Nat. Struct. Biol.*, **1**, 701.
- [68] Schlichting, I., Berendzen, J., Phillips, G., and Sweet, R. (1994) Crystal structure of photolysed carbonmonoxy-myoglobin. *Nature*, **371**, 808.
- [69] Hartmann, H., Zinser, S., Komninos, P., Schneider, R., Nienhaus, G., and Parak, F. (1996) X-ray structure determination of a metastable state of carbonmonoxy myoglobin after photodissociation. *Proc. Natl. Acad. Sci.*, **93**, 7013.
- [70] Nienhaus, G., Chu, K., and Jesse, K. (1998) Structural heterogeneity and ligand binding in carbonmonoxy myoglobin crystals at cryogenic temperatures. *Biochemistry*, **37**, 6819.
- [71] Schlichting, I. and Chu, K. (2000) Trapping intermediates in the crystal: ligand binding to myoglobin. *Curr. Opin. Struct. Biol.*, **10**, 744.
- [72] Brunori, M., Vallone, B., Cutruzzolà, F., Travaglini-Allocatelli, C., Berendzen, J., Chu, K., Sweet, R., and Schlichting, I. (2000) The role of cavities in protein dynamics: crystal structure of a photolytic intermediate of a mutant myoglobin. *Proc. Natl. Acad. Sci.*, **97**, 2058.
- [73] Nienhaus, K., Deng, P., Kriegl, J., and Nienhaus, G. (2003) Structural dynamics of myoglobin: Effect of internal cavities on ligand migration and binding. *Biochemistry*, **42**, 9647.
- [74] Lutz, S., Nienhaus, K., Nienhaus, G., and Meuwly, M. (2009) Ligand migration between internal docking sites in photodissociated carbonmonoxy neuroglobin. *J. Phys. Chem. B*, **113**, 15334.
- [75] Lim, M., Jackson, T., and Anfinrud, P. (1995) Mid-infrared vibrational spectrum of CO after photodissociation from heme: Evidence for a ligand docking site in the heme pocket of hemoglobin and myoglobin. *J. Chem. Phys.*, **102**, 4355.
- [76] Nienhaus, K., Deng, P., Belyea, J., Franzen, S., and Nienhaus, G. (2006) Spectroscopic study of substrate binding to the carbonmonoxy form of dehaloperoxidase from *Amphitrite ornata*. *J. Phys. Chem. B*, **110**, 13264.

- 
- [77] Henry, E., Sommer, J., Hofrichter, J., Eaton, W., and Gellert, M. (1983) Geminate recombination of carbon monoxide to myoglobin. *J. Mol. Biol.*, **166**, 443.
- [78] Nienhaus, K. and Nienhaus, G. (2005) Probing heme protein-ligand interactions by UV/visible absorption spectroscopy. *Methods Mol. Biol.*, **305**, 215.
- [79] Cantor, C. and Schimmel, P. (1980) *Biophysical Chemistry, Part III: The behavior of biological macromolecules*. WH Freeman, San Francisco.
- [80] Copeland, R. (2000) *Enzymes: a practical introduction to structure, mechanism, and data analysis*. Wiley-Vch, NY, 2nd edn.
- [81] Hesse, M., Meier, H., and Zeeh, B. (2005) *Spektroskopische Methoden in der organischen Chemie*. Georg Thieme Verlag, Stuttgart.
- [82] Lopez, X. and Marques, M. (2006) Biochromophores. *Time-Dependent Density Functional Theory*, Springer, Berlin Heidelberg.
- [83] Ormö, M., Cubitt, A., Kallio, K., Gross, L., Tsien, R., and Remington, S. (1996) Crystal structure of the *Aequorea victoria* green fluorescent protein. *Science*, **273**, 1392.
- [84] Barth, A. and Zscherp, C. (2002) What vibrations tell us about proteins. *Q. Rev. Biophys.*, **35**, 369.
- [85] Dong, A., Huang, P., and Caughey, W. (1990) Protein secondary structures in water from second-derivative amide I infrared spectra. *Biochemistry*, **29**, 3303.
- [86] Barth, A. (2007) Infrared spectroscopy of proteins. *Biochim. Biophys. Acta - Bioenergetics*, **1767**, 1073.
- [87] Oberg, K., Ruysschaert, J., and Goormaghtigh, E. (2004) The optimization of protein secondary structure determination with infrared and circular dichroism spectra. *Eur. J. Biochem.*, **271**, 2937.
- [88] Caughey, W., Alben, J., McCoy, S., Boyer, S., Charache, S., and Hathaway, P. (1969) Differences in the infrared stretching frequency of carbon monoxide bound to abnormal hemoglobins. *Biochemistry*, **8**, 59.
- [89] Choc, M. and Caughey, W. (1981) Evidence from infrared and <sup>13</sup>C NMR spectra for discrete rapidly interconverting conformers at the carbon monoxide binding sites of hemoglobins A and Zurich. *J. Biol. Chem.*, **256**, 1831.

- 
- [90] Shimada, H. and Caughey, W. (1982) Dynamic protein structures. Effects of pH on conformer stabilities at the ligand-binding site of bovine heart myoglobin carbonyl. *J. Biol. Chem.*, **257**, 11893.
- [91] McNaught, A. D. and Wilkinson, A. (1997) *IUPAC. Compendium of Chemical Terminology. 2nd ed. (the "Gold Book")*. Blackwell Scientific Publications, Oxford, 2nd edn.
- [92] Ray, G., Li, X., Ibers, J., Sessler, J., and Spiro, T. (1994) How far can proteins bend the FeCO unit? Distal polar and steric effects in heme proteins and models. *J. Am. Chem. Soc.*, **116**, 162.
- [93] Vogel, K., Kozlowski, P., Zgierski, M., and Spiro, T. (1999) Determinants of the FeXO (X= C, N, O) vibrational frequencies in heme adducts from experiment and density functional theory. *J. Am. Chem. Soc.*, **121**, 9915.
- [94] Li, X. and Spiro, T. (1988) Is bound carbonyl linear or bent in heme proteins? Evidence from resonance Raman and infrared spectroscopic data. *J. Am. Chem. Soc.*, **110**, 6024.
- [95] Vogel, K., Kozlowski, P., Zgierski, M., and Spiro, T. (2000) Role of the axial ligand in heme-CO backbonding; DFT analysis of vibrational data. *Inorg. Chim. Acta*, **297**, 11.
- [96] Li, T., Quillin, M., Phillips Jr, G., and Olson, J. (1994) Structural determinants of the stretching frequency of CO bound to myoglobin. *Biochemistry*, **33**, 1433.
- [97] Park, K., Guo, K., Adebodun, F., Chiu, M., Sligar, S., and Oldfield, E. (1991) Distal and proximal ligand interactions in heme proteins: correlations between CO and Fe-C vibrational frequencies, oxygen-17 and carbon-13 nuclear magnetic resonance. *Biochemistry*, **30**, 2333.
- [98] Das, T., Weber, R., Dewilde, S., Wittenberg, J., Wittenberg, B., Yamauchi, K., Van Hauwaert, M., Moens, L., and Rousseau, D. (2000) Ligand binding in the ferric and ferrous states of Paramecium hemoglobin. *Biochemistry*, **39**, 14330.
- [99] Yeh, S., Couture, M., Ouellet, Y., Guertin, M., and Rousseau, D. (2000) A cooperative oxygen binding hemoglobin from *Mycobacterium tuberculosis*. *J. Biol. Chem.*, **275**, 1679.
- [100] Littlejohn, T., Takikawa, O., Skylas, D., Jamie, J., Walker, M., and Truscott, R. (2000) Expression and purification of recombinant human indoleamine 2,3-dioxygenase. *Protein Express. Purif.*, **19**, 22.

- 
- [101] Austin, C., et al. (2004) Optimised expression and purification of recombinant human indoleamine 2,3-dioxygenase. *Protein Express. Purif.*, **37**, 392.
- [102] Papadopoulou, N., Mewies, M., McLean, K., Seward, H., Svistunenکو, D., Munro, A., and Raven, E. (2005) Redox and spectroscopic properties of human indoleamine 2,3-dioxygenase and a His303Ala variant: implications for catalysis. *Biochemistry*, **44**, 14318.
- [103] Nienhaus, K. and Nienhaus, G. (2008) Ligand dynamics in heme proteins observed by Fourier transform infrared spectroscopy at cryogenic temperatures. *Methods Enzymol.*, **437**, 347.
- [104] Berendzen, J. and Braunstein, D. (1990) Temperature-derivative spectroscopy: a tool for protein dynamics. *Proc. Natl. Acad. Sci. USA*, **87**, 1.
- [105] Lehle, H., Kriegl, J., Nienhaus, K., Deng, P., Fengler, S., and Nienhaus, G. (2005) Probing electric fields in protein cavities by using the vibrational Stark effect of carbon monoxide. *Biophys. J.*, **88**, 1978.
- [106] Kriegl, J., Bhattacharyya, A., Nienhaus, K., Deng, P., Minkow, O., and Nienhaus, G. (2002) Ligand binding and protein dynamics in neuroglobin. *Proc. Natl. Acad. Sci. USA*, **99**, 7992.
- [107] Terentis, A., Thomas, S., Takikawa, O., Littlejohn, T., Truscott, R., Armstrong, R., Yeh, S., and Stocker, R. (2002) The heme environment of recombinant human indoleamine 2,3-dioxygenase. *J. Biol. Chem.*, **277**, 15788.
- [108] Macchiarulo, A., Nuti, R., Bellocchi, D., Camaioni, E., and Pellicciari, R. (2007) Molecular docking and spatial coarse graining simulations as tools to investigate substrate recognition, enhancer binding and conformational transitions in indoleamine 2,3-dioxygenase (IDO). *Biochim. Biophys. Acta - Proteins Proteomics*, **1774**, 1058.
- [109] Frauenfelder, H., Parak, F., and Young, R. (1988) Conformational substates in proteins. *Annu. Rev. Biophys. Biophys. Chem.*, **17**, 451.
- [110] Elber, R. and Karplus, M. (1987) Multiple conformational states of proteins: a molecular dynamics analysis of myoglobin. *Science*, **235**, 318.
- [111] Noguti, T. and Gō, N. (1989) Structural basis of hierarchical multiple substates of a protein. I: Introduction. *Proteins*, **5**, 97.

- 
- [112] Hong, M., Braunstein, D., Cowen, B., Frauenfelder, H., Iben, I., Mourant, J., Ormos, P., Scholl, R., Schulte, A., and Steinbach, P. (1990) Conformational substates and motions in myoglobin. external influences on structure and dynamics. *Biophys. J.*, **58**, 429.
- [113] Johnson, J., Lamb, D., Frauenfelder, H., Müller, J., McMahon, B., Nienhaus, G., and Young, R. (1996) Ligand binding to heme proteins. VI. interconversion of taxonomic substates in carbonmonoxymyoglobin. *Biophys. J.*, **71**, 1563.
- [114] Di Pace, A., Cupane, A., Leone, M., Vitrano, E., and Cordone, L. (1992) Protein dynamics. Vibrational coupling, spectral broadening mechanisms, and anharmonicity effects in carbonmonoxy heme proteins studied by the temperature dependence of the Soret band lineshape. *Biophys. J.*, **63**, 475.
- [115] Ansari, A., et al. (1987) Rebinding and relaxation in the myoglobin pocket. *Biophys. Chem.*, **26**, 337.
- [116] O’Keefe, D., Ebel, R., Peterson, J., Maxwell, J., and Caughey, W. (1978) An infrared spectroscopic study of carbon monoxide bonding to ferrous cytochrome P-450. *Biochemistry*, **17**, 5845.
- [117] Park, J., Kim, J., Lee, T., and Lim, M. (2007) Rebinding dynamics of CO to guanidine HCl-denatured heme proteins. *Conference on Lasers and Electro-Optics-Pacific Rim, 2007. CLEO/Pacific Rim 2007*.
- [118] Alben, J., et al. (1982) Infrared spectroscopy of photodissociated carboxymyoglobin at low temperatures. *Proc. Natl. Acad. Sci.*, **79**, 3744.
- [119] Yang, F. and Phillips Jr, G. (1996) Crystal structures of CO-, deoxy- and met-myoglobins at various pH values. *J. Mol. Biol.*, **256**, 762.
- [120] Vojtechovsky, J., Chu, K., Berendzen, J., Sweet, R., and Schlichting, I. (1999) Crystal structures of myoglobin-ligand complexes at near-atomic resolution. *Biophys. J.*, **77**, 2153.
- [121] Sugimoto, H., Oda, S., Otsuki, T., Yotsuya, K., Hino, T., Yoshida, T., and Shiro, Y. (2007) X-ray structure and reaction mechanism of human indoleamine 2,3-dioxygenase. *International Congress Series*, **1304**, 85.
- [122] Chauhan, N., et al. (2009) Reassessment of the reaction mechanism in the heme dioxygenases. *J. Am. Chem. Soc.*, **131**, 4186.
- [123] Capece, L., Arrar, M., Roitberg, A., Yeh, S., Marti, M., and Estrin, D. (2010) Substrate stereo-specificity in tryptophan dioxygenase and indoleamine -2,3-dioxygenase. *Proteins: Struct., Funct., and Bioinf.*, **78**, 2961.

- 
- [124] Frauenfelder, H., McMahon, B., Austin, R., Chu, K., and Groves, J. (2001) The role of structure, energy landscape, dynamics, and allostery in the enzymatic function of myoglobin. *Proc. Natl. Acad. Sci.*, **98**, 2370.
- [125] Lamb, D., Nienhaus, K., Arcovito, A., Draghi, F., Miele, A., Brunori, M., and Nienhaus, G. (2002) Structural dynamics of myoglobin. *J. Biol. Chem.*, **277**, 11636.
- [126] Lim, M., Jackson, T., and Anfinrud, P. (1997) Modulating carbon monoxide binding affinity and kinetics in myoglobin: the roles of the distal histidine and the heme pocket docking site. *J. Biol. Inorg. Chem.*, **2**, 531.
- [127] Nienhaus, K., Palladino, P., and Nienhaus, G. (2008) Structural dynamics of myoglobin: FTIR-TDS study of NO migration and binding. *Biochemistry*, **47**, 935.
- [128] Ormos, P., Ansari, A., Braunstein, D., Cowen, B., Frauenfelder, H., Hong, M., Iben, I., Sauke, T., Steinbach, P., and Young, R. (1990) Inhomogeneous broadening in spectral bands of carbonmonoxymyoglobin. the connection between spectral and functional heterogeneity. *Biophys. J.*, **57**, 191.
- [129] Ormos, P., Száraz, S., Cupane, A., and Nienhaus, G. (1998) Structural factors controlling ligand binding to myoglobin: a kinetic hole-burning study. *Proc. Natl. Acad. Sci. USA*, **95**, 6762.
- [130] Nienhaus, K., Nickel, E., Lu, C., Yeh, S., and Nienhaus, G. (2011) Ligand migration in human indoleamine-2,3 dioxygenase. *IUBMB life*, **63**, 153.
- [131] Lu, C., Lin, Y., and Yeh, S. (2010) Spectroscopic studies of ligand and substrate binding to human indoleamine 2,3-dioxygenase. *Biochemistry*, **49**, 5028.
- [132] Nickel, E., Nienhaus, K., Lu, C., Yeh, S., and Nienhaus, G. (2009) Ligand and substrate migration in human indoleamine 2,3-dioxygenase. *J. Biol. Chem.*, **284**, 31548.
- [133] Sono, M. (1989) Enzyme kinetic and spectroscopic studies of inhibitor and effector interactions with indoleamine 2,3-dioxygenase. 2. evidence for the existence of another binding site in the enzyme for indole derivative effectors. *Biochemistry*, **28**, 5400.
- [134] Hamilton, G. (1969) Mechanisms of two-and four-electron oxidations catalyzed by some metalloenzymes. *Adv. Enzymol. Relat. Areas Mol. Biol.*, **32**, 55.

- 
- [135] Chung, L., Li, X., Sugimoto, H., Shiro, Y., and Morokuma, K. (2008) Density functional theory study on a missing piece in understanding of heme chemistry: the reaction mechanism for indoleamine 2,3-dioxygenase and tryptophan 2,3-dioxygenase. *J. Am. Chem. Soc.*, **130**, 12299.
- [136] Lewis-Ballester, A., Batabyal, D., Egawa, T., Lu, C., Lin, Y., Marti, M., Capece, L., Estrin, D., and Yeh, S. (2009) Evidence for a ferryl intermediate in a heme-based dioxygenase. *Proc. Nat. Acad. Sci.*, **106**, 17371.
- [137] Muller, A., DuHadaway, J., Donover, P., Sutanto-Ward, E., and Prendergast, G. (2005) Inhibition of indoleamine 2,3-dioxygenase, an immunoregulatory target of the cancer suppression gene Bin1, potentiates cancer chemotherapy. *Nature Med.*, **11**, 312.
- [138] Metz, R., DuHadaway, J., Kamasani, U., Laury-Kleintop, L., Muller, A., and Prendergast, G. (2007) Novel tryptophan catabolic enzyme IDO2 is the preferred biochemical target of the antitumor indoleamine 2,3-dioxygenase inhibitory compound D-1-methyl-tryptophan. *Cancer Res.*, **67**, 7082.
- [139] Murray, M. (2007) The human indoleamine 2,3-dioxygenase gene and related human genes. *Curr. Drug Metab.*, **8**, 197.
- [140] Ball, H., Yuasa, H., Austin, C., Weiser, S., and Hunt, N. (2009) Indoleamine 2,3-dioxygenase-2; a new enzyme in the kynurenine pathway. *Int. J. Biochem. Cell Biol.*, **41**, 467.
- [141] Dolusic, E., et al. (2011) Tryptophan 2,3-dioxygenase (TDO) inhibitors. 3-(2-(pyridyl)ethenyl)indoles as potential anticancer immunomodulators. *J. Med. Chem.*, **54**, 5320.



## Danksagung

Bei all denjenigen, die zum Gelingen dieser Arbeit beigetragen haben, möchte ich mich an dieser Stelle herzlich bedanken.

Zunächst möchte ich mich bei Professor Gerd U. Nienhaus bedanken, der mir die Gelegenheit gegeben hat, in seiner Abteilung meine Dissertation anzufertigen und ohne den diese Arbeit nicht zustande gekommen wäre. Er hat die bestmöglichen Voraussetzungen für das Gelingen der Arbeit geschaffen und mir die wissenschaftliche Herangehensweise an fachliche Fragestellungen und Probleme nahe gebracht.

Ein herzliches Dankeschön ist an Karin Nienhaus gerichtet, die mich hervorragend betreut hat, jederzeit ein offenes Ohr für meine Fragen hatte und auch zum tausendsten Mal "germinate" re-binding - fast - kommentarlos korrigiert hat. Die Diskussionen mit ihr waren sehr konstruktiv und haben mich immer sehr motiviert, auch wenn sie sich hundertmal im Kreis gedreht haben. Ihr Interesse an meiner Arbeit hat mich zusätzlich angespornt.

My sincere thanks to Prof. Yeh for providing the opportunity to work in her lab for a couple of month. I had a great time in your lab, learned a lot of things very useful for my experiments and the discussions were very helpful. Many thanks to Ariel Lewis who taught me the handling of the Raman setup. I had a really good time in NY. Thanks!

Der Auslandsaufenthalt wurde vom Karlsruhe House of Young Scientists (KHYS) gefördert.

Einen herzlichen Dank an die Ulmer TAs, insbesondere an Uwe Theilen, der mich in die Proteinexpression eingewiesen hat, an Renate Nikopoulos, die einige Flash Messungen für mich durchgeführt hat und eine tolle Bürokollegin war und an Florian Junginger, der immer dafür gesorgt hat, das die IR und die Flash Anlage gut gepflegt und einsatzbereit zur Verfügung standen.

Auch an Susanne Matschulo, die zahllose Mutanten exprimiert und aufgereinigt hat und an Alexander Hepting, ohne den die IR Anlage in Karlsruhe vermutlich noch nicht wieder laufen würde, ein großes Dankeschön.

An Robert Rieger und Andrei Kobitski, die mir bei der Auswertung der Daten mit MatLab behilflich waren.

Last but not least: Meine lieben Kollegen. Tja, was soll ich sagen .. ich hatte ne wirklich schöne Zeit mit Euch.



## List of Publications

Nienhaus, K., Nickel, E., Lu, C., Yeh, S. R., und Nienhaus, G. U. (2011) Ligand migration in human indoleamine-2,3 dioxygenase, *IUBMB Life*, **63**, 153-159.

Nickel, E., Nienhaus, K., Lu, C., Yeh, S. R., und Nienhaus, G. U. (2009) Ligand and substrate migration in human indoleamine 2,3-dioxygenase, *J. Biol. Chem.*, **284**, 31548.

Nienhaus, K., Nickel, E., Davis, M. F., Franzen, S., und Nienhaus, G. U. (2008) Determinants of substrate internalization in the distal pocket of dehaloperoxidase hemoglobin of *Amphitrite ornata*, *Biochemistry*, **47**, 12985.



## List of Poster

Nickel, E., Nienhaus, K., Lu, C., Yeh, S. R. and Nienhaus, G.U. (2011) Spectroscopic Studies of Ligand and Substrate Binding to Heme Containing Indoleamine 2,3-Dioxygenase, Biophysical Society Meeting, Baltimore, USA

Nickel, E., Nienhaus, K., Lu, C., Yeh, S. R. and Nienhaus, G.U. (2010) Ligand and Substrate Migration in Human Indoleamine 2,3-Dioxygenase, Jahrestagung 2010 der Deutschen Gesellschaft für Biophysik, Bochum, Germany

Nickel, E., Nienhaus, K., Lu, C., Yeh, S. R. and Nienhaus, G.U. (2010) Spectroscopic Studies of Substrate Binding to Human Indoleamine 2,3-Dioxygenase, XVIth International Conference on Oxygen Binding and Sensing Proteins, Antwerp, Belgium

Nickel, E., Nienhaus, K., Lu, C., Yeh, S. R. and Nienhaus, G.U. (2009) Spectroscopic Studies of Ligand and Substrate Binding to Indoleamine 2,3-Dioxygenase, 7th European Biophysics Congress (EBSA), Genua, Italy

Nickel, E., Nienhaus, K., Lu, C., Yeh, S. R. and Nienhaus, G.U. (2008) Spectroscopic Studies of Ligand and Substrate Binding to Heme Containing Indoleamine 2,3-Dioxygenase, Jahrestagung 2008 der Deutschen Gesellschaft für Biophysik, Berlin, Germany



## Lebenslauf

Name	Elena Nickel
Geburtsdatum	20.07.1981
Geburtsort	Ahlen, NRW
Staatsangehörigkeit	deutsch

### Promotion

10/2007 - heute	Promotionsthema: Ligand and Substrate Migration in Human Indoleamine 2,3-Dioxygenase
10/2009 - 07/2011	Wissenschaftliche Mitarbeiterin; AG Prof. Nienhaus, Institut für Angewandte Physik, Karlsruher Institute für Technologie (KIT), Karlsruhe
09/2010 - 12/2010	Forschungsaufenthalt; Physiology and Biophysics, Albert Einstein College of Medicine, NY (USA)
10/2007 - 09/2009	Wissenschaftliche Mitarbeiterin; Institut für Biophysik, Fakultät für Naturwissenschaften, Universität Ulm, Ulm

### Universitäre Ausbildung

10/2001 - 06/2007	Studium der Biologie; Universität Osnabrück, Osnabrück Abschluss: Diplom
09/2004 - 06/2005	Auslandsaufenthalt; University of Hull, Hull (UK)

### Schulbildung

07/1992 - 05/2001	Gymnasium Wolbeck, Münster Abschluss: Abitur
07/1989 - 06/1992	Ludgerusgrundschule Albersloh, Sendenhorst

